Multidirectional flow and LRG1 in endothelial cells: potential atheroprotective role

Kuin Tian Pang

Department of Bioengineering

Imperial College London

A thesis submitted for the degree of

Doctor of Philosophy and Diploma of Imperial College

January 2020

Declaration

I hereby declare that this thesis is my original work and it has been written by me in its entirety. I have duly acknowledged all the sources of information which have been used in the thesis. Work carried out with the assistance of others has been appropriately acknowledged.

This thesis has not been submitted to any institution of higher learning for a degree or an award.

Kuin Tian Pang

Copyright

Abstract

Haemodynamic wall shear stress affects the function of arterial endothelial cells (ECs). Low magnitude, oscillatory and multidirectional shear have all been postulated to stimulate endothelial activation, whereas high magnitude and uniaxial shear are thought to promote endothelial homeostasis. The effects of shear interact with the effects of pro-inflammatory cytokines; they are mediated by complex signal transduction pathways and together may account for the patchy nature of atherosclerosis.

The swirling-well system was used to investigate shear-induced endothelial activation. The method involves culturing ECs in standard multi-well plates on the platform of an orbital shaker to induce complex flow profiles. Computational fluid dynamic (CFD) simulation revealed that the swirling medium produces low magnitude multidirectional flow (LMMF) in the centre of the well and high magnitude uniaxial flow (HMUF) at the edge. A disadvantage of the method is that sheared ECs may release soluble mediators that become mixed in the swirling medium, and corrupt of apparent relations between shear and ECs properties. This drawback was resolved using a novel coating method that restricts cell growth to specific regions of the well. This modification permitted the demonstration that ECs do indeed release anti-inflammatory soluble mediators under HMMF.

Leucine-rich α-2-glycoprotein 1 (LRG1) is a pro-angiogenic protein intimately linked with inflammation. Its role in endothelial activation was investigated. ECs activated by TNF-α treatment and LMMF showed higher LRG1 expression. The protein suppressed endothelial NF-κB signalling, EC adhesion molecules expression, and monocyte recruitment. Mechanistically, LRG1 caused TNFR1 shedding via the ALK5-SMAD2 pathway and the activation of ADAM10. LRG1 was highly expressed in ECs of stenotic arteries; it was found at high concentrations in the serum of critical limb ischemia patients and correlated with sTNFR1 concentrations. These data are consistent with a novel role for LRG1 in endothelial activation and a significant influence on atherogenesis.

Acknowledgement

First and foremost, I would like to give thanks to the Triune God for giving me the wisdom, knowledge, and ability to undertake and complete this study.

I owe my supervisors—Professor Peter Weinberg and Dr Xiaomeng Wang—a debt of gratitude. There is a Chinese proverb that says:'He who teaches me for even one day, I should regard him as my father for life' (translation of 一日为师, 终身为父). My supervisors have been very supportive and nurturing in my research training, for which I will forever be grateful for. They have turned a mechanical engineering-trained novice into a qualified multidisciplinary researcher through their years of guidance. I am very grateful to them for accepting me as their student despite my bizarre education background.

One of the favourite phrases that Professor Peter Weinberg says in a meeting is 'This is a very interesting data...but why?'; this phrase always reminds me to be curious about everything—especially unexpected results from experiments,. The phrase shall be my motto in my research career. He has also been a great role model who shows me the qualities of a good scientist.

I owe a great deal of thanks to my 'Daigo' (oldest brother or gang leader)—Dr Chee Wai Fhu, and my 'boss'—Dr Mean Ghim. They have been great mentors who provided many advise and guidance in my work. I would like to thank Dr Chee Wai Fhu for the countless hours he has spent on the phone talking to an

inexperience student like me, and Dr Mean Ghim for the daily coffee session to discuss about research idea in the cold outside the campus (he forced me to drink outside because he had to vape). I wish to thank Dr Christina Warboys for 'the only molecular biologist' in the lab who provided me mentorship and help in molecular biology work (and for saving my *ss when my reagents ran out). I would like to thank Dr Ethan Rowland for his help in my writing and for putting up with my weak writing skill. I would also like to thank Dr-to-be Mehwish Arshad for her help in CFD work, MATLAB coding, for her comradeship and our nonsense chat in the lab. I am also grateful for Xuan Rui Ng (whom i like to call Xuan-Xuan) for teaching me laboratory techniques (although he always got grumpy when I forgot the protocols).

I have been enjoying working in a multidisciplinary team. I would like to thank, in no particular order, lab mates from Weinberg's lab (Dr Marta Dazzi, Dr Yean Chooi, Kai Riemer,Dr Yumnah Mohamied, Dr Eleni Bazigou, Dr Zahra Mohri, Piotr Sowinski) and XW lab (Dr Rui Ning Chia, Dr Chenghao Liu, Dr Yuet Ping Kwan, Dr Beiying Qiu, Seok Ting Lim, Sze Yuan Ho, Michelle Tan, Alison Tan, Melissa Teo, Johanna Howson, Dr Koon Hwee Ang, Fangcheng Wong, Azizah, and Dr Daniel Lio) for their friendship. I am also grateful to have buddies—Dr Worrapong Kit-anan and Jack Chen—who have been a great support and companion throughout my PhD.

Lastly, I would like to thank my wife Pei Wen Law for her unconditional love and support throughout this journey. I must also thank her for pretending to understand my PhD project and holding back her yawn in every one of our conversations about my work.

I am grateful for the A*STAR Graduate Scholarship (Overseas), without which this PhD would not have been possible. I would also like to acknowledge the research grants that support the work presented in this thesis: British Heart

Foundation project grant (awarded to Professor Peter Weinberg), National Medical Research Council Singapore Cooperative Basic Research Grant and Large Collaborative Grant DYNAMO (awarded to Dr Xiaomeng Wang).

For

my wife Pei Wen,

who showers me with her love and affection

(and sometimes with annoyance)

along this journey of life.

&

For

Jehovah God Almighty, the Maker of all things;

Lord Jesus Christ, my Saviour and Redeemer;

Holy Spirit, the Giver of life.

The heavens declare the glory of God;

the skies proclaim the work of His hands.

(Psalm 19:1)

Contents

List of Figures

List of Tables

List of Abbreviations

ADAM10	A Disintegrin and metalloproteinase domain-containing protein 10
ADAM17	A Disintegrin and metalloproteinase domain-containing protein 17
Akt	Protein kinase B
ALK1	Activin receptor-like kinase 1
ALK5	TGFβ receptor 1
ANCA	Antineutrophil cytoplasmic antibody
ANOVA	Analysis of variance
ApoE	Apolipoprotein E
APS	Ammonium Persulfate
AUC	Area under curve
BCL3	B-cell lymphoma 3-encoded protein
BSA	Bovine serum albumin
cDNA	Complementary DNA
CFD	Computational fluid dynamics
ChIP	Chromatin immunoprecipitation
CLI	Critical limb ischemia
CVD	Cardiovascular disease
DI water	Deionised water
DISC	Death signalling inducing signalling complex
DMSO	Dimethyl sulfoxide
DNA	Deoxyribonucleic acid

DNAse	Deoxyribonuclease
EBM-2	Endothelial Cell Growth Basal Medium 2
ECs	Endothelial cells
EDTA	Ethylenediaminetetraacetic acid
EGM-2	Endothelial Growth Medium 2
ELISA	Enzyme-linked immunosorbent assay
ELK1	E26 transformation-specific like-1 protein
EMT	Epithelial-mesenchymal transition
ENG	Endoglin
eNOS	Endothelial nitric oxide synthase 3
ERK	Extracellular signal–regulated kinases
EVG stain	Elastic Van Gieson stain
FADD	Fas associated protein with death domain
FAK	Focal adhesion kinase
FBS	Fetal bovine serum
FH	Familial hypercholesterolemia
GAPDH	Glyceraldehyde 3-phosphate dehydrogenase
GFP	Green fluorescence protein
HAECs	Human aortic endothelial cells
HCV	Hepatitis C virus
HEK293F	Freestyle human embryonic kidney 293
HIF-1α	Hypoxia inducible factor 1 subunit alpha
HMUF	High magnitude uniaxial flow
HUVECs	Human umbilical vein endothelial cells
IκB	Inhibitor of κB
ICAM-1	Intercellular adhesion molecule 1
ICAM-2	Intercellular adhesion molecule 2
IHD	Ischemic heart disease

IKK	IκB kinase
IL-1β	Interleukin-1β
IL-6	Interleukin 6
iNPH	Idiopathic normal pressure hydrocephalus
JAM	Junctional adhesion molecules
KLF2	Kruppel-like factor 2
KLF4	Kruppel-like factor 4
LDL	Low-density lipoprotein
LFA-1	Lymphocyte function-associated antigen 1
LMMF	Low magnitude multidirectional flow
LRG1	Leucine-rich α-2-glycoprotein 1
$Lrg^{-/-}$	LRG1 knock out
LRR	Leucine-rich repeat
M-CSF	Macrophage colony-stimulating factor
Mac1	macrophage-1 antigen
MAPK	Mitogen-activated protein kinase
MCP-1	Monocyte Chemoattractant Protein-1
mRNA	Messenger RNA
MSC	Mesenchymal stem cells
NF-κB	Nuclear factor kappa B
NO	Nitric oxide
OSI	Oscillatory shear index
Ox-LDL	Oxidised LDL
PAD	Peripheral arterial disease
PBS	Phosphate-buffered saline
PCR	Polymerase chain reaction
PCRT	Pre-operative chemoradiotherapy
PDMS	Polydimethylsiloxane

PECAM-1	Platelet endothelial cell adhesion molecule
PFA	Paraformaldehyde
PVDF	Polyvinylidene fluoride
qRT-PCR	Quantitative reverse transcription polymerase chain reaction
RFU	Relative fluorescence units
rhLRG1	Recombinant human LRG1
RIPA	Radioimmunoprecipitation assay
RNA	Ribonucleic acid
ROC	Receiver operating curve
ROS	Reactive oxygen species
RPM	Revolutions per minute
RUNX1	Runt-related transcription factor 1
SDS-PAGE	Sodium dodecyl sulfate-polyacrylamide gel electrophoresis
SMCs	Smooth muscle cells
SODD	silencer of death domain
sTNFR1	Soluble TNFR1
TβRII	TGF-β Receptor II
T2D	Type 2 diabetes
TAWSS	Time-averaged wall shear stress
TBS	Tris-buffered saline
TBST	Tris-buffered saline with TWEEN 20
TFBS	Transcription factor binding sites
TGF-β1	Transforming growth factor-beta 1
TGF-β3	Transforming growth factor-beta 3
THP-1 cells	Human acute monocytic leukaemia suspension line
TNF-α	Tumour necrosis factor-α
TNFR1	Tumour necrosis factor receptor 1
TNFR2	Tumour necrosis factor receptor 2

TRADD	TNFR-associated death domain protein
TRAF1	TNFR-associated factor 1
TransWSS	Transverse wall shear stress
UTRs	Untranslated regions
VCAM-1	Vascular cell adhesion molecule 1
VE-Cadherin	Vascular endothelial cell cadherin
VEGFR2	Vascular endothelial growth factor receptor 2
VLA-4	Integrin $\alpha 4\beta 1$ (very late antigen-4)
VOF	Volume of fluid
WSS	Wall shear stress
ZO-1	Zonula occludens-1

List of Symbols

ω	Angular velocity
Bo	Bond number
U	Characteristic velocity
ρ	Density
g	Gravitational acceleration
d	Medium height
a	Orbital radius of an orbital shaker
σ	Surface tension
t	Time
T	Time taken for one revolution
$\mathbf{u}$	Velocity vector
μ	Viscosity
τ	Wall shear stress vectors
We	Weber number
R	Well radius

Publications

Part of the work presented in this thesis have been published, submitted for publication, or presented at conferences.

Journal articles

Published

Ghim, M.[#], **Pang, K.T.** [#], Arshad, M., Wang, X., Weinberg, P.D., A novel method for segmenting growth of cells in sheared endothelial culture reveals the secretion of an anti-inflammatory mediator. Journal of Biological Engineering 12, 15 (2018)

Co-first author

Manuscripts in preparation

Pang, K.T., Ghim, M., Fhu, C.W., Tay, H.M., Hou, H.W., Chia, R.N., Sarathchandra,P., Chester, A.H., Yacoub, M., Wilkinson, F.L., Weston, R., Warboys, C.M., Weinberg, P.D.*, Wang, X.*, LRG1 is a novel regulator of endothelial activation.

∗ Co-corresponding author

Pang, K.T. [#], Ghim, M.[#], Arshad, A., Wang, X., Weinberg, P.D., Segmenting growth of endothelial cells in an orbiting 6-well plate for mechanobiology

study. Invited by Journal of visualized experiments (JoVE).

Conference contributions

Oral presentation

Pang, K.T., Fhu, C.W., Ghim, M., Tay, H.M., Hou, H.W., Lu, Q., Warboys, C.M., Wang, X., Weinberg, P.D., LRG1 is a novel regulator of endothelial activation and is shear dependent: a potential therapeutic target? Presented at the Frontiers in Cardiovascular Biology 2018 meeting, 2018, Vienna, Austria.

Pang, K.T., Fhu, C.W., Ghim, M., Tay, H.M., Hou, H.W., Lu, Q., Warboys, C.M., Wang, X., Weinberg, P.D., LRG1 is a novel regulator of endothelial activation and is shear dependent: a potential therapeutic target? Presented at 86th EAS Conress, 2018, Lisbon, Portugal.

Pang, K.T., LRG1 is a shear dependent protein and a novel regulator of endothelial activation. Presented at the 2nd LKCMedicine Retreat, Singapore.

Pang, K.T., Ghim, M., Arshad, M., Wang, X., Weinberg, P.D., Segmentation of endothelial cell growth in a swirling well plate allows investigation of the shear-dependent release of soluble mediators. Presented at the 17th International Conference on Biomedical Engineering, Singapore.

Poster presentation

Pang, K.T., Fhu, C.W., Warboys, C., Ghim, M., Wang, X., Weinberg, P.D., Could LRG1 be a novel regulator of shear stress-induced endothelial activation? A preliminary study. Presented at The 12th International Symposium on Biomechanics in Vascular Biology and Cardiovascular Disease, 2017, Rotterdam, The Netherlands.

Pang, K.T., Fhu, C.W., Ghim, M., Warboys, C., Wang, X., Weinberg, P.D., LRG1 expression is shear dependent and regulates endothelial activation. Presented at British Atherosclerosis Society Autumn Meeting, 2017, Cambidge, UK.

Pang, K.T., Fhu, C.W., Ghim, M., Tay, H.M., Hou, H.W., Lu, Q., Warboys, C.M., Wang, X., Weinberg, P.D., LRG1 is a novel regulator of endothelial activation and is shear dependent: a potential therapeutic target? Presented at The 13th International Symposium on Biomechanics in Vascular Biology and Cardiovascular Disease, 2018 , Atlanta, USA.

Pang, K.T.$^{\#}$, Ghim, M.$^{\#}$, Arshad, M., Weinberg, P.D., Segmentation of endothelial cell growth in a swirling well plate allows investigation of the shear-dependent release of soluble mediators. Presented at the 8th World Congress on Biomechanics, 2018, Dublin, Republic of Ireland.

Pang, K.T., Ghim, M., Wang, X., Weinberg, P.D., Suppression of endothelial activation depends on the type and duration of applied shear stress in vitro. Presented at The 14th International Symposium on Biomechanics in Vascular Biology and Cardiovascular Disease, 2019, London, UK.

Chapter 1

Introduction

Cardiovascular disease (CVD) is one of the leading causes of mortality and morbidity in the world and in the UK alone, it is responsible for 27% of deaths (Townsend et al., 2015). Atherosclerosis, a chronic inflammatory disease characterised by the accumulation of lipids and fibrous elements in the walls of large arteries, is the primary cause of CVD. Atherosclerosis progression results in ischemic heart disease (IHD), ischemic stroke, and peripheral arterial disease (PAD) (Herrington et al., 2016).

Atherosclerosis is not a 'modern' disease; arterial lesions have been found in well preserved ancient Egyptian and hunter-gatherer remains (Allam et al., 2009; Thompson et al., 2013). A whole-genome study revealed that a 5300-year-old glacier mummy exhibited several single nucleotide polymorphisms that are associated with CVD (Zink et al., 2014). These observations suggest that understanding atherosclerosis as solely the result of modern-day diets and lifestyles is not sufficient; atherogenesis is much more complex and more investigation is required.

One striking feature of atherosclerosis is that it forms preferentially at certain

arterial sites that experience 'disturbed' flow (Enos et al., 1953, 1955), hence it is essential to consider this biomechanical factor while investigating atherogenesis. Endothelial cells (ECs), cells that line the interior surface of blood vessels, are subjected to chronic shear stress *in vivo*; their activation by some shear stress profiles and pro-inflammatory cytokines is well recognised as an important step in the initiation of atherosclerosis (Ross et al., 1977). NF-κB is known as a central pathway that mediates endothelial activation (Pober, 2002). Despite the importance of biomechanical force in EC homeostasis and activation, many *in vitro* studies are performed in static culture—this ignores and undermines the role of biomechanical forces.

The swirling-well system (Warboys et al., 2019) is gaining attention as a simple and effective method of subjecting cultured ECs to complex flow; it is capable of generating both uniaxial and multidirectional flow in a single well. The system can be a very useful tool to study EC mechanobiology. But ECs are known to secrete soluble mediators (Sage et al., 1981; Tunica et al., 2009; Griffoni et al., 2011); such mediators are mixed by the swirling medium and influence cells everywhere in the well, thus masking the true effect of specific shear on ECs behaviour. Rectifying this flaw will make this system a better *in vitro* tool to study EC mechanobiology.

In search of a novel regulator in endothelial activation and atherogenesis, Leucine-rich α-2-glycoprotein 1 (LRG1), a pro-angiogenic protein (Wang et al., 2013b), was found to be relevant. LRG1 is intimately linked to inflammation, and possibly to the NF-κB pathway; pro-inflammatory cytokine and mechanical strain induce LRG1 expression (Wang et al., 2017b; Gao et al., 2019). Serum LRG1 of patients with inflammatory, autoimmune, and cardiovascular diseases (Xie et al., 2018; Ha et al., 2014; Serada et al., 2012; Watson et al., 2011; Yin et al., 2014; Pek et al., 2015) is also higher than that of

healthy controls. Understanding the role of LRG1 in endothelial activation, by pro-inflammatory cytokines and shear stress, could provide a new avenue for therapeutic discovery in atherosclerotic diseases.

Presented in this chapter is an introduction to the background knowledge and recent discoveries made in the field. The pathogenesis of atherosclerosis and the role of haemodynamics in atherosclerosis are detailed in Section 1.1 and Section 1.2. An introduction to EC mechanobiology is detailed in Section 1.3 and Section 1.4. The role of endothelial activation in atherosclerosis, NF-κB pathway in endothelial activation, regulation of NF-κB pathway by receptor shedding, and endothelial-monocyte interaction are detailed in Section 1.5, Section 1.6, Section 1.7 and Section 1.8, respectively. Section 1.9 presents the literature review of the use of the swirling-well system, and its advantages and limitations. In Section 1.10, LRG1 is introduced and discussed. Finally the research aims are laid out in Section 1.11 and the outline of this thesis is given in Section 1.12.

1.1 Pathogenesis of atherosclerosis

Atherosclerosis is a complex condition that progressively develops over decades. It is thought to be initiated by endothelial activation (Hunt and Jurd, 1998) and deposition of low-density lipoprotein (LDL) in the sub-endothelial matrix (Mundi et al., 2018). Accumulated LDL is oxidised to form oxidised LDL (ox-LDL), which triggers the production of pro-inflammatory cytokines by ECs, resulting in monocyte recruitment to vascular walls (Li and Mehta, 2005). Ox-LDL also stimulates the expression of endothelial cell adhesion molecules such as intercellular adhesion molecule 1 (ICAM-1) and vascular cell adhesion molecule 1 (VCAM-1) (Kita et al., 2001); upregulation of these molecules

promotes the capture, adhesion, and transmigration of monocytes across the endothelium (Mestas and Ley, 2008).

Recruited monocytes then differentiate into macrophages due to the effects of macrophage colony-stimulating factor (M-CSF) (Qiao et al., 1997). Macrophages ingest ox-LDL and become foam cells due to reactive oxygen species (ROS). The death of these foam cells results in accumulation of lipid-rich cell debris, resulting in a growing necrotic core within the vascular wall (Yu et al., 2013). Subsequently, smooth muscle cells (SMCs) proliferate and migrate to the intima; they accumulate and secrete fibrous elements that help develop a plaque with a fibrous cap (Basatemur et al., 2019). Although plaques remain asymptomatic for decades, they can eventually grow large enough to restrict blood flow causing symptoms such as angina. Fibrous cap rupture or superficial erosion of endothelium may cause acute vessel occlusion due to thrombosis, with or without embolisation, resulting in myocardial infarction or stroke (Lusis, 2000). The pathological process of atherosclerosis is illustrated in Figure 1.1.

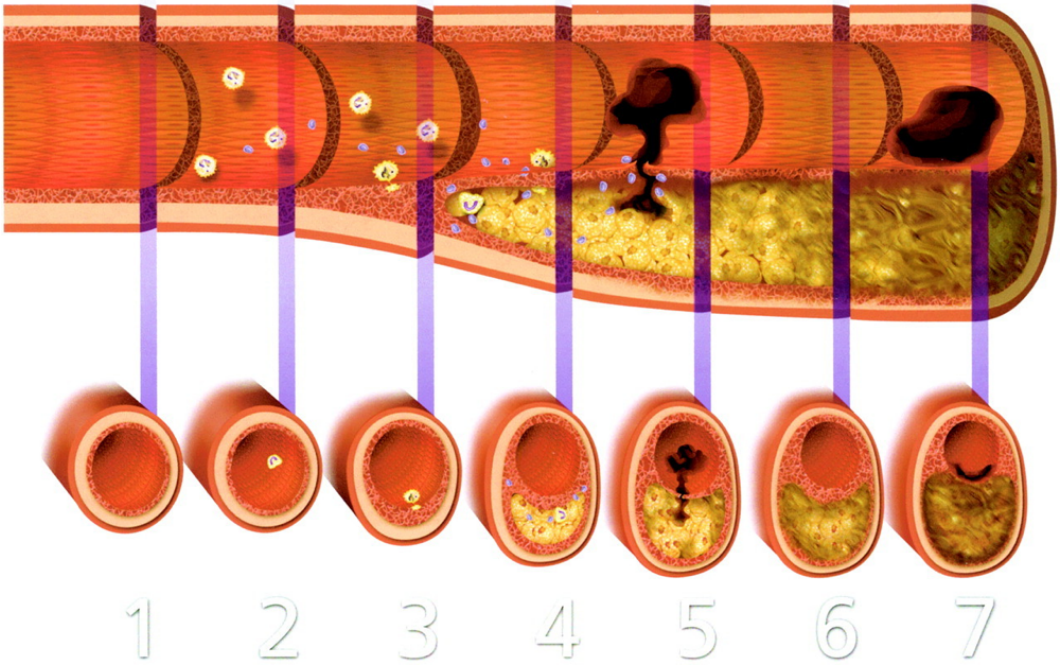

Figure 1.1: Atherogenesis. Longitudinal section (top) and cross section (bottom) of an artery showing the progression of atherogenesis from a normal artery to a stenotic atheroma in humans. (1) A normal artery that shows no sign of atherogenesis should have unobstructed lumen with no thickening of vessel wall. (2) Initiation of lesion formation as a result of endothelial activation, LDL deposition, and monocyte recruitment. (3) Recruited monocytes differentiate into macrophages and engulf LDL. (4) Macrophages become foam cells and their death results in accumulation of lipid-rich cell debris, thereby causing a growing necrotic core within the vascular wall. Proliferation and migration of SMCs results in the formation of a plaque with a fibrous cap. (5) Fibrous cap ruptures can cause acute vessels occlusion due to thrombosis. (6) Increased collagen accumulation and SMCs growth after thrombus resolution may cause significant stenosis. (7) In some cases, superficial erosion of the endothelium may cause occlusive thrombus. Reprinted with permission from Wolters Kluwer Health, Inc.: Circulation (Libby, 2001).

Numerous risk factors for atherosclerosis have been identified through epidemiological studies in the last 50 years, these include age, high plasma cholesterol, smoking, obesity and family history (Lusis, 2000). These risk factors interact to accelerate disease progression.

In addition to these risk factors, biomechanical forces have emerged as an essential feature of atherogenesis. The human body is sustained by nutrients

and other essentials circulating in a branching system of tubes with a complex geometry. Geometry complexity results in heterogeneous flow characteristics, which might be an important factor that initiates atherosclerosis. This will be discussed further in the next section.

1.2 Haemodynamics and its role in atherosclerosis

Atherosclerotic lesions form preferentially at certain arterial sites. For example, DeBakey et al. (1985) found that lesions mainly occur in the vicinity of the major branches of the aortic arch, coronary arteries, carotid arteries, and abdominal aorta. Autopsies performed on 200 young American soldiers (average age of 22.1 years) who were killed in the Korean War showed that 77% of them had varying degrees of vascular thickening and occlusion in one or more of the major vessels; most lesions were found to be at or near points of bifurcation in blood vessels (Enos et al., 1953, 1955). The predilection for lesions to occur at branches and bifurcations suggests that local flow disturbance is an important factor in disease initiation.

Many theories have been proposed over the past few decades to explain the association between atherogenesis and haemodynamics. Most theories are based on wall shear stress (WSS)—the frictional force per unit area between the blood and the endothelium. Time-averaged WSS (TAWSS), the temporal average of the magnitude of the instantaneous WSS vectors, is commonly used to describe the magnitude of WSS.

Fry (1969) proposed that the formation of lesions downstream of branches is due to elevated WSS. Following that, Caro et al. (1971) argued that high WSS

is actually atheroprotective. They postulated that high WSS promotes lipid efflux from the vascular wall to the blood due to the presence of favourable steep concentration gradients; instead, it is low WSS that leads to lipid accumulation. Ku et al. (1985) extended this hypothesis to incorporate the oscillatory nature of WSS by developing a new metric: the oscillatory shear index (OSI) (He and Ku, 1996) to describe the oscillatory nature of flow.

Today, the low and oscillatory shear stress theory is a widely accepted consensus by researchers in the field. However, a systematic review by Peiffer et al. (2013b) revealed that the low and oscillatory WSS theory is less robust than claimed. Of 18 studies that spatially assessed association between WSS and disease, only 10 supported the accepted hypothesis. When rigorous point-by-point comparisons are made, no studies support the low and oscillatory WSS theory.

The term disturbed flow is widely used, but vaguely defined as acknowledged by Himburg and Friedman (2006). The commonly used index, OSI, also fails to capture the multidirectional nature of blood flow. In the same year when Peiffer et al. (2013b) conducted a systematic review, they published another article to propose a novel metric, the transverse WSS (transWSS) (Peiffer et al., 2013a). TransWSS is calculated by averaging the magnitude of the WSS components perpendicular to the mean WSS vector (Peiffer et al., 2013a). Mohamied et al. (2014) found strong and significant correlations between maps of atherosclerotic lesion prevalence and transWSS in rabbits but no significant correlations were found with other commonly used WSS metrics. The transWSS theory is further supported by Wang et al. (2013a) who recently showed that flow applied perpendicular to the long axis of ECs stimulates reactive oxygen and NF-κB translocation (thought to be atherogenic), whereas parallel flow promotes endothelial nitric oxide synthase 3 (eNOS) phosphorylation

and nitric oxide (NO) synthesis (thought to be atheroprotective). Note that this is relevant to the transWSS hypothesis because ECs are thought to align with the mean WSS vector.

It is, however, important to note that transWSS cannot differentiate between purely forward flow and pulsatile flow with reversal; hence transWSS should be used in complement TAWSS and OSI, instead of replacing them (Mohamied et al., 2014) .The illustration of TAWSS, OSI, and transWSS is shown in Figure 1.2.

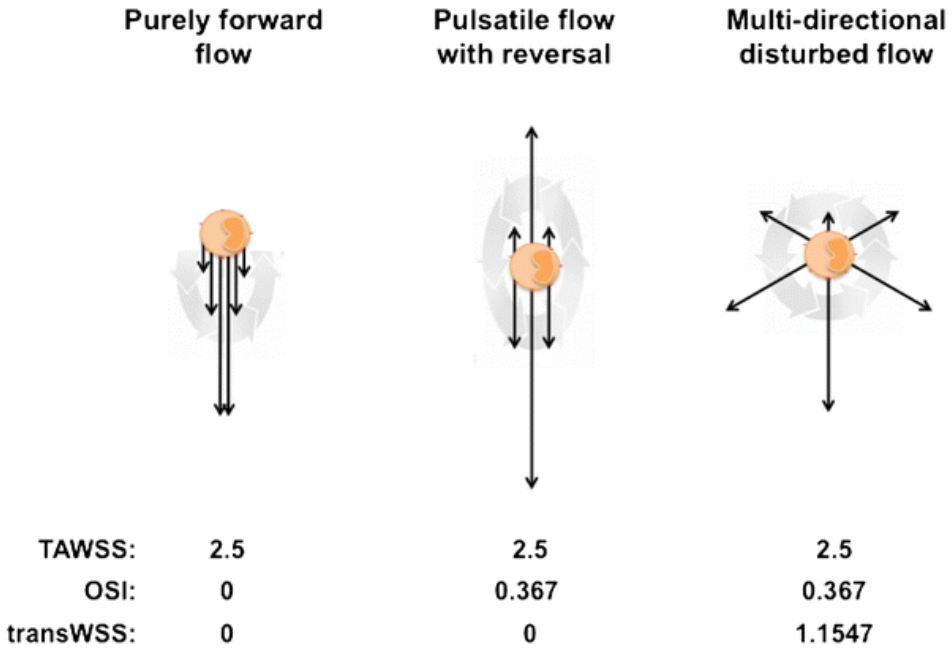

Figure 1.2: TAWSS, OSI, and transWSS. Instantaneous WSS is represented by each black arrow, and the evolution of WSS vectors with time during the cardiac cycle is represented by grey arrows. With the same TAWSS, OSI is able to distinguish between purely forward flow and oscillatory flow; but it fails to capture the multidirectional nature of flow. TransWSS has the capability to differentiate multidirectional flow from the pure oscillatory flow. TransWSS should be used in complement with TAWSS and OSI because it cannot distinguish between purely forward flow and pulsatile flow with reversal. Adapted from Mohamied et al. (2014).

1.3 Mechanosensing by endothelial cells

ECs that line the interior surface of blood vessels have a variety of receptors and mechanotransducers that can sense blood flow and convert mechanical stimuli to biochemical signals. Examples of mechanosensors are adhesion receptors, glycocalyx components, integrins, ion channels, and cytoskeletal molecules (Fang et al., 2019). For example, Tzima et al. (2005) demonstrated that platelet endothelial cell adhesion molecule (PECAM-1), vascular endothelial cell cadherin (VE-Cadherin), and vascular endothelial growth factor receptor 2 (VEGFR2) form a mechanosensory complex. PECAM-1 transduces mechanical forces directly and the cells deficient in any of these molecules did not activate protein kinase B (Akt) and were not aligned in the direction of flow (both of which are known responses of ECs to shear application). PECAM-1 knockout mice also do not show NF-κB activation and F-actin organisation (Tzima et al., 2005).

The glycocalyx is a mix of glycoproteins, glycolipids and absorbed circulating molecules which is found on the luminal side of the endothelium (Weinbaum et al., 2007). In an experiment in which enzymes were used to digest heparan sulfate, the dominant glycosaminoglycan of the glycocalyx, from cultured ECs impaired the responses of ECs to shear stress (Florian et al., 2003). Disruption of the glycocalyx also compromised the reorganisation of the actin cytoskeleton in response to shear stress (Thi et al., 2004).

There are many other mechanosensors and mechanotransduction pathways, but how various mechanosensors work together in response to shear stress is still unknown.

1.4 Mechanoregulation of endothelial cells

Shear stress has been shown to affect endothelial stiffness (Potter et al., 2012; Merna et al., 2018), alignment (Ghim et al., 2017; Levesque and Nerem, 1985; Potter et al., 2011), elongation (Levesque and Nerem, 1985; Potter et al., 2011), and cytoskeleton organisation (Merna et al., 2018; Birukov et al., 2002). Cultured ECs exposed to high magnitude laminar flow (putatively atheroprotective flow) are elongated and aligned with the flow direction, whereas those exposed to low magnitude or disturbed flow (putatively atherogenic flow) exhibit cobblestone morphology; their morphology *in vivo* is similar at atheroprone and atheroprotected regions, respectively (Nerem et al., 1981; Sato and Ohshima, 1994).

In addition to physical and morphological changes, shear stress has also been shown to regulate gene expressions in ECs (Chen et al., 2001; García-Cardeña et al., 2001; Serbanovic-Canic et al., 2017). Atherogenic flow was reported to increase NF-κB activation (Baeriswyl et al., 2019; Feaver et al., 2013), apoptosis (Pan et al., 2017; Heo et al., 2011; Warboys et al., 2014), permeability (Ghim et al., 2017), oxidative stress (Passerini et al., 2004), and leukocyte recruitment (Hsiai et al., 2003). On the other hand, atheroprotective flow was reported to upregulate atheroprotective mechanism such as the phosphorylation of eNOS (Jin et al., 2003; Fleming et al., 2005) and increases the level of the transcription factor Kruppel-like factor 2 (KLF2) (Dekker et al., 2002; Wang et al., 2006). A summary of these phenotypic changes in ECs in response to flow is shown in Figure 1.3.

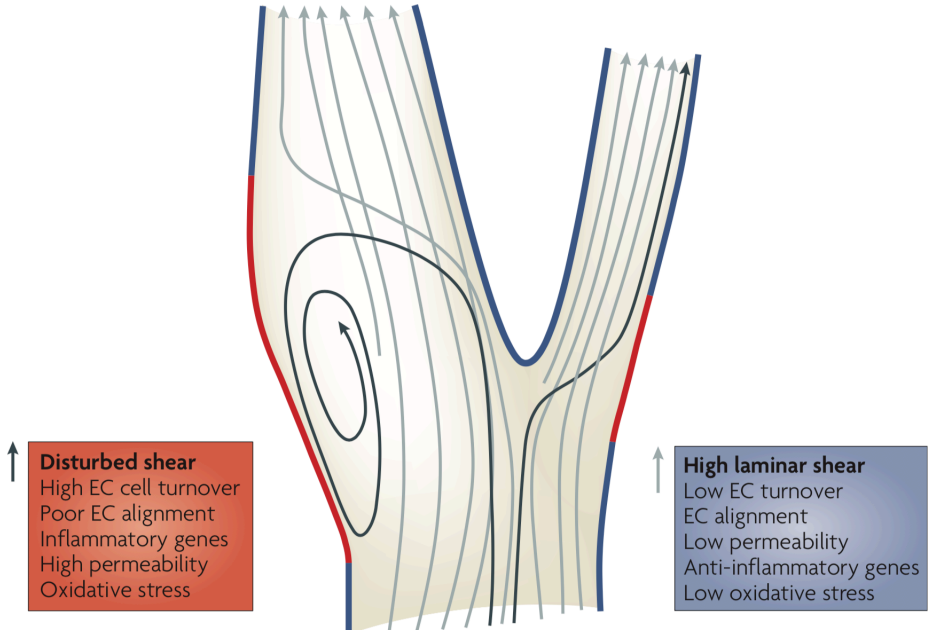

Figure 1.3: Phenotype of ECs in regions of different flow profile. ECs in regions of disturbed shear are activated, exhibit a pro-inflammatory phenotype that is characterised by high cell turnover, poor alignment, increased inflammatory genes expression and permeability, and high oxidative stress. ECs in regions of high laminar shear are quiescent, exhibit an anti-inflammatory phenotype that is characterised by low cell turnover, alignment in flow direction, low permeability and oxidative stress, and increased in anti-inflammatory genes expression. Reprinted with permission from Springer Nature: Nature Reviews Molecular Cell Biology (Hahn and Schwartz, 2009).

1.5 Endothelial activation in atherosclerosis

ECs are critical players in maintaining circulatory function and vascular wall homeostasis. They form a semi-permeable barrier that facilitates the exchange of nutrients, fluid, and metabolic waste between the blood and vascular tissues. ECs maintain tight cellular junctions with non-adhesive and non-thrombogenic surfaces in the physiological state (Fleming et al., 2017).

The response-to-injury hypothesis states that atherogenesis is a result of ECs response to injuries (Ross et al., 1977). Pro-inflammatory cytokines and

atherogenic flow are two known stimuli that trigger endothelial injury (Sedger and Mcdermott, 2014; Chappell et al., 1998). Structurally intact ECs respond to these stimuli by increasing permeability and LDL transcytosis (Mundi et al., 2018; Ghim et al., 2017; Zhang et al., 2014), increasing cell adhesion molecules (Chappell et al., 1998), and recruiting leukocytes (Mestas and Ley, 2008); this process was termed endothelial activation by Pober (1988).

1.6 NF-κB pathway in endothelial activation

The NF-κB pathway is a key pathway in endothelial activation (Pober, 2002). NF-κB, an important transcription factor in the pathway, was first discovered by Sen and Baltimore (1986). NF-κB is a general name which includes 5 subunits, namely RelA (p65), NF-κB1 (p50), and NF-κB2 (p52), c-Rel, and RelB. Two of these abundant subunits, p65/p50, form a heterodimer complex, which is often referred to as NF-κB. In the non-activated state, NF-κB is sequestered in the cytoplasm by inhibitor kappa B alpha (IκBα) (Karin and Ben-neriah, 2000).

The NF-κB pathway can be activated by many extracellular stimuli such as tumour necrosis factor-α (TNF-α) via tumour necrosis factor receptor 1 (TNFR1) and tumour necrosis factor receptor 2 (TNFR2) (Brockhaus et al., 1990); TNFR1 is primarily associated with inflammation and apoptosis (Fischer et al., 2015). Binding of TNF-α to TNFR1 activates the IκB kinase (IKK), leading to IκB phosphorylation, resulting in IκB ubiquitination and degradation, which allows the translocation of NF-κB from the cytosol to the nucleus (Karin, 1999; Traenckner et al., 1995). Akt phosphorylation has also been shown to be required in NF-κB activation (Ozes et al., 1999).

NF-κB activation then triggers many cellular processes, including inflammation and apoptosis. NF-κB translocation results in transcriptional regulation of a wide range of pro-inflammatory genes, including VCAM-1 and ICAM-1.

Binding of TNF-α to TNFR1 also induces apoptotic signalling: this activation results in the release of the silencer of death domain (SODD) protein and the recruitment of intracellular 'death signalling inducing signalling complex' (DISC) proteins (including TNFR-associated death domain protein (TRADD), Fas associated protein with death domain (FADD) and the TNFR-associated factor 1 (TRAF1)). The formation of this complex creates a scaffold which then recruits pro-caspase-8. Proteolytic cleavage of pro-caspase-8 releases an active form of caspase-8, which then enzymatically cleaves caspase-3 into an active enzyme. The activation of caspase-3 then causes apoptotic cell death by targeting a latent deoxyribonuclease (DNAse) that degrades genomic deoxyribonucleic acid (DNA) (Sedger and Mcdermott, 2014).

1.7 Regulation of NF-κB pathway by TNFR1 shedding

TNFR1 shedding is a mechanism which involves irreversible release of TNFR1 from the cell membrane that generates soluble TNR1. The mechanism plays a critical role in the regulation of NF-κB activation. TNFR1 shedding reduces the number of signal competent receptors on cell membranes and results in attenuated NF-κB activation (Fischer et al., 2015). On the other hand, shed TNFR1, or soluble TNFR1 (sTNFR1), acts as intrinsic TNF-α inhibitor in the circulation (Giai et al., 2013). Mutated non-cleavable TNFR1 in knock-in mice results in inflammatory and autoimmune disorders (Xanthoulea et al.,

2004). Patients with a rare genetic disease—TNF receptor-associated periodic syndrome (TRAPS) exhibit non-cleavable TNFR1; this is partially responsible for their prolonged and unprovoked episodes of fever and inflammation of multiple organs (McDermott et al., 1999).

ADAM17, also commonly known as TNF-α converting enzyme (TACE), is the most studied enzyme that proteolytically cleaves the extracellular domain of membrane TNFR1 into the extracellular space (Moss and Minond, 2017). In ECs, however, soluble full-length 55-kDa TNFR1 is released into the extracellular space in exosome-like vesicles (Hawari et al., 2004); this process also requires ADAM17.

In addition to ADAM17, ADAM10 has also been recently found to play a role in TNFR1 shedding (Yang et al., 2015, 2017). For instance, Epigallocatechin-3-gallate (EGCG), a catechin that is abundant in green tea, causes ADAM10-dependent shedding of TNFR1: depletion of ADAM10 in cells prevented TNFR1 shedding induced by EGCG (Yang et al., 2016).

1.8 Endothelial-monocyte interactions in atherosclerosis

Monocyte recruitment to ECs is an important hallmark of atherosclerosis. Healthy ECs in the physiological state do not bind monocytes while endothelial activation triggers a tightly regulated monocyte recruitment cascade.

Activated ECs express P-, E-selectin, VCAM-1 and ICAM-1. Selectins mediate the initial capture and rolling of monocytes from the circulation to the endothelium, which is facilitated by the expression of P-selectin glycoprotein

ligand-1 (PSGL-1) on all monocytes (McEver, 2002). Blocking P-selectin on ECs or PSGL-1 on leukocyte impairs the capture and rolling of leukocyte on ECs (Ramos et al., 1999). Genetic deletion of P-selectin, E-selectin, or ICAM-1 in apolipoprotein E (ApoE) knockout mice significantly reduced atherosclerotic lesions formation (Collins et al., 2000; Bourdillon et al., 2000).

VCAM-1 expressed on ECs then binds to Integrin $\alpha 4\beta 1$ (VLA-4) on monocytes to facilitate slow rolling and firm adhesion of monocytes on ECs. Blocking VLA-4 or VCAM-1 inhibited the slow rolling and firm adhesion of monocytes in ECs (Huo et al., 2000, 2001). VCAM-1 deficiency in mice significantly reduced lesion formation, suggest that it plays a key role in initiating atherogenesis (Cybulsky et al., 2001).

Firm adhesion is followed by monocyte spreading and crawling to identify preferred sites for transmigration (Wong et al., 2010). Crawling is mediated by lymphocyte function-associated antigen-1 (LFA-1), macrophage-1 antigen (Mac1), ICAM-1 and Intercellular adhesion molecule 2 (ICAM-2); blocking these molecules was shown to disrupt monocyte locomotion on endothelium (Schenkel et al., 2004). Finally, monocytes polarise and transmigrate through the endothelial junctions via PECAM-1 and junctional adhesion molecules (JAM) (Ostermann et al., 2002; Muller et al., 1993). The monocyte adhesion cascade is summarised and illustrated in Figure 1.4.

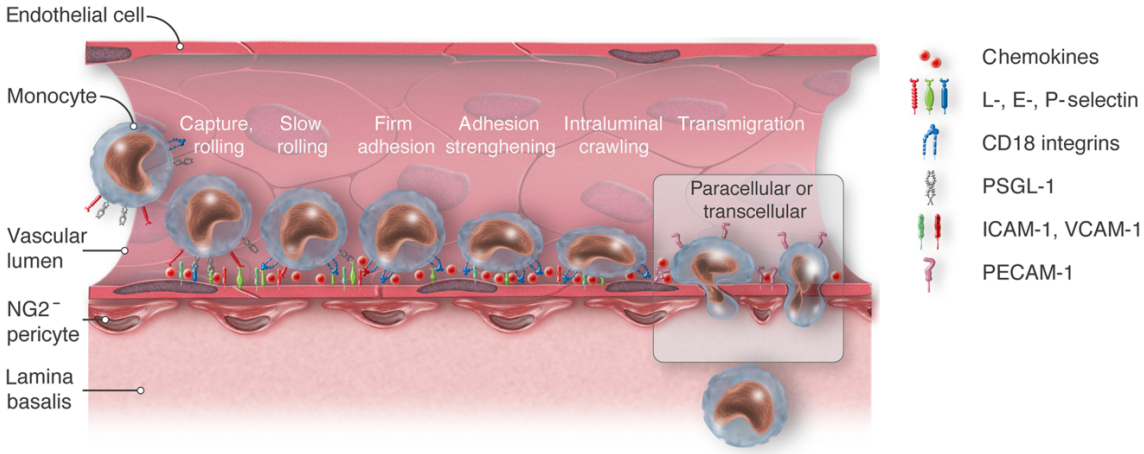

Figure 1.4: Monocyte adhesion cascade. A sequential multistep cascade of monocyte capture, slow rolling, firm adhesion, crawling, and transmigration. Reprinted with permission from Oxford University Press: Cardiovascular Research (Gerhardt and Ley, 2015).

1.9 Use of the swirling-well system in the study of endothelial activation

The most commonly used devices for shearing cells include the cone-and-plate viscometer and parallel-plate flow chamber (Schnittler et al., 1993; Levesque and Nerem, 1985). Many studies have employed these devices to apply steady laminar, oscillatory, and pulsatile flow; but only uniaxial and spatially uniform flow can be applied. Several methods have been developed to produce more complex flow, including flow chambers with tapered (Baeriswyl et al., 2019), branching geometries (Moonen et al., 2015), or with a backward-facing step (Haidekker et al., 2001; Nagel et al., 1999; Chiu et al., 2003). Tissue-engineered 3-dimensional artery models (Robert et al., 2013) and microfluidic chip models (Venugopal Menon et al., 2018) have also been developed to mimic the complex geometry and flow in blood vessels. However, these devices are either complicated to set up or do not permit multidirectional flow with cyclical

changes.

An alternative method is to culture ECs in multi-well plates on an orbital shaker. The orbital shaker method, also known as the swirling-well system, is capable of inducing a complex flow environment. Orbital motion causes the medium in a well plate to swirl, which results in the variation in WSS from the centre to the edge of a well. The swirling-well system has attracted increasing attention because this method allows high throughput and chronic exposure of the ECs to shear.

1.9.1 Flow characterisation

Flow behaviour in a swirling-well system is complex, hence a comprehensive characterisation is required to understand the WSS values at the base of the well.

Simplistic analytical approaches (Ley et al., 1989; Kraiss et al., 2000) ignore wall effects and medium volume and estimate WSS values that differ by one order of magnitude to those obtained by more involved numerical solutions (Salek et al., 2011; Dardik et al., 2005). In addition, the analytical equation assumed that the majority of cells in a swirling well experienced near maximal WSS; however, this is not true.

Instead, computational fluid dynamics (CFD) can be used to solve the governing fluid flows numerically. CFD provides a higher accuracy than the analytic method because it accounts for the spatial and temporal variation of WSS in a swirling-well (Alpresa et al., 2018).

CFD simulations performed by multiple groups have successfully captured the free surface of the swirling medium and shown that the maximum medium

height is located at the edge of the swirling well (Salek et al., 2011; Alpresa et al., 2018; Thomas et al., 2011; Berson et al., 2008). WSS magnitudes remain relatively constant over time in the centre, but fluctuate at the edge of the well (Thomas et al., 2011; Ghim et al., 2017; Chakraborty et al., 2012). Time average WSS magnitude increases with radial distance from the centre of the well, and then drops to zero at the wall because of the no-slip condition (Salek et al., 2011; Thomas et al., 2011; Berson et al., 2008). WSS vectors in the centre rotate at a constant rate, suggesting a multidirectional flow behaviour, and the multi-directionality decreases towards the edge of the well (Chakraborty et al., 2012; Ghim et al., 2017). Ghim et al. (2017) have computed the two metrics that measure the multi-directionality: OSI and transWSS. Both metrics decrease with increasing radial distance from the well centre. In summary, the centre and edge of a swirling well experience low magnitude multidirectional flow, and high magnitude uniaxial flow, respectively.

1.9.2 Properties of endothelial cells sheared using the swirling-well system

Despite exhibiting a rich flow environment, the swirling-well system was used by some studies simply to compare the effect of flow with no flow in static controls, without considering WSS variation within the well. For example, compared with the static control, flow induced by the swirling-well system has been shown to reduce granulocyte and monocyte adhesion to ECs (Ley et al., 1989; Tsao et al., 1995) and E-selectin expression (Kraiss et al., 2003). Transforming growth factor-beta 3 (TGF-β3) signalling, KLF2, and NO production were induced by flow in the swirling-well system (Walshe et al., 2013; Tsao et al., 1995). Warboys et al. (2010) adopted the same model, by incorporating Transwell® filter inserts within the well, to compare the effect of flow (and its

duration) with no flow on endothelial permeability.

WSS variation within the swirling-well system can be harnessed to investigate the effect of different flows on ECs. Low magnitude multidirectional flow in the centre and high magnitude uniaxial flow at the edge, respectively, are putatively atherogenic and atheroprotective flow profiles. Most studies that employed the system compared ECs properties in the centre and the edge of the well.

ECs at the edge of the swirling-well system are elongated and aligned, whereas those in the centre exhibit cobblestone morphology with no alignment (Chakraborty et al., 2012; Dardik et al., 2005; Chakraborty et al., 2016). ECs at the edge are also stiffer than those in the centre (Potter et al., 2012).

Flow in the centre was shown to induce endothelial senescence (Dardik et al., 2005; Warboys et al., 2014) via the p53-p21-dependent pathway (Warboys et al., 2014), which is accompanied by higher rates of proliferation (Dardik et al., 2005; Chakraborty et al., 2012). On the other hand, the expression of Kruppel-like factor 4 (KLF4) and eNOS, both of which are atheroprotective genes, is higher at the edge (Warboys et al., 2014; Filipovic et al., 2016).

Flow in the centre of the swirling well can induce endothelial activation; ECs in the centre have significantly higher VCAM-1 (Mahmoud et al., 2016), ICAM-1(Dardik et al., 2005; Chakraborty et al., 2016; Mahmoud et al., 2016), E-selectin (Chakraborty et al., 2016; Warboys et al., 2014), and Interleukin 6 (IL-6) (Chakraborty et al., 2016) expression than those at the edge, and the same flow also triggers NF-κB activation (Feng et al., 2017). Transendothelial transport of macromolecules has also been shown to be higher in the centre of the well, and decreases gradually towards the edge (Ghim et al., 2017).

1.9.3 Pros and cons of the swirling-well system

As discussed, the complex and rich flow environment in the swirling-well system makes this method an attractive *in vitro* method to study the mechanobiology of EC as it is possible to compare the effects of atherogenic and atheroprotective flow in a single well (Warboys et al., 2019).

The swirling-well system requires nothing more than standard multi-well plates and an orbital shaker, hence it is cheap to use and easy to set up. It is also a high-throughput system because multiple multi-well plates can be stacked on the orbiting platform. The use of standard cell culture plasticware means that chronic shear stress can be applied with minimal risk of contamination; Warboys et al. (2010) have used this system to apply shear stress on ECs for up to 9 days.

Compared with a flow chamber or a microfluidic chip, the swirling-well system only requires a small volume of culture media without large fluid reservoirs. Hence, only minimal amounts of recombinant protein, inhibitors, and drugs are required to investigate their effects on ECs in a flow environment.

However, the swirling-well system does have some drawbacks. Firstly, it is challenging to harvest cells for gene expression and protein analysis accurately from a specific region in the well. This limitation can be overcome by measuring cell phenotype with spatially-resolved microscopy techniques (Ghim et al., 2017). Secondly, ECs release soluble mediators (Sage et al., 1981; Tunica et al., 2009; Griffoni et al., 2011) and this process is shear-dependent (Burghoff and Schrader, 2011). Such mediators are mixed by the swirling medium and affect cells everywhere in the well, thus masking the true effect of a specific shear on ECs behaviour at one location in the well. Studies have shown that the effect

of this type accounts for the apparently identical influence of different shear profiles on transcellular transport of large particles (Ghim et al., 2017) and baseline proliferation in cells (Dardik et al., 2005).

1.10 Leucine-rich α-2-glycoprotein 1 (LRG1)

Leucine-rich α-2-glycoprotein 1 (LRG1) is a member of leucine-rich repeat (LRR) family of proteins (Ng et al., 2011), many of which are abundant in various organism ranging from bacteria to man and are involved in various crucial functions such as cell adhesion, development, DNA repair, transcription and signal transduction (Kobe and Deisenhofer, 1995). LRG1 is a secreted glycoprotein and is highly expressed in the liver and granuloytes (Uhlén et al., 2015).

1.10.1 LRG1 in human disease

LRG1 concentration in human serum or plasma is increased in different type of cancers (Sandanayake et al., 2011; Ivancic et al., 2020; Shinozaki et al., 2018; Zhao et al., 2015; Liu et al., 2012; Wu et al., 2013; Kakisaka et al., 2007), inflammatory diseases (Serada et al., 2010; Kimura et al., 2017; Rainer et al., 2017), cardiovascular diseases (Xuan et al., 2019; Pek et al., 2015; Watson et al., 2011), infectious diseases (Hashida et al., 2017; Choi et al., 2014; Fish-Low et al., 2019), and diabetic kidney disease (Hong et al., 2019; Liu et al., 2017). Differential concentrations of LRG1 in urine (Yap et al., 2019; Jiang et al., 2020; Chokchaichamnankit et al., 2019), cerebrospinal fluid (Chong et al., 2018; Chen et al., 2016; Li et al., 2007), and peritoneal fluid (Ferrero et al., 2009) have also been reported in various diseases. Many of these studies have proposed using

LRG1 as a biomarker to diagnose diseases due to its outstanding performance in discriminating diseased groups from healthy controls.

LRG1 expression is a predictive marker of poor survival in cancer (Zhang et al., 2018; Sun et al., 2017; Walker et al., 2015; Xie et al., 2019) and chronic kidney disease (Glorieux et al., 2015). The protein is also capable of predicting the efficacy of chemoradiotherapy in esophageal cancer (Nambu et al., 2019) and shunt surgery in idiopathic normal pressure hydrocephalus patients (Nakajima et al., 2011). High expression of LRG1 is also associated with high mortality in elderly individuals (Orwoll et al., 2018).

Table 1.1 summarises the reported expression of LRG1 in various human diseases.

Diseases	**Samples**	**Reported expression of LRG1 (Compared with healthy control, unless otherwise stated)**	**References**
Acute appendicitis	Plasma, blood cells	Upregulated	Rainer et al., 2017
Acute appendicitis (paediatric)	Urine	Upregulated	Yap et al., 2019 Salö et al., 2016 Kentsis et al., 2012 Kentsis et al., 2010
Acute kidney injury induced by cisplatin	Urine	Upregulated	Jiang et al., 2020
Acute lymphoblastic leukemia	Serum	Upregulated	Cavalcante et al., 2016
Amyotrophic lateral sclerosis	Cerebrospinal fluid	Downregulated	Chen et al., 2016
Antineutrophil cytoplasmic antibody (ANCA)-associated vasculitides	Serum	Upregulated	Ishizaki et al., 2017
Asthma	Sputum	Upregulated	Honda et al., 2016
Bacterial meningitis	Cerebrospinal fluid	Upregulated, compared with febrile patients	Chong et al., 2018
Biliary tract cancer	Serum	Upregulated	Sandanayake et al., 2011
Cervical cancer	Urine	Upregulated	Chokchaichamnankit et al., 2019
Chronic kidney disease	Plasma	Upregulated, high expression is a predictive marker of poor survival outcome	Glorieux et al., 2015

Colorectal Cancer	Serum	Upregulated	Ivancic et al., 2020 Shinozaki et al., 2018
	Tissue, plasma	Upregulated, high expression is a predictive marker of poor survival outcome	Zhang et al., 2018
	Plasma, tissue	Upregulated	Zhou et al., 2017
	Tissue	Upregulated	Zhang et al., 2016b
	Plasma	Upregulated	Choi et al., 2013 Ladd et al., 2012
	Tissue, plasma	Associated with microvessel density, and high expression is a predictive marker of poor survival outcome	Sun et al., 2017
Coronary artery dilatation caused by Kawasaki disease	Serum	Upregulated	Zhang et al., 2016a
Diabetic kidney disease	Tissue, plasma	Upregulation of LRG1 mRNA in Glomeruli EC, high expression is a predictive marker of worse renal outcome	Hong et al., 2019
	Plasma	Upregulated, high expression is a predictive marker of albuminuria and chronic kidney disease	Liu et al., 2017
Early-onset myocardial infarction	Serum	Upregulated	Xuan et al., 2019
Esophageal cancer-response to pre-operative chemoradiotherapy (PCRT)	Serum	Downregulated in responder group (compared with non-responder group)	Nambu et al., 2019

Esophageal squamous cell carcinoma	Plasma	Upregulated	Zhao et al., 2015
Familial hypercholesterolemia (FH)	Plasma	Downregulated in FH patients with coronary artery disease (compared with FH patients with no coronary artery disease)	Bos et al., 2017
Galactosemia	Urine	Upregulated	Staubach et al., 2016
Glioblastoma	Plasma	Upregulated	Miyauchi et al., 2018
H1N1 infection	Plasma	Upregulated	Choi et al., 2014
Head and neck squamous cell carcinoma	Tissue	Downregulated	Wang et al., 2017a
Heart failure	Serum	Upregulated	Watson et al., 2011
Hepatocellular carcinoma	Tissue	Downregulated (compared with periphery non-cancerous tissue)	Zhang et al., 2015
		Upregulated (compared with periphery non-cancerous tissue)	Chaerkady et al., 2008
	Serum	Upregulated	Sarvari et al., 2014
Hypertrophic scar	Skin/Dermis	Upregulated	Gao et al., 2019
Idiopathic nephrotic syndrome	Urine	Upregulated	Suresh et al., 2016
Idiopathic normal pressure hydrocephalus (iNPH)	Cerebrospinal fluid	Upregulated	Li et al., 2006 Li et al., 2007
		Upregulated in shunt responsive group, compared with nonresponsive group. High expression is a predictive marker of shunting outcome in iNPH patients	Nakajima et al., 2011

Idiopathic pulmonary arterial hypertension	Serum	Upregulated	Zhang et al., 2009
Ischemic-dilated cardiomyopathy	Tissue	Downregulated	Liu et al., 2019
Kawasaki disease	Serum	Upregulated	Kimura et al., 2017
Leptospirosis	Plasma	Upregulated	Fish-Low et al., 2019
Liver fibrosis in Hepatitis C virus (HCV) infected patients	Serum	Downregulated in severe fibrosis, compared with non-fibrosis	Cheung et al., 2009
Mortality risk	Serum	High expression is a predictive marker of 5-year mortality risk	Orwoll et al., 2018
Musculoskeletal disorder	Plasma	Upregulated	Ghafouri et al., 2016
Myelodysplastic syndrome	Plasma	Upregulated in advanced disease groups, compared with low-risk disease group	Majek et al., 2015
		Upregulated	Majek et al., 2014
Non-small cell lung cancer	Plasma	High expression is a predictive marker of poor survival	Walker et al., 2015
	Urinal exosomes, lung tissue	Upregulated	Li et al., 2011
	Serum, tissue	Upregulated, compared with febrile patients	Liu et al., 2012
Non-muscle invasive bladder cancer	Urine, tissue	Upregulated	Lindén et al., 2012
Oral squamous cell carcinoma	Plasma	Upregulated	Tung et al., 2013

Ovarian cancer	Serum	Upregulated	Wu et al., 2013 Wu et al., 2015 Boylan et al., 2010
	Urine	High abundance of LRG1 peptides in diseased samples, and near absence in healthy control	Smith et al., 2014
	Urine	Upregulated	Mu et al., 2013
	Serum, tissue	Upregulated	Andersen et al., 2010
Pancreatic cancer	Plasma	Upregulated	Kakisaka et al., 2007
Pancreatic ductal adenocarcinoma	Tissue	Upregulated, high expression is a predictive marker of poor survival and a late tumour stage	Xie et al., 2019
	Plasma	Upregulated	Park et al., 2017
Peripheral arterial disease (PAD)	Plasma	Upregulated (compared with type 2 diabetic patients without PAD)	Pek et al., 2015
Post-stroke depression	Plasma	Downregulated (compared with stroke patients without depression)	Zhan et al., 2014
Proliferative diabetic retinopathy	Plasma	Upregulated	Zhang et al., 2019 Hase et al., 2017
Psoriasis	Serum	Upregulated	Nakajima et al., 2017
Refractory anemia with excess blasts subtype 1	Plasma	Upregulated	Májek et al., 2012
Retinoblastomas	Tissue	Upregulated	Amer et al., 2018
Rheumatoid arthritis	Serum	Upregulated	Ha et al., 2014
Rheumatoid arthritis, Crohn's disease	Serum	Upregulated (compared with healthy control), and downregulated after anti-TNF therapy	Serada et al., 2010

Sepsis	Hemofilter adsorbates, serum	Upregulated	Hashida et al., 2017
Stress urinary incontinence	Urine	Upregulated	Koch et al., 2016
Traumatic brain injury	Serum	Upregulated	Anada et al., 2018
Ulcerative colitis	Serum	Upregulated, correlated with endoscopic disease activity and mucosal healing	Shinzaki et al., 2017
		Upregulated	Serada et al., 2012
Uterine leiomyomas	Plasma	Upregulated	Lin et al., 2012
	Peritoneal fluid	Upregulated	Ferrero et al., 2009

Table 1.1: Reported expression of LRG1 in human disease.

1.10.2 Functions of LRG1

Despite overwhelming evidence for the involvement of LRG1 in human diseases, the role of LRG1 in these diseases is not fully understood. Only a few studies have shed light on the mechanisms of LRG1 action in pathological processes. LRG1 activates runt-related transcription factor 1 (RUNX1) (Zhou et al., 2017), Hypoxia-inducible factor 1 subunit alpha (HIF-1α) (Zhang et al., 2016a), the TGF-β1-SMAD2/3 pathway (Zhong et al., 2015), and the p38/MAPK pathway (Xie et al., 2019) to promote cancer cell proliferation, migration, invasion, and epithelial-mesenchymal transition (EMT). LRG1 modulates fibrosis through the regulation of the TGF-β pathway (Honda et al., 2017; Liu, 2019; Sng et al., 2018).

One of the most comprehensive investigations of LRG1 was conducted by Wang

et al. (2013b); they characterised the molecular mechanisms of LRG and its interaction with TGF-β pathway in angiogenesis. Recombinant LRG1 promotes angiogenesis. Wang et al. (2013b) suggested that the complex interaction of LRG1 with various receptors of the TGF-β pathway, namely TGF-β Receptor II (TβRII), Activin receptor-like kinase 1 (ALK1), TGFβ receptor 1 (ALK5), and Endoglin (ENG), is involved in tuning the stoichiometry of the TGF-β receptors to promote angiogenesis in endothelial cells. The angiogenic switch is activated via the TβRII-ALK1-SMAD1/5/8 pathway by binding of LRG1 to the accessory receptor ENG in the presence of TGF-β1 to the complex of TβRII /ALK1 receptors. This pathway can only be activated in the presence of ENG. On the other hand, LRG1 and TGF-β1 binds to the TβRII /ALK5 complex to activate the ALK5-SMAD2/3—an anti-angiogenic pathway; the ALK5-SMAD 2/3 pathway is activated only in the absence of ENG as ENG attenuates TβRII/ALK5/LRG1 complex formation in the presence of TGF-β1. The proposed working model of LRG1 in endothelial cell signalling is shown in Figure 1.5.

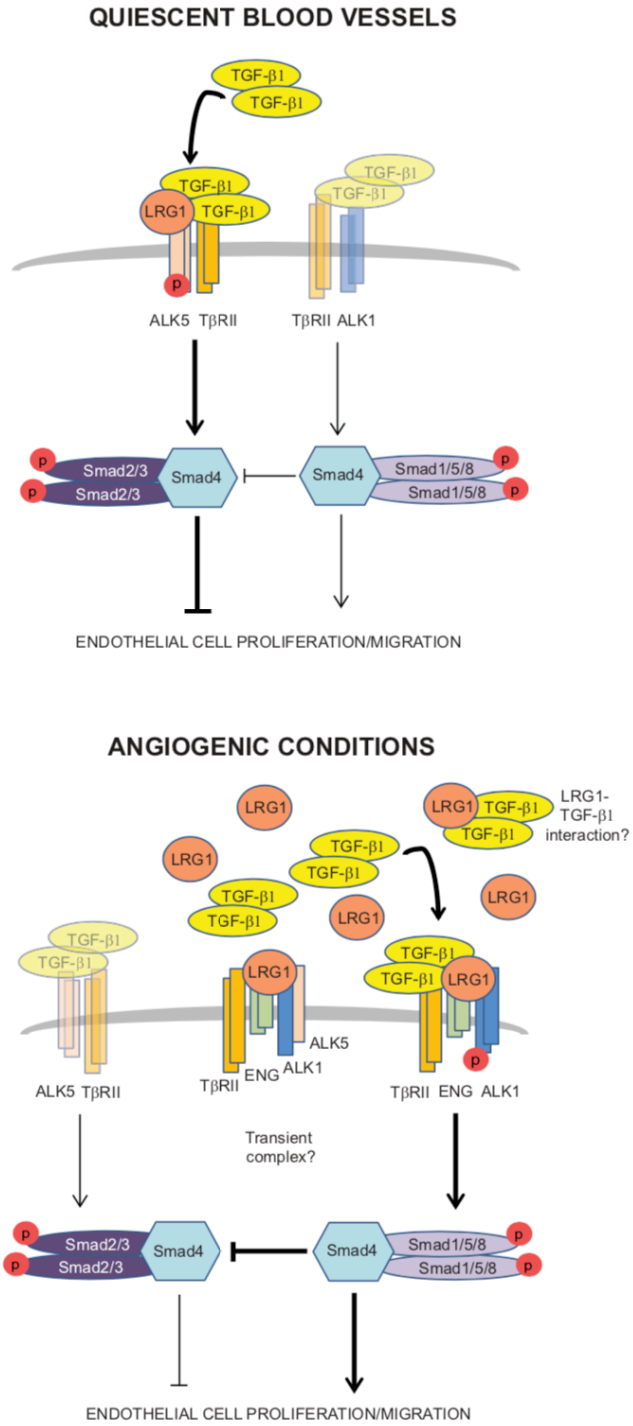

Figure 1.5: Proposed working model of LRG1-mediated TGF-β signalling in endothelial cells. In the quiescent state, LRG1 and TGF-β1 signalling in ECs is predominantly through the TβRII-ALK5-SMAD2/3 pathway, which maintains vascular homeostasis. Under pathological conditions, production of LRG1 and ENG is increased. LRG1 interacts with TGF-β1 to facilitate ENG/TβRII/ALK1 receptor complex formation, resulting in ALK1-SMAD1/5/8 pathway activation. Reprinted with permission from Macmillan Publishers Ltd: Nature (Wang et al., 2013b).

LRG1 is intimately linked with inflammation and endothelial activation. LRG1 binds to cytochrome c (Cummings et al., 2006), and this process protects lymphocytes against toxic effects of exogenous cytochrome c (Codina et al., 2010). The protein also promotes T helper cell differentiation by upregulating IL-6 receptor expression via TGF-β-SMAD2 activation (Urushima et al., 2017). Neutrophil granulocytes undergoing differentiation synthesise and release LRG1 that antagonises the inhibitory effect of TGF-β1 on colony growth of human lymphohematopoietic stem cells and myeloid progenitors (Druhan et al., 2017). Pro-inflammatory cytokines such as Interleukin-1β (IL-1β) and IL-6 upregulate LRG1 expression in epithelial cells (Lee et al., 2018) and liver cancer cells (Shirai et al., 2009), respectively. TNF-α upregulates endothelial LRG1 expression via p38 and NF-κB activation (Wang et al., 2017b).

Table 1.2 summarises the functions and mechanisms of LRG1 in various cell types.

Cell Type	Functions of LRG1	Mechanisms/Signalling	References
Bone marrow mesenchymal stem cell (MSC)	Promotes MSC migration	via TNF-α-induced LRG1 expression in endothelial cells that promotes MSC recruitment	Wang et al., 2017b
Colon cancer cell	Promotes proliferation and suppressed apoptosis	Through RUNX1 activation	Zhou et al., 2017
	Promotes EMT, migration, and invasion	Through HIF-1α activation	Zhang et al., 2016a
Endothelial cell	Promotes angiogenesis	Binds directly to endoglin in the presence of TGF-β1 and promotes SMAD1/5/8 signalling pathway	Wang et al., 2013b
		LRG1 is upregulated by TNF-α through p38 and NF-κB pathway	Wang et al., 2017b
Fibroblast	Promotes lung fibrosis	Modulates TGF-β-induced SMAD2 phosphorylation (independent of endoglin)	Honda et al., 2017
	Inhibits fibrosis by reduced cardiac fibroblast activation	LRG1 is regulated by TGF-β1 via SMRT. Competes with TGF-β1 for receptor binding.	Liu, 2019
	Rescues the fibrotic phenotype of PPARβ/δ-deficient fibroblast	LRG1 is regulated by PPARβ/δ. Attenuates the expression of pSMAD3 and α-SMA induced by TGF-β1	Sng et al., 2018
	Promotes proliferation, migration, angiogenesis	LRG1 is upregulated by mechanical stretch through FAK/ERK/ELK1 pathway	Gao et al., 2019
Glomeruli endothelial cell	Promotes angiogenesis	Through ALK1-SMAD1/5/8 activation	Hong et al., 2019
Glioma cell	Promotes proliferation, migration, and invasion	Activates TGF-β1 and SMAD2/3	Zhong et al., 2015
Hepatocellular carcinoma cell	Inhibits migration and invasion	-	Zhang et al., 2015

Lymphocyte	Protects lymphocytes against toxic effects of exogenous cytochrome c	Binds to cytochrome c	Codina et al., 2010
Neuroblastoma cell lines	Promotes invasion and migration	LRG1 is downregulated by MiRNA-335	Lynch et al., 2012
Neutrophils	Antagonises the inhibitory effects of TGF-β1 on colony growth of human CD34+ cells and myeloid progenitors	LRG1 is synthesised and released during neutrophil granulocyte differentiation. Binds cytochrome c	Druhan et al., 2017
Pancreatic ductal adenocarcinoma cell line	Promotes viability, proliferation, migration, and invasion	Interacts with EGFR and activates p38/MAPK pathway	Xie et al., 2019
T helper cell	Promotes T helper cell differentiation	Increases IL-6 receptor expression via TGF-β-SMAD2 activation	Urushima et al., 2017

Table 1.2: Functions and mechanisms of LRG1.

1.10.3 Mechanical activation of LRG1

Two studies have shown that mechanical stimulation leads to LRG1 activation. Mechanical stretch induces LRG1 expression in human dermal fibroblast; this is a result of focal adhesion kinase (FAK) sensitisation, which leads to extracellular signal–regulated kinases (ERK) translocation into the nucleus and E26 transformation-specific like-1 protein (ELK1) phosphorylation, and results in its binding to the LRG1 promoter region (Gao et al., 2019). ECs exposed to pathologically-elevated unidirectional shear stress of 75 dynes/cm^2 have higher LRG1 gene expression than those exposed to the atheroprotective unidirectional shear stress of 15 dynes/cm^2 (GEO DataSet GDS3868, White

et al., 2011).

1.11 Research aims

The overarching aim of this thesis is to further our understanding of the role and the interaction of low magnitude multidirectional flow (LMMF) and LRG1 in TNF-α- and LMMF-induced endothelial activation. The thesis builds on previous work that shows atherogenic effects of LMMF and novel roles of LRG1 in human pathophysiology.

The swirling-well system is used to induce multidirectional flow on ECs, but the flow characteristics of swirling 6-well plates, used in this study, have not been characterised under the specific parameters used in our laboratory. The first research aim is therefore to employ CFD simulation to characterise the flow in a swirling 6-well plate on our orbital shaker. The second research aim is to improve the swirling-well system by eliminating the general mixing of soluble mediators whose secretion by ECs is shear-dependent in the swirling-well system. This can be achieved by using surface modification to permit ECs growth only in specific regions of the well. It is hypothesised that the surface modification can successfully eliminate the general mixing of secreted soluble mediators, and thus will lead to new understandings of endothelial responses to shear stress.

LRG1 is intimately linked with inflammation and endothelial activation, and is upregulated in many inflammatory and cardiovascular diseases. However, its role in endothelial activation and in these diseases is not known. It is postulated that the upregulation of LRG1 in pathogenesis has a direct role in the regulation of endothelial activation. Hence, the third aim is to decipher

the role of LRG1 in TNF-α- and LMMF-induced endothelial activation. The molecular mechanism of LRG1 in the regulation of endothelial activation is also investigated. Finally, the clinical relevance of LRG1 in atherosclerotic diseases will be explored.

These aims are summarised as follow:

1. To characterise the flow behaviour and WSS metrics in a swirling 6-well;
2. To develop a coating method that restricts ECs growth in 6-well plates to eliminate the effect of the general mixing of soluble mediators secreted by ECs exposed to different shear profiles;
3. To investigate the effect of different flows generated by swirling 6-well plates on endothelial activation in full and segmented wells;
4. To characterise the expression of LRG1 in ECs activated by TNF-α and LMMF, and to investigate its functional role;
5. To decipher the molecular and signalling mechanisms of LRG1 in endothelial activation;
6. To evaluate the clinical relevance of LRG1 in atherosclerotic diseases.

1.12 Thesis outline

Following this introduction is a series of chapters addressing the research aims listed above. Chapter 2 presents the CFD simulation of a swirling 6-well plate. Qualitative data on ECs morphology is also discussed. The data from Chapter 2 are used to guide the experimental design in the work presented in the subsequent chapter, Chapter 3, that describes a novel coating method to

segment EC adhesion in 6-well plates. The effects of different shear stress on endothelial activation in full and segmented wells are discussed.

Chapter 4 describes a novel role of LRG1 in endothelial activation. The expression of LRG1 in ECs activated by TNF-α and LMMF, its functional role in monocyte-endothelial interactions, and its molecular mechanisms are also discussed. LMMF is induced using the swirling-well system discussed in Chapter 3. Chapter 5 discusses the clinical relevance of LRG1. This is examined using clinical samples of human serum and coronary artery sections from atherosclerotic patients.

Lastly, conclusions are presented in Chapter 6, with suggestions for future work.

Chapter 2

CFD simulation of a swirling 6-well plate

2.1 Background

Vascular endothelial cells (ECs) can sense the shear stress generated by the flow of blood over them and respond by altering their stiffness and morphology, regulating their interactions and communications with neighbouring cells, and activating transcription factors (Wang et al., 2013a; Tzima et al., 2005; Potter et al., 2011; Nagel et al., 1999), amongst other changes. Such responses, when coupled with the variation in wall shear stress (WSS) that occurs from site to site within vessels, can explain local differences in endothelial properties and may also account for the patchy development of diseases such as atherosclerosis (Asakura and Karino, 1990; Giddens et al., 1993; Bond et al., 2011). Their physiological and pathological importance has stimulated many studies on the effects of shear on ECs in culture.

Devices that are commonly employed for shearing cells include the cone-and-

plate viscometer and the parallel-plate flow chamber. Both devices allow cells to be exposed to steady, oscillatory and pulsatile flow (Schnittler et al., 1993; Levesque and Nerem, 1985), but the flow is uniaxial and spatially uniform. Several methods have been developed to overcome these restrictions, including flow chambers with tapered or branching geometries, or with a backward-facing step (Haidekker et al., 2001; Chiu et al., 2003; Nagel et al., 1999).

An alternative method is to culture ECs in standard petri dishes or culture plates on an orbital shaker. The orbital motion leads to variation in shear pattern from the centre to the edge of the dish or well. In addition, this technique permits a high throughput and chronic exposure of the ECs to flow, making it possible to study a wide range of ECs responses. For example, it has enabled the demonstration that chronic and acute shear stress have opposite effects on endothelial permeability to macromolecules (Warboys et al., 2010).

These more complex methods require the use of computational fluid dynamics (CFD) to characterise the spatial variation in flow. For example, in a swirling 12-well plate, CFD has been used to show that cells at the centre of the well experience multidirectional shear stress while cells closer to the edge experience a nearly uniaxial shear stress (Ghim et al., 2017). The capacity to generate multidirectional shear stress is important as recent studies have suggested that it is correlated with lesion formation *in vivo* (Mohamied et al., 2014; Peiffer et al., 2013b).

A 6-well plate was chosen for the present work instead of a 12-well plate, which has been well characterised in our lab (Alpresa, 2017; Ghim, 2016), because it has a larger surface area for sufficient cells to be harvested for protein and gene expression analysis. In addition, 6-well plate, due to its larger radius, is capable of generating higher circumferential velocity, which might result in a higher WSS magnitude. Many groups have investigated

the fluid dynamics of a swirling 6-well plate experimentally or numerically (Dardik et al., 2005; Salek et al., 2011; Filipovic et al., 2016; Velasco et al., 2016), but the specific parameters (orbital radius of 5mm, angular velocity of 150 revolutions per minute (rpm), medium height of 2mm) used in our lab have not been characterised.

This chapter will describe the swirling-well system in more detail, following the work of Ghim (2016) and Alpresa (2017), but adapted to human umbilical vein endothelial cells (HUVECs) and 6-well plates. A CFD simulation was performed to determine the shear stresses on the base of the well. The morphology of HUVECs cultured in 6-well plates and subjected to swirling flow is imaged and the qualitative data are discussed here.

2.2 Methods and Materials

2.2.1 Computational fluid dynamics

Flow simulations were carried out with StarCCM+ (version 11.02.009, CD-Adapco, USA). A single well of a 6-well plate was represented as a cylinder with height 10 mm and radius 17.4 mm. The geometry was discretised using a structured cylindrical mesh with 360,000 grid elements (Figure 2.1). To capture the boundary layers adequately, a finer element was generated at the base and walls of the cylinder.

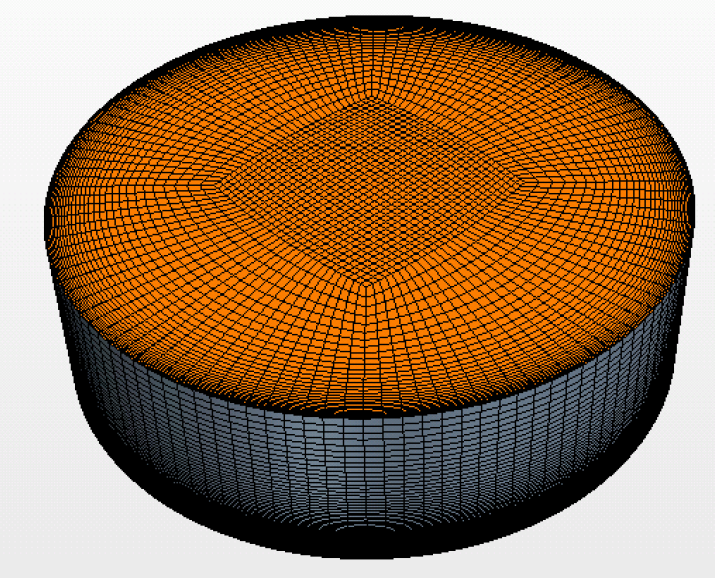

Figure 2.1: Structured cylindrical mesh with 360,000 grid elements.

The Volume of Fluid (VOF) model was used to track the free surface of the medium (Hirt and Nichols, 1981). When stationary, the medium had a height of 2 mm; the remainder of the domain was air. Both were modelled as Newtonian fluids (gas and liquid) using the continuity and unsteady incompressible Navier-Stokes equation:

$$\frac{\partial \rho_i}{\partial t} + \nabla \cdot \rho_i \boldsymbol{u}_i = 0 \tag{2.1}$$

$$\frac{\partial \boldsymbol{u}_i}{\partial t} + \boldsymbol{u}_i \cdot \nabla \boldsymbol{u}_i = -\frac{1}{\rho}\nabla p + \nu \nabla^2 \boldsymbol{u}_i \tag{2.2}$$

where the subscript i denotes the gas and liquid phase, ν and ρ are, respectively, the kinematic viscosity and density of the medium and air, t is the time variable, **u** is the velocity vector, and p is the pressure.

The medium was modelled with dynamic viscosity, and density of 0.78 $\times$ 10^3 Pa.s and 1003 kg/m^3 respectively, and the gas was modelled as an ideal gas with dynamic viscosity and density of 18.688 x $10^{-}6$ Pa.s and 1.1115 kg/m^3 respectively. A no-slip condition was imposed at all walls. The top surface of

the cylinder was defined as a pressure outlet.

The orbital motion of the well was modelled by introducing a translating gravitational force of the form:

$$[x, y, z] = [a\omega^2 cos(\omega t), a\omega^2 sin(\omega t), -9.81] \tag{2.3}$$

where a is the orbital radius of the shaker, ω is the angular velocity and t is time. The orbital shaker used in this study (POS-300, Grant Instruments) has an orbital radius of 5mm and angular velocity of 150 rpm. These parameters were simulated. The swirling-well system is illustrated in Figure 2.2.

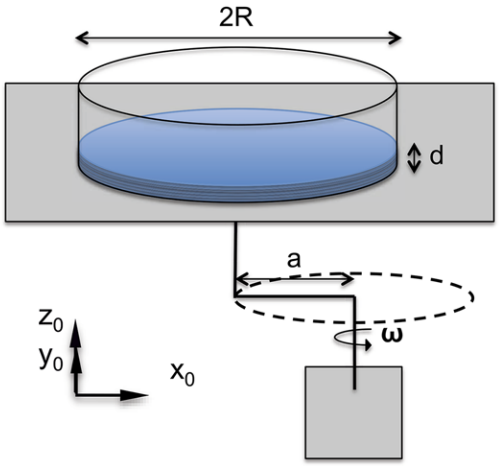

Figure 2.2: Schematic diagram of the orbital shaker model. The orbital motion of the 6-well plate was simulated with a as the orbital radius and ω as the angular velocity of the shaker. Medium height when stationary is illustrated as d. Reprinted with permission from AIP Publishing: Physics of Fluids (Alpresa et al., 2018)

.

The influence of surface tension forces in a swirling 6-well is examined by Bond (Bo) and Weber (We) numbers, that measure the ratio of gravitational forces and fluid's inertia, respectively, to the surface tension forces (Salek et al., 2011):

$$Bo = \frac{(\rho_l - \rho_g)g(2R)^2}{\sigma} \tag{2.4}$$

$$We = \frac{(\rho_l)U^2(2R)}{\sigma} \tag{2.5}$$

where ρ_l is the liquid density (1003 kg/m^3), ρ_g is the gas density (1.1115 kg/m^3), g is the gravitational acceleration (9.81 m/s^2), R is the well radius (0.0174 m), U is the characteristic velocity (estimated by ωa = 0.0786 m/s), and σ is the surface tension between the two phases (0.073 N/m). *Bo* and *We* are of the order of 100 and 10 (which is $\gg 1$), respectively, hence the surface tension was neglected in this simulation.

Time steps of 1×10^{-4} s were each iterated 5 times. Maximum WSS at the base of the well was used to assess convergence. A mesh independence study was performed using 720,000 grid elements, and no difference was observed. The method described in this section was developed and optimised by Dr Paola Alpresa (Alpresa, 2017).

2.2.2 Computation of shear metrics

MATLAB was employed to post-process to obtain the WSS acting on the base of the well, and hence cell monolayer. The instantaneous WSS vectors ($\vec{\tau_w}$) from one complete revolution (0.4 s) were used to calculate time-average WSS (TAWSS), the Oscillatory Shear Index (OSI) (Ku et al., 1985), and transverse WSS (transWSS) (Peiffer et al., 2013a), reflecting, respectively, the temporal average of the instantaneous vectors, the tendency of the instantaneous vectors to deviate from the direction of the mean vector, and the average of the components of the instantaneous vectors acting perpendicular to the mean vector:

$$TAWSS = \frac{1}{T}\int_0^T \mid \vec{\tau_w} \mid dt, where \mid \vec{\tau_w} \mid = \sqrt{\tau_x^2 + \tau_y^2 + \tau_z^2} \tag{2.6}$$

$$OSI = \frac{1}{2}\left(1 - \frac{|\int_0^T \vec{\tau_w} dt|}{\int_0^T |\vec{\tau_w}| dt}\right) \tag{2.7}$$

$$transWSS = \frac{1}{T}\int_0^T \left|\vec{\tau_w} \cdot \left(\vec{n} \times \frac{\vec{\tau}_{mean}}{|\vec{\tau}_{mean}|}\right)\right| dt \tag{2.8}$$

where T is the time taken for one revolution, τ_x, τ_y, and τ_z are the instantaneous WSS vectors in the x-, y-, and z-direction, respectively, and τ_w is the magnitude of these WSS vectors.

2.2.3 HUVECs isolation and culture

HUVECs were isolated as described in Jaffe et al. (1973) with minor modification to cords obtained from donors with uncomplicated labour at Hammersmith Hospital, UK. The setup of the isolation is illustrated in Figure 2.3. Isolation and culture of HUVECs was approved for research purposes by the Hammersmith hospital research ethics committee (ref. 06/Q0406/21).

Before isolation, the cord was gently massaged to remove residual blood in the vein. The proximal end was cannulated with a three-way tap, and the vein was washed three times by injecting 20 mL of phosphate-buffered saline (PBS) using a syringe. The distal end of the cord was then clamped before 10 mL of collagenase solution (1 mg/mL, dissolved in M199 medium (Sigma-Aldrich, UK)) was added through the tap into the vein. The cord was incubated at 37°C for 15 minutes on a tray in a humidified incubator. After the incubation, the collagenase solution was collected in a 50 mL centrifuge tube and centrifuged at 200 g for 5 minutes to obtain a pellet of cells. The cell pellet was resus-

pended in Endothelial Cell Growth Medium-2 (EGM-2) containing the EGM-2 supplement kit (Lonza, Switzerland). The cell suspension was transferred to a flask coated with 0.1% gelatin and placed in a humidified incubator at 37°C under 95% air/5% CO_2. The medium was replaced with fresh EGM-2 after 24 h, and cells were allowed to grow to confluence. HUVECs between passage 3-5 were used for experiments.

Figure 2.3: Setup of the isolation of HUVECs.

2.2.4 Application of shear stress

Once the ECs were confluent, the medium in each well was replaced with 1.9 mL of fresh medium (to achieve 2 mm medium height), and the 6-well plate was placed on the horizontal platform of an orbital shaker at 37°C in a humidified incubator under 95% air/5% CO_2 for 3 days. The platform orbited in the horizontal plane with an orbital radius of 5 mm and an angular velocity of 150 rpm. The setup of the swirling-well system is illustrated in Figure 2.4.

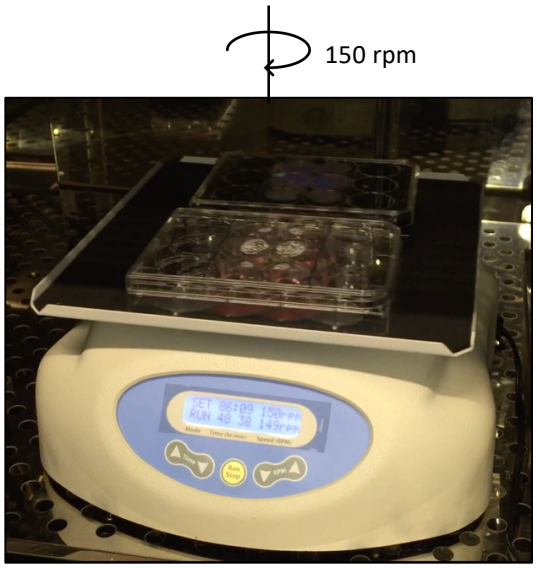

Figure 2.4: Setup of the well-plate on an orbital shaker.

2.3 Results

2.3.1 Flow field of a swirling 6-well plate

The movement of the orbital shaker platform causes the medium to swirl. This motion is captured in the CFD simulation, which showed a wave travelling around the well periodically at the rotational speed of the orbital shaker. Maximum medium height is located at the edge of the well, while the minimum height is located at the opposite side (Figure 2.5).

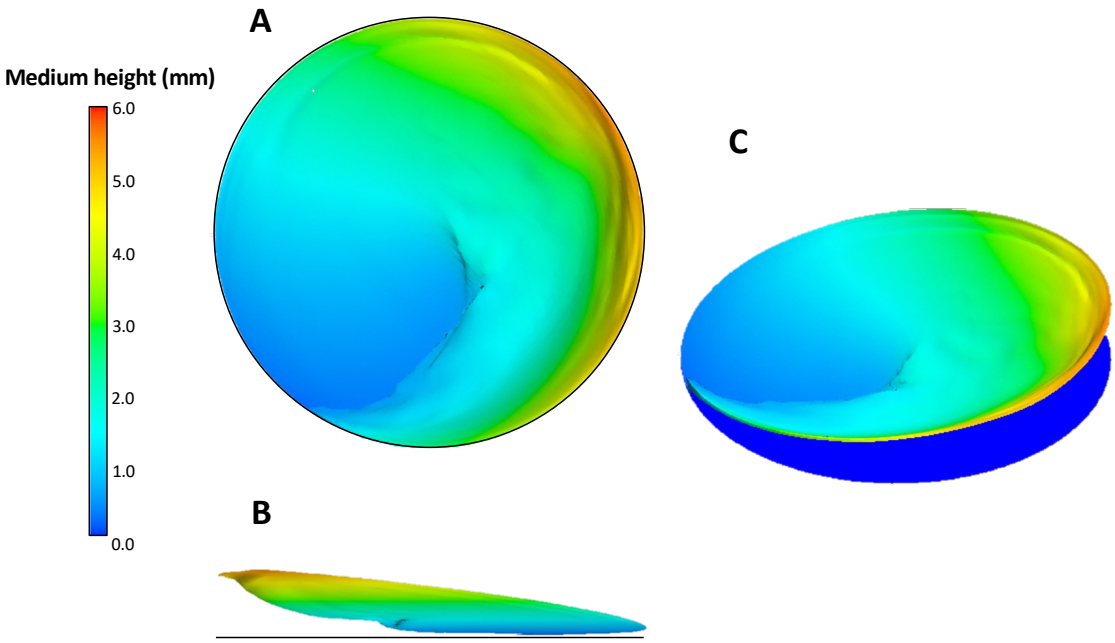

Figure 2.5: Medium height map from a simulated swirling 6-well plate. (A) Top view, (B) side view, and (C) isometric view are shown.

The velocity field, which rotates at the rotational speed of the orbital shaker, moves in synchrony with the wave of medium. Velocity vectors at the centre of the well rotated at a constant rate, resulting in a perfectly multidirectional flow behaviour; this behaviour was suppressed at the edge of the well, resulting in a nearly uniaxial flow profile. Medium travelled at the highest velocity at the edge of the well (Figure 2.6).

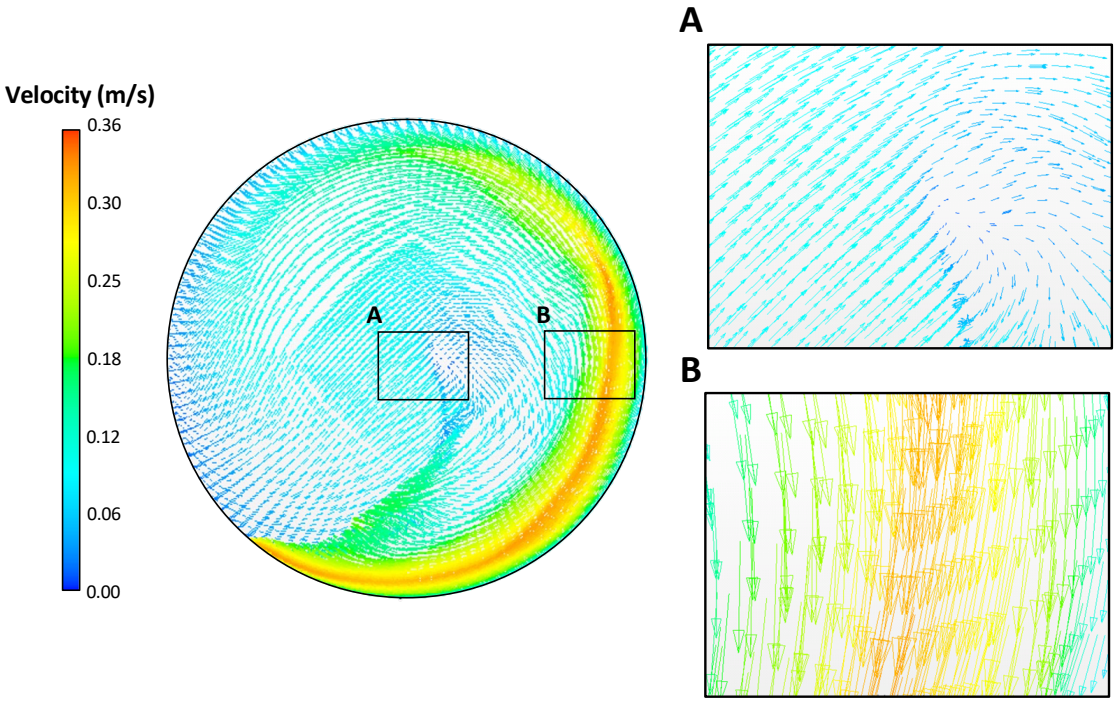

Figure 2.6: Velocity magnitude map from a simulated swirling 6-well plate. Close-up view of the (A) centre and the (B) edge of the velocity magnitude map.

2.3.2 Wall shear stress at the base of a swirling 6-well plate

The directionality of the flow is also reflected in the WSS vectors. Figure 2.7 shows a polar plot, which represents both their magnitude and direction. Each point on the curve represents the tip of an instantaneous WSS vector, with its radius as the WSS magnitude. In the central region of the well (radial distances of 0.01mm, 4.01mm, and 8.01), the direction of the WSS vectors rotated around the well at a constant rate with low magnitude, whereas the WSS vectors towards the edge of the well (radial distances of 14.01mm and 16.01mm) were mainly distributed in the second and third quadrant, suggesting uniaxial flow behaviour, with high magnitude.

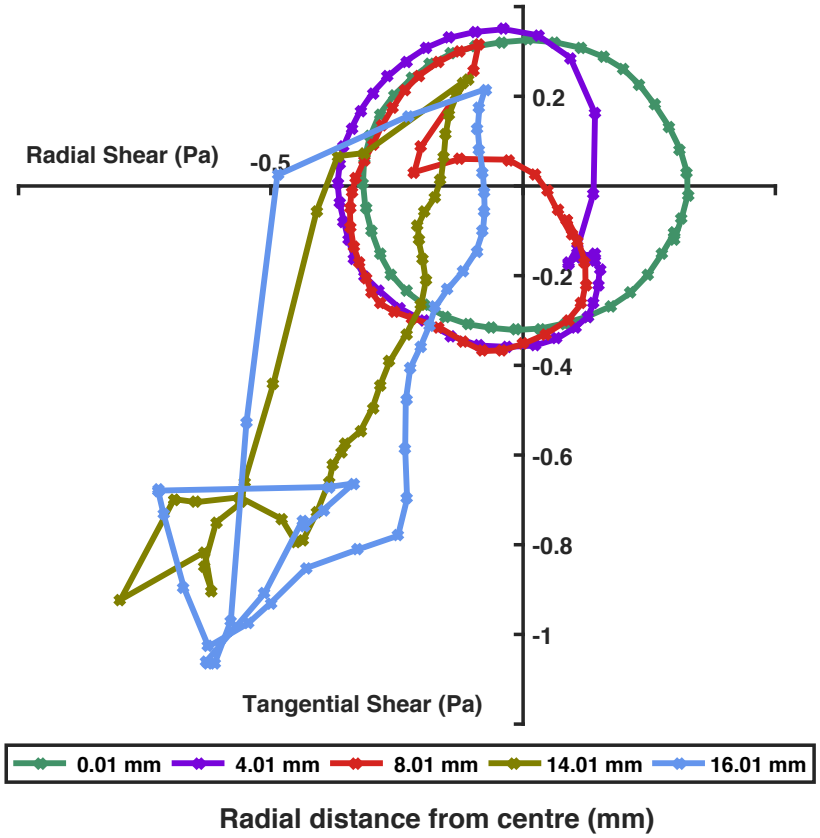

Figure 2.7: Polar plot of the magnitude and direction of instantaneous WSS vectors during one cycle. Each curve applies to one radial distance from the centre of the well. The curve represents the path travelled by the tip of the WSS vector, with its origin at 0,0. Points on the curves are spaced at 10 ms intervals.

Another way of displaying the polar plot is shown in Figure 2.8. Each instantaneous WSS vector is represented by an arrow pointing away from origin (0,0), with the length as the WSS magnitude. Multi-directionality decreases as radial distance from the centre of the well increases. WSS vectors in the region with radial distance between 0.01mm and 4.01mm rotated in all four quadrants. Between 6.01m and 10.01mm, WSS vectors rotated in three quadrants. In these regions, flow was multidirectional with low magnitude. From 12.01mm onwards, WSS vectors are distributed only in two quadrants with high magnitude. On average, the centre and the edge of the well experience low magnitude multidirectional flow (LMMF) and high magnitude uniaxial

flow (HMUF) respectively.

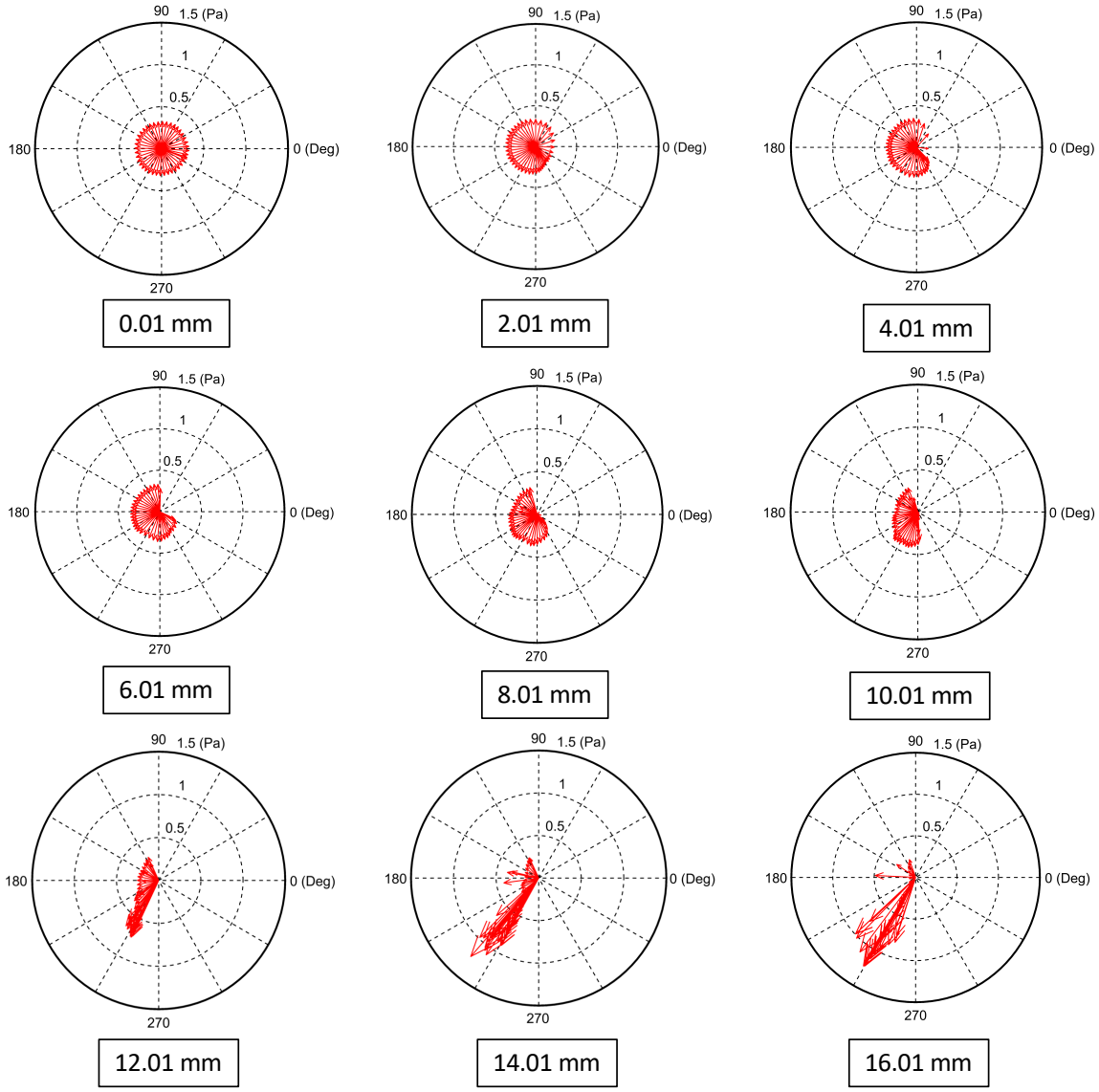

Figure 2.8: Individual polar plots of the magnitude and direction of instantaneous WSS vectors during one cycle. Each plot applies to one radial distance from the centre of the well. Each arrow represents an instantaneous WSS vector, whose length represents its magnitude, which is plotted at angles corresponding to the shear direction.

Figure 2.9 shows a snapshot of the shear stress produced on the base of the well. At the centre of the well, the magnitude of WSS was approximately constant at 0.3 Pa during each orbit, but an oscillation with increasing maximum WSS is observed towards the edge; instantaneous WSS at the edge ranged between

0.2 Pa and 1.2 Pa.

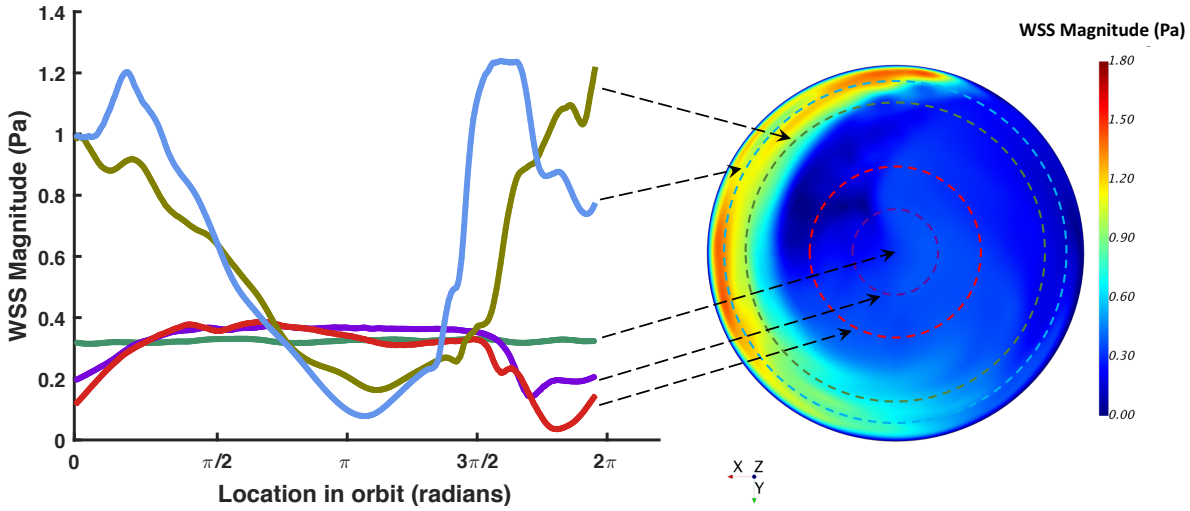

Figure 2.9: Plot and map of the instantaneous WSS magnitude. Plot of WSS magnitude at different radial distances from the centre throughout one cycle (2π radians), and map of the instantaneous WSS magnitude acting on the base of a 6-well plate on the orbital shaker. Arrows indicate the radial position for each curve on the WSS magnitude map.

TAWSS, OSI, and transWSS are plotted in Figure 2.10 as a function of the radial distance from the centre of the well. TAWSS was relatively low (around 0.3 Pa) from the centre to a radial distance of 10.5 mm, and it then increased to its peak of 0.7 Pa before it dropped sharply due to the no-slip condition at the wall. OSI and transWSS—two indices of multidirectional shear stress—were higher in the centre than at the edge.

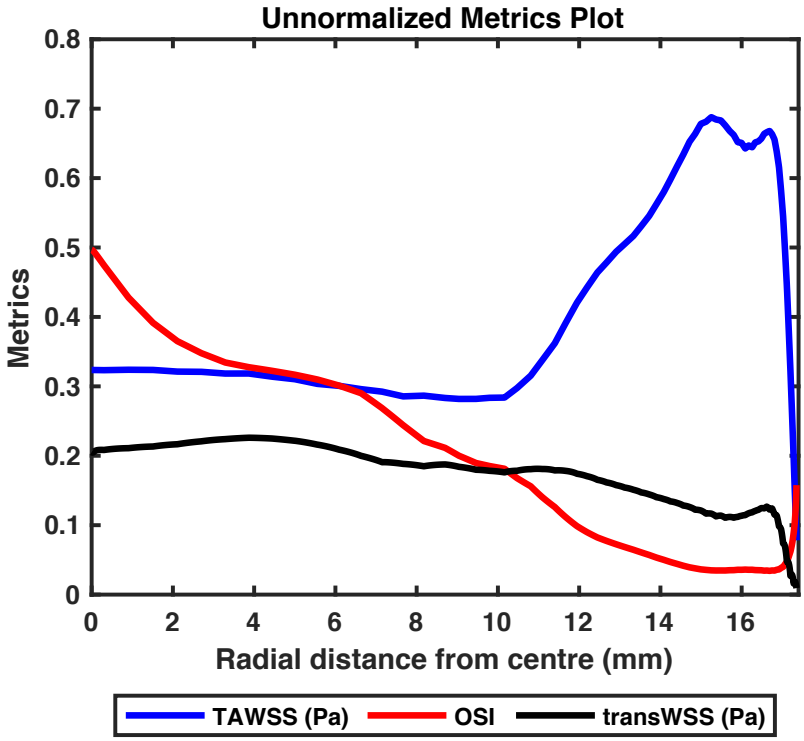

Figure 2.10: Plots of three WSS metrics—TAWSS, OSI, and transWSS—with respect to radial distance from the centre of the well.

2.3.3 Morphology of sheared HUVECs

Isolated HUVECs were sheared using a swirling 6-well. HUVECs at the centre exhibited a cobblestone morphology, while HUVECs at the edge were elongated and aligned (Figure 2.11). A more quantitative analysis is presented in the next chapter.

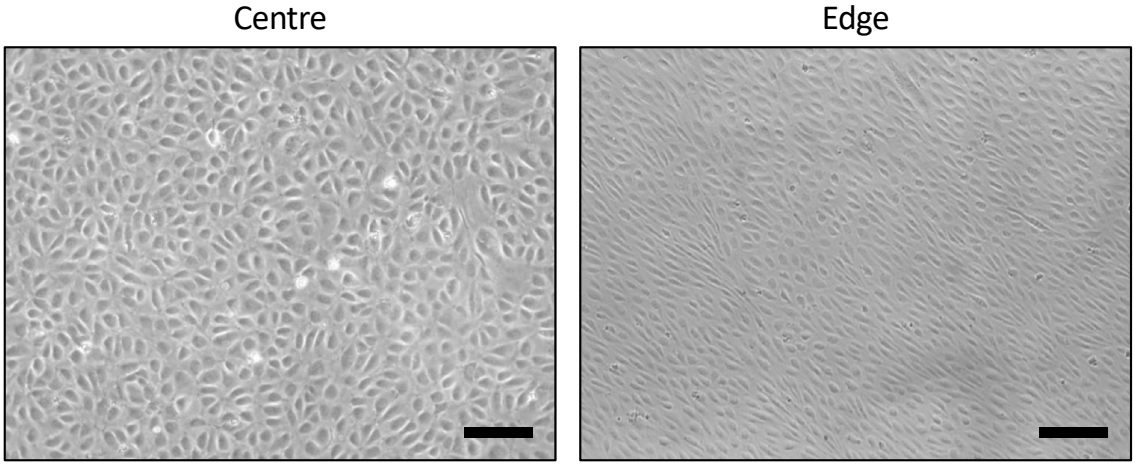

Figure 2.11: Morphology of sheared HUVECs using a swirling 6-well. (scale bar = 200 μm)

2.4 Discussion

The use of the swirling-well system to examine the effects of multidirectional flow and uniaxial flow on cultured endothelium simultaneously has increased substantially in recent years (summarised by Alpresa et al. (2018) and (Warboys et al., 2019)). The system allows cells to be exposed to a range of physiological shear stress profiles depending on the location of the cells within the well. For example, cells at the centre of the well experience multidirectional shear stress while cells nearer to the edge experience pulsatile uniaxial shear stress resembling that seen in straight, unbranched arterial segments *in vivo* (Ghim et al., 2017; Filipovic et al., 2016). The capacity to generate multidirectional shear stress is important because recent studies have suggested anatomical co-localisation of transWSS with a high predilection for lesion formation (Mohamied et al., 2014; Peiffer et al., 2013b).

The parameters used in our lab (orbital radius of 5mm, angular velocity of 150 rpm, medium height of 2mm) were simulated, and results show that the

WSS magnitudes at the centre and the edge mimic the pathological low magnitude and physiological high magnitude of WSS, respectively, in human arteries (Giddens et al., 1993; Gimbrone et al., 2000). The WSS vectors at the edge also closely mimic the physiological pulsatile flow. We termed the flow at the centre and the edge of a swirling well as low magnitude multidirectional flow (LMMF) and high magnitude uniaxial flow (HMUF), respectively.

As discussed, characterisation of flow in a swirling 6-well (numerically or experimentally) conducted by other studies used different parameters (Dardik et al., 2005; Salek et al., 2011; Filipovic et al., 2016; Velasco et al., 2016), hence no quantitative comparison can be made. However, all these studies showed an observation consistent with our CFD data—low magnitude WSS in the centre, and high magnitude WSS at the edge of the well.

Simulated medium height shows that the bottom of a swirling 6-well is never exposed to air; this is relevant for biological cell experiment because cells need to be submerged in culture medium at all time.

The morphology of HUVECs sheared using a swirling 6-well plate is consistent with previous studies performed using a swirling 6-well plate (although different parameters were used) (Salek et al., 2011; Filipovic et al., 2016). In the following chapter, the morphology of sheared HUVECs will be investigated quantitatively.

The CFD characterisation presented in this chapter provide an in-depth understanding of the flow behaviour in a swirling 6-well plate. This information will be used to guide the experimental design in the subsequent work in this thesis to understand the effect of shear stress on ECs.

Chapter 3

A novel method for segmenting growth of cells in sheared endothelial culture reveals the secretion of anti-inflammatory mediators

3.1 Background

The previous chapter has demonstrated that a swirling 6-well is capable of generating low magnitude multidirectional flow (LMMF) and high magnitude uniaxial flow (HMUF) in the centre and the edge of a well, respectively. This system is an ideal *in vitro* model to study the mechanobiology of endothelial cells (ECs).

The properties of cells in one region are widely assumed to be related to the

shear stresses occurring in the same region, allowing comparisons to be made between sites. However, there is a potential flaw in this system: ECs release soluble mediators and microparticles (Sage et al., 1981; Tunica et al., 2009; Griffoni et al., 2011), a process that, as mentioned above, can depend on flow characteristics (Burghoff and Schrader, 2011). These mediators affect cells in regions other than the one where they were released, due to general mixing in the swirling medium on an orbital shaker. This may corrupt or hide true effects of shear on cell behaviour. Ghim et al. (2017) have speculated that an effect of this type accounts for the apparently identical influence of different shear profiles on transcellular transport of large particles.

In a previous study (Dardik et al., 2005), cells were seeded only in specific regions of the well. This theoretically avoids the aforementioned flaw: if cells are restricted to one area, which corresponds to one shear profile, the properties of those cells cannot be influenced by mediators from cells exposed to other shear profiles, and they cannot influence such cells. However, we show below that cells seeded in one location can spread to other regions over time.

This chapter will describe and evaluate methods for promoting cell adhesion in some regions of devices while using surface passivation to prevent growth elsewhere, even after prolonged culture. We demonstrate a specific effect of shear on cell behaviour that would otherwise be masked if cells are allowed to grow over the entire well rather than being restricted to specific segments of it. More specifically, we demonstrate that ECs release anti-inflammatory mediators when exposed to a certain shear pattern, a finding that may be important for understanding atherogenesis. The demonstration that important shear responses are revealed only when using the new methods mandates their wider use.

3.2 Methods and materials

3.2.1 HUVECs isolation and culture

The protocol for HUVECs isolation and culture is described in Section 2.2.3.

3.2.2 Region-specific coating

Region-specific coating was achieved by coating the region of interest with fibronectin (Sigma-Aldrich, UK), and the remaining surface was passivated using 1% Pluronic F-127 solution (Sigma-Aldrich, UK). Only non tissue culture-treated wells were used. Polydimethylsiloxane (PDMS) rings (Figure 3.1) were casted in a master mould (Figure 3.2) that was designed using computer-aided design software (Solidworks 2016) and printed with an Ultimaker 2+ 3-D printer using polylactic acid filaments. A mixture of PDMS base and curing agent (90.9% base and 9.1% curing agent, Farnell, UK) was poured directly into the mould, degassed and cured at 80°C for 1 h before removal.

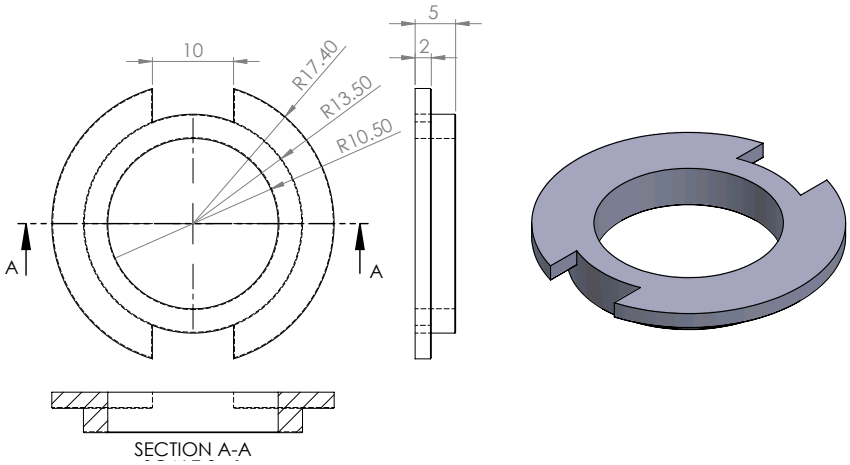

Figure 3.1: Engineering drawing of the PDMS ring used to segment the wells. Dimensions are in mm.

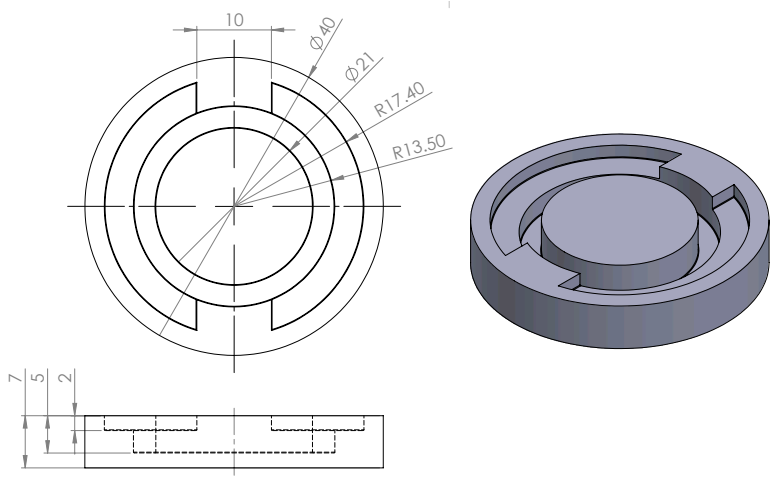

Figure 3.2: Engineering drawing of the PDMS mould. Dimensions are in mm.

A PDMS ring was placed in each well and secured using a custom-made stainless steel module (Figure 3.3) and a 35 mm diameter retaining ring (Misumi, UK) to give a tight seal between the bottom of the PDMS ring and the base of the well. One mL of 5 μg/mL fibronectin solution was pipetted into the centre

or the edge of a well and left for 30 minutes at 37°C. The fibronectin solution and then the PDMS ring were removed from the well, which was washed three times with PBS. The non-fibronectin coated region was passivated by the addition of a 1% Pluronic F-127 solution (Sigma-Aldrich, UK) to the well for 1 h. The Pluronic solution was removed and the wells washed three times with PBS. The coating procedure is summarised in Figure 3.4. Wells coated only with fibronectin, without segmentation, allow cells to grow over the entire base of the well and were used as a control.

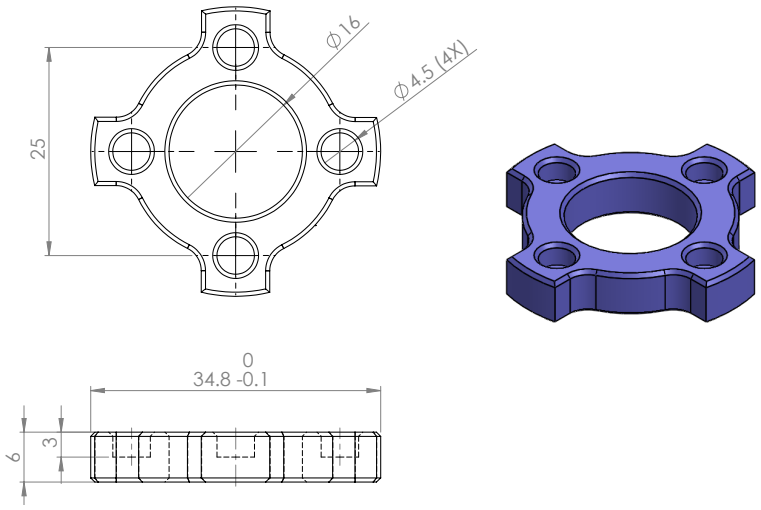

Figure 3.3: Engineering drawing of the stainless-steel module. Dimensions are in mm

HUVECs were seeded at 1.5×10^5 cells/well, and medium was replaced after 24 h to remove the non-adhered cells. They were cultured for another 2 days until confluent.

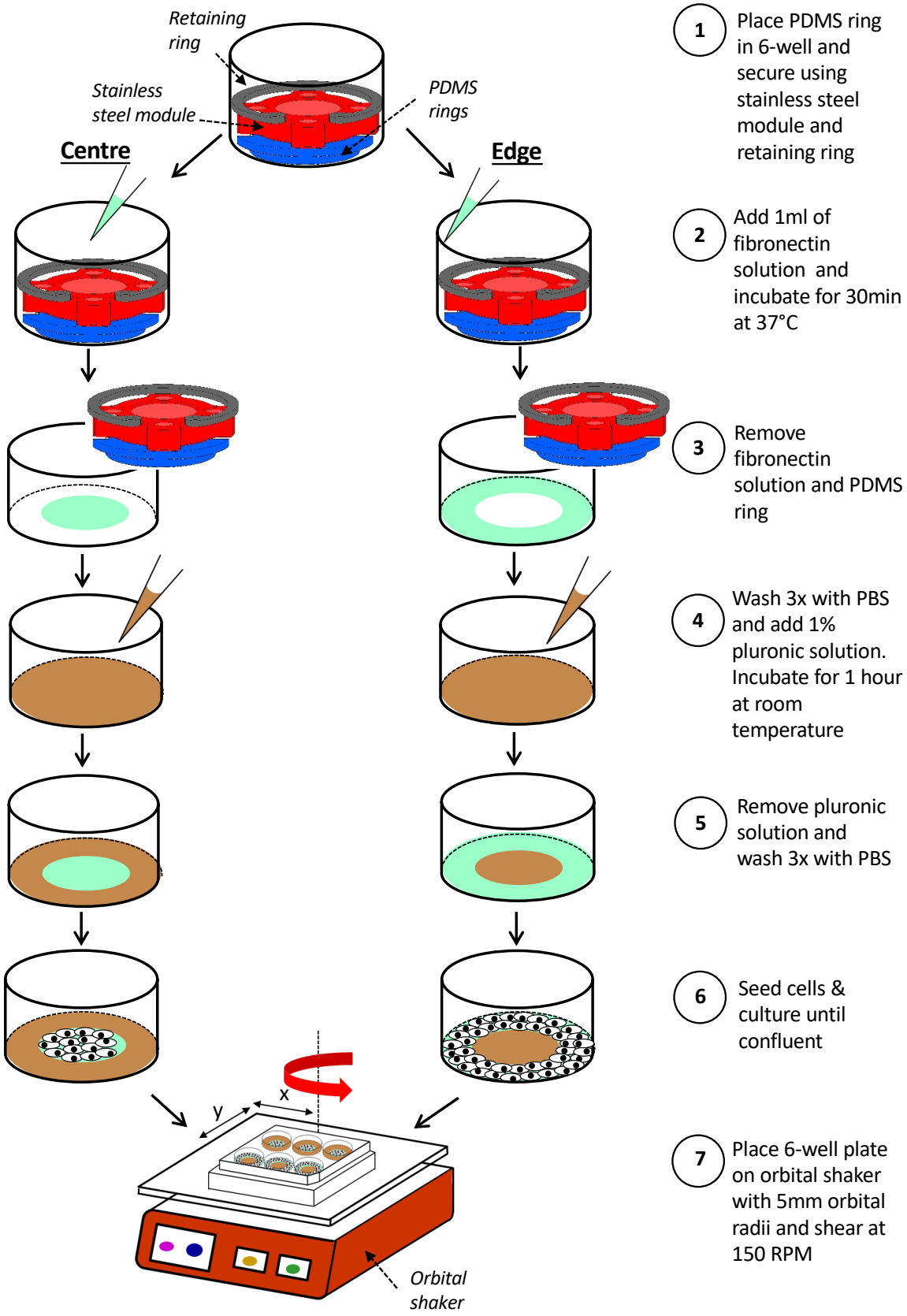

Figure 3.4: Schematic of the method for allowing cell growth only in the centre or at the edge of a 6-well plate.

3.2.3 THP-1 cell culture

Human acute monocytic leukaemia suspension line (THP-1 cells) were obtained from the American Type Culture Collection (USA). They were maintained in RPMI 1640 supplemented with 10% FBS, 2 mM L-glutamine, 100 U/mL penicillin and 100 μg/mL streptomycin (all from Sigma-Aldrich, UK). THP-1 cells at passages 6–20 were used for this study. THP-1 cells were maintained at 37°C in a humidified incubator under 95% air/5% CO_2.

3.2.4 Application of shear stress

HUVECs were sheared using a swirling-well system as described in Section 2.2.4.

3.2.5 TNF-α treatment in a swirling-well system

Tumour Necrosis Factor-α (TNF-α, PeproTech, UK) at a concentration of 10 ng/mL was used to induce endothelial activation. TNF-α was added after 2 days of shear, and left for another day on an orbital shaker. PBS was used as a control.

3.2.6 Immunofluorescence staining of ZO-1

After the exposure to shear, HUVECs were fixed with 4% Paraformaldehyde (PFA, Sigma-Aldrich, UK) for 10 minutes, permeabilised with 0.1% Triton X-100 (Sigma-Aldrich, UK) for 5 minutes and blocked with 1% bovine serum albumin (BSA) for 1 h at room temperature. Cells were then incubated with

rabbit anti-human zonula occludens-1 (ZO-1) (#13663, Cell Signaling Technology, USA) at a 1:200 dilution in 1% BSA overnight at 4°C, followed by three washes in PBS and incubation with Alexa Fluor 488-labelled goat anti-rabbit IgG (A11008, ThermoFisher Scientific, USA) at a 1:300 dilution in PBS at room temperature for 1 h. Nuclei were stained with DRAQ5 at a 1:1000 dilution in PBS for 15 minutes. ZO-1 staining was imaged with an inverted Leica TCS SP5 laser scanning confocal microscope (Leica, UK) using a 10× objective, 488 nm excitation and detection at 505-535 nm. DRAQ5 was excited at 633 nm and detected at 670-750 nm.

3.2.7 Nuclear orientation and shape index

Following 3 days of shear, cells were fixed with 4% PFA for 10 minutes. The wells were washed 3 times with PBS and nuclei stained with DRAQ5. Z-stack of 43 slices each were obtained from the edge to the centre with an inverted Leica TCS SP5 laser scanning confocal microscope.

The images were post-processed using ImageJ and a custom MATLAB script. A maximum intensity projection image was created from the 43 slices in each z-stack. Area and intensity thresholding were used to distinguish nuclei from the background. Individual images in the tile scan were stitched together using the image stitching plugin in ImageJ (Preibisch et al., 2009) and then subdivided into 1 mm intervals along the radius. Ellipses were fitted to the nuclei and the orientation of each nucleus was calculated as the angle between the long axis of the fitted ellipse and a vector running from the centre of the well to the centroid of the ellipse (y-axis), with positive numbers indicating that the end of the nucleus nearest the centre of the well was displaced to the right of the reference vector.

The shape index (SI) of each nucleus was defined as (Levesque et al., 1986):

$$SI = \frac{4\pi A}{P^2} \tag{3.1}$$

where A is the area and P is the perimeter of the ellipse. An SI of 1 indicates a circle, whereas a value of 0 indicates a line. The MATLAB script was written, and analysis was performed by Mehwish Arshad, Imperial College London, UK.

3.2.8 Counting HUVECs

HUVECs nuclei were stained with Hoechst 33342 (2 μg/mL, Thermofisher Scientific, USA) at a 1:1000 dilution in the incubator for 15 minutes, prior to fixation with 4% PFA for 10 minutes. Ten random fields were imaged at each location of interest using an inverted SP105F fluorescence microscope (Brunel Microscopes, UK) with a 20× objective, 365/50 nm excitation filter, 400 nm dichroic mirror and 460/50 nm emission filter. The number of HUVECs was quantified using a custom script written in MATLAB which distinguished stained nuclei by intensity and area thresholding. The MATLAB script was written by Dr Mean Ghim and Mehwish Arshad, Imperial College London, UK.

To quantify the number of HUVECs as a function of distance along a radius, a tile scan was performed from the edge to the centre of the well using the inverted TCS SP5 laser scanning confocal microscope with a 10× objective. Prior to that, cell nuclei were stained with DRAQ5 and fixed as described above.

3.2.9 Fluorescent labelling of THP-1 cells with Calcein AM

THP-1 cells were pelleted by centrifugation at 200 g for 5 minutes and resuspended in RPMI 1640 medium to reach the final concentration at 1×10^6 cells/mL. One μl of a 1 mg/mL Calcein AM solution (Life Technologies, USA) was added to 1 mL of the THP-1 cell suspension and incubated for 30 minutes at 37°C in a humidified incubator under 95% air/5% CO_2 to label the cells. Calcein AM-labelled THP-1 cells were centrifuged again at 200 g and resuspended in EGM-2 medium.

3.2.10 THP-1 cell adhesion assay in a swirling-well system

Calcein AM-labelled THP-1 cells were applied to the monolayers of pre-sheared HUVECs in 6-well plates at a density of 1 million per well and left for 1 h at 37°C in a humidified incubator under 95% air/5% CO_2 under static condition. Three washes with pre-warmed RPMI 1640 medium removed unbound THP-1 cells. Adhered THP-1 cells were fixed with 4% PFA for 15 minutes. Ten random fields were imaged at locations of interest using an inverted fluorescence microscope (SP105F, Brunel Microscopes) with a 20× objective, 470/40 nm excitation filter, 495 nm dichroic mirror and 525/50 nm emission filter. The number of adhered THP-1 cells was quantified using a custom MATLAB script that distinguished stained nuclei by intensity and area thresholding. The number of adhered THP-1 cells was normalised to the number of HUVECs. The MATLAB script was written by Dr Mean Ghim, Imperial College London, UK.

3.2.11 SDS-PAGE and Western blotting

ECs were lysed using radioimmunoprecipitation assay (RIPA) buffer (Sigma-Aldrich, UK) supplemented with Halt protease and phosphatase inhibitor (Thermo-Fisher Scientific, USA). Cell lysates were mixed with 4x Laemmli buffer (Biorad, UK) before boiling at 95°C for 5 minutes to denature the protein.

Denatured proteins were separated by sodium dodecyl sulfate-polyacrylamide gel electrophoresis (SDS-PAGE) through a 10% resolved gel. Resolved proteins were transferred onto a polyvinylidene fluoride (PVDF) membrane (Merck Millipore, USA), and the blot was blocked for 1 h with 5% skimmed milk in Tris-buffered saline with TWEEN 20 (TBST). Blots were incubated with respective primary antibodies (diluted in TBST containing 5% skimmed milk) overnight at 4°C, followed by the incubation of horseradish peroxidase-conjugated secondary antibodies (diluted in TBST containing 5% skimmed milk) for 1 h at room temperature. A list of antibodies is given in Table 3.1. Glyceraldehyde 3-phosphate dehydrogenase (GAPDH) and Calnexin were used as a housekeeping proteins for static and shear experiments, respectively. Blots were incubated using Clarity ECL substrate (Biorad, USA) before the bands were imaged using Biospectrum imaging system (UVP, UK). Densitometry was performed using Image Studio Lite software (LI-COR, USA). The list of buffers and reagents and their components are summarised in Table 3.2.

Antibody	Host Species	Dilution	Catalogue number	Company	Country of Origin
Primary Antibodies					
VCAM-1	Rabbit	1:2000	sc-8304	Santa Cruz Biotechnology	USA
ICAM-1	Rabbit	1:2000	sc-7891	Santa Cruz Biotechnology	USA
Phospho-Ikbα	Rabbit	1:1000	2859s	Cell Signaling Technology	USA
Ikbα	Rabbit	1:2000	sc-371	Santa Cruz Biotechnology	USA
Calnexin	Mouse	1:2000	LS-C179860	Source BioScience	UK
p-eNOS	Rabbit	1:1000	9571s	Cell Signaling Technology	USA
eNOS	Rabbit	1:2000	9572s	Cell Signaling Technology	USA
Secondary Antibodies					
Mouse anti-rabbit IgG-HRP	Mouse	1:5000	sc-2357	Santa Cruz Biotechnology	USA
Goat anti-mouse IgG-HRP	Goat	1:5000	sc-2005	Santa Cruz Biotechnology	USA

Table 3.1: List of antibodies used in Western blotting.

Buffers	Components		Remarks
10x Running buffer	• Tris	60.55 g	Dilute to 1x before use
	• Glycine	288 g	
	• 20% SDS	100 ml	
	• DI water	Top up to 2 L	
10x Transfer buffer	• Tris	60.55 g	Dilute to 1x before use
	• Glycine	288 g	
	• DI water	Top up to 2 L	
20x Tris-buffered saline	• Tris	96.8 g	Adjust pH to 7.6
(TBS)	• NaCl	320 g	
	• DI water	Top up to 2 L	
TBS with Tween (TBST)	• 20X TBS	100 ml	
	• Tween 20	2 ml	
	• DI water	Top up to 2 L	
20% SDS	• SDS	10 g	
	• DI water	Top up to 50 ml	
1.5M Tris-HCl, pH 8.8	• Tris	18.15g	
	• Adjust pH to 8.8		
	• DI water	Top up to 100ml	
1.0M Tris-HCl, pH 6.8	• Tris	12.114g	
	• Adjust pH to 6.8		
	• DI water	Top up to 100ml	
10% APS	• Ammonium Persulfate	1g	Aliquot and store in -20°C
	• DI water	Top up to 10ml	
10% Resolving gel (5 ml)	• 30% Acrylamide mix	1 ml	
	• 1.5M Tris-HCl, pH 8.8	1.3 ml	
	• 20% SDS	0.025 ml	
	• 10% APS	0.05 ml	
	• TEMED	0.004 ml	
	• DI water	2.6 ml	
Stacking gel (1ml)	• 30% Acrylamide mix	0.17 ml	
	• 1.0M Tris-HCl, pH 6.8	0.13 ml	
	• 20% SDS	0.005 ml	
	• 10% APS	0.01 ml	
	• TEMED	0.001 ml	
	• DI water	0.68 ml	

Table 3.2: List of buffers and reagents used in Western blotting.

3.2.12 Statistical analysis

Data are presented as mean ± standard error of the mean. Statistical analyses were performed by unpaired two-tailed Student's t-test or one-way or two-way ANOVA using GraphPad Prism 6 (GraphPAD Software Inc., USA). The criterion for significance was $p < 0.05$ (*$p < 0.05$; **$p < 0.01$; ***$p < 0.001$; ****$p < 0.0001$).

3.3 Results

3.3.1 Region-specific culture of endothelial cells

The choice of dimensions for the regions was based on results from the flow simulations. Fibronectin was applied to a circular region having the same centre as the well and a radius of 10.5 mm to expose cells to LMMF alone. For exposure to HMUF alone, the fibronectin-coated region was an annulus with the same centre, an inner radius of 13.5 mm and an outer boundary at the wall of the well (radius of 17.4 mm). The areas of the centre and the edge regions are 346.36 mm^2 and 378.59 mm^2, respectively, and differed by less than 10%.

Pluronic passivation abrogated adhesion of cells to the region that was not coated with fibronectin; growth was restricted to the fibronectin-coated region even after 6 days of culture. If the passivation step was omitted, cells were able to attach and spread to the regions that were not coated with fibronectin and proliferated there (Figure 3.5).

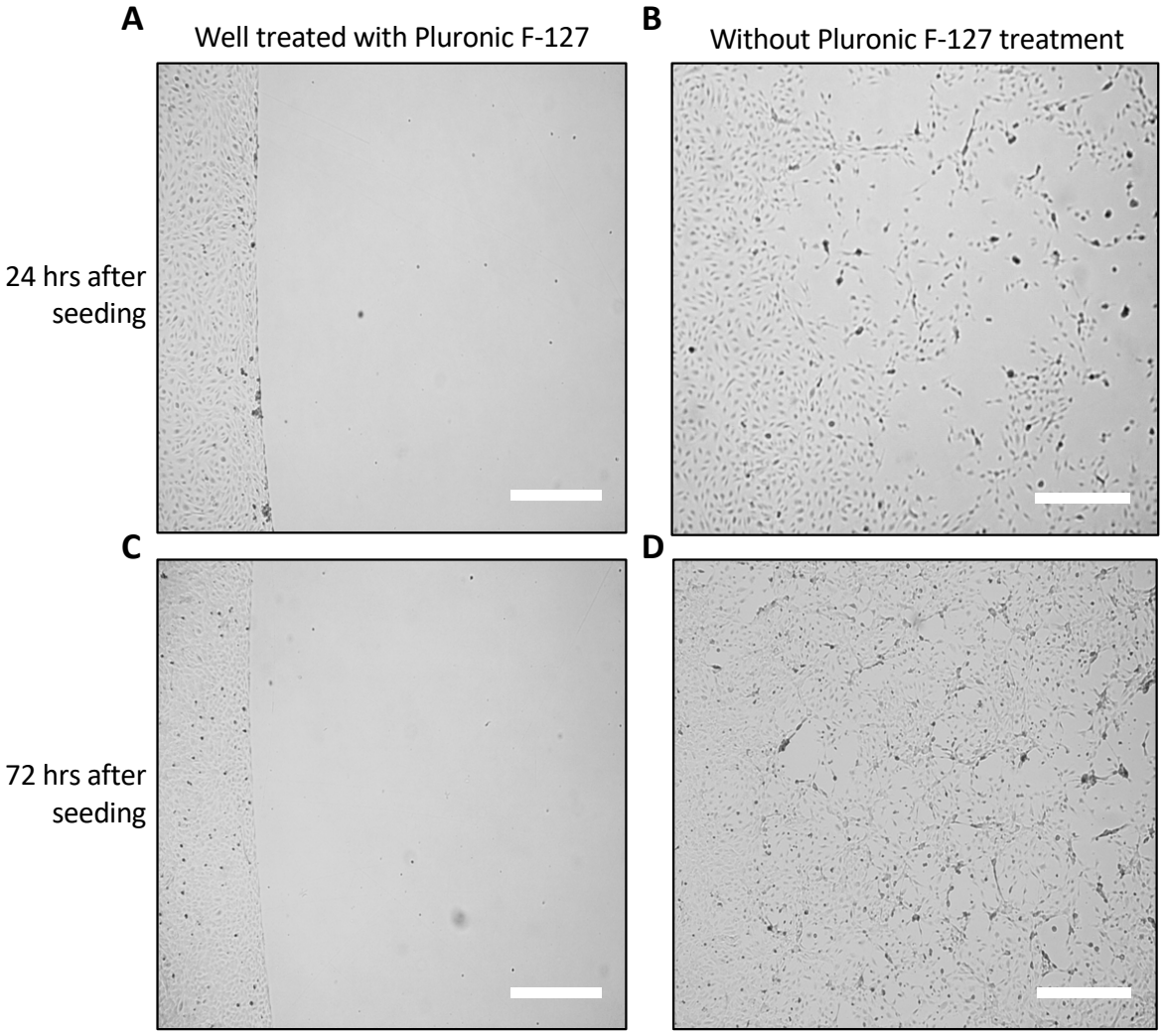

Figure 3.5: Microscope images showing that Pluronic F-127 prevented HUVECs adhesion to the region without fibronectin coating. No HUVECs were attached to the part of the well surface that was not pretreated with fibronectin and then passivated with Pluronic F-127, after 24 h (A) and 72 h (C) of growth. Without Pluronic F-127 passivation, HUVECs were attached to the surface without fibronectin 24 h after seeding (B) and had proliferated further by 72 h (D). (Scale bar = 500 μm)

3.3.2 Morphology and orientation in segmented wells and full wells

HUVECs in the annulus were visibly aligned and elongated, while HUVECs at the centre of the well exhibited a cobblestone morphology and lack of alignment

(Figure 3.6 A-B).

Nuclear roundness was quantified as their Shape Index; it decreased with distance along the radius, demonstrating that the nuclei become more elongated under HMUF (Figure 3.6 E). At each radial location, there was no statistically significant difference in Shape Index between HUVECs grown in segmented wells and full wells. The same result was obtained after TNF-α treatment. The treatment did have a tendency to increase elongation, but this trend was inconsistent, reaching statistical significance at only a few radial locations.

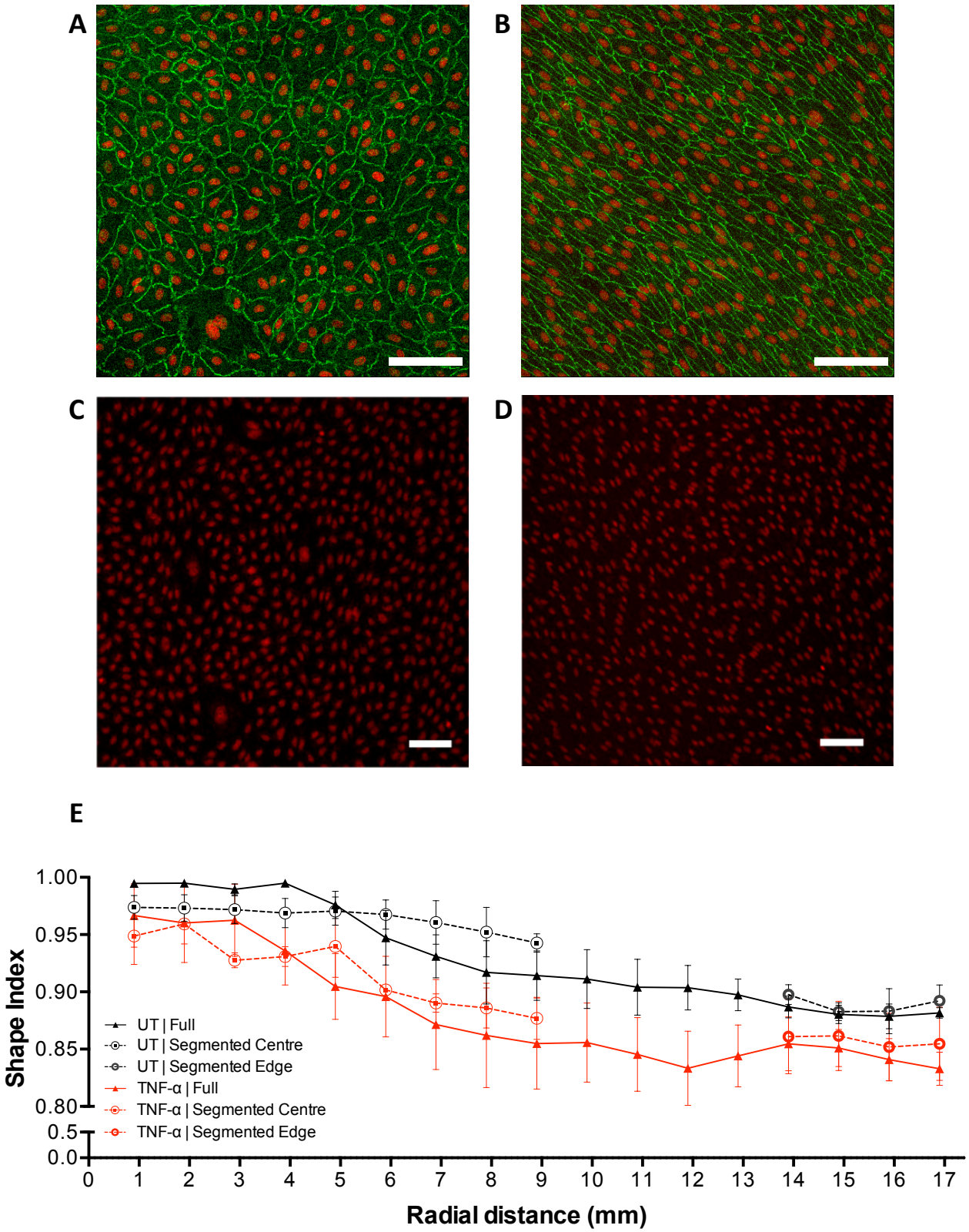

Figure 3.6: (Continued on the following page.)

Figure 3.6: The morphology of sheared HUVECs in a segmented or full well. Nuclear (red) stain shows the morphology of sheared HUVECs (A) in the centre and (B) at the edge of a full well, and (C) in the centre and (D) at the edge of a segmented well (scale bar = 100 μm). (A) and (B) also show cell outlines, delineated by ZO-1 immunostaining. Note the alignment and elongation of cells at the edge but not at the centre, and the lack of difference between full and segmented wells. (E) No significant difference in nuclear Shape Index, indicating roundness, between nuclei of HUVECs grown in full wells and segmented wells was seen for untreated or TNF-α treated HUVECs. Cells were more elongated near the edge than in the centre of the well. A tendency for greater elongation in TNF-α-treated HUVECs was not consistently significant across locations. (Two-way ANOVA and Bonferroni's post hoc test; n = 3)

Similarly, at each radial location and for both untreated and TNF-α treated HUVECs, there was no statistically significant difference in alignment between cells grown in a segmented well compared with a full well (Figure 3.7 – 3.8). There was again a small effect of TNF-α at some radial locations and, for unknown reasons, there was a larger standard error in the alignment of HUVECs grown in a full wells compared with those grown in segmented wells at radial distances between approximately 4 mm and 9 mm.

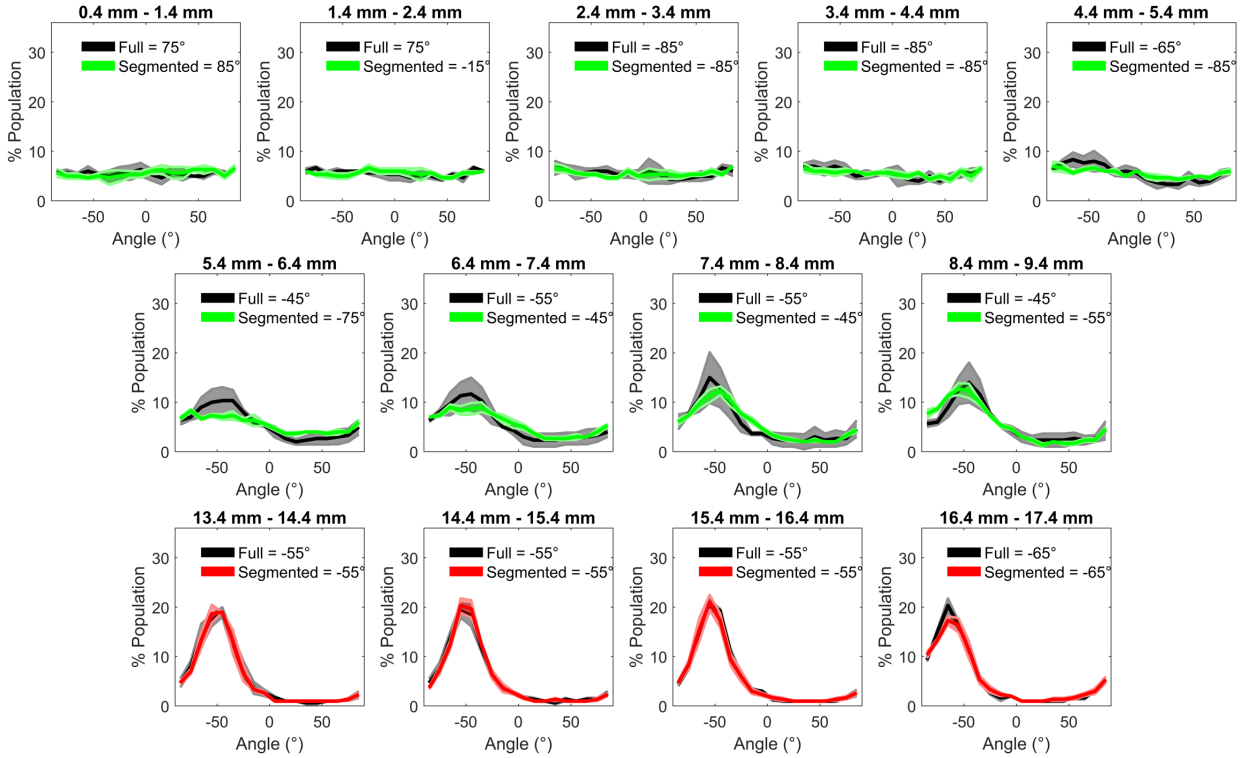

Figure 3.7: Orientation of untreated HUVECs nuclei in wells where the cells were growing only in the central region (green), only near the edge (red) or everywhere (grey). Each panel shows a different radial distance from the centre of the well. Mean data are presented as lines of best fit (obtained using seventh-order polynomials) and shaded areas show the standard error of the mean for 3 independent experiments. The modal orientation, with and without segmentation, is shown at the top of each panel. Note the absence of alignment near the well centre.

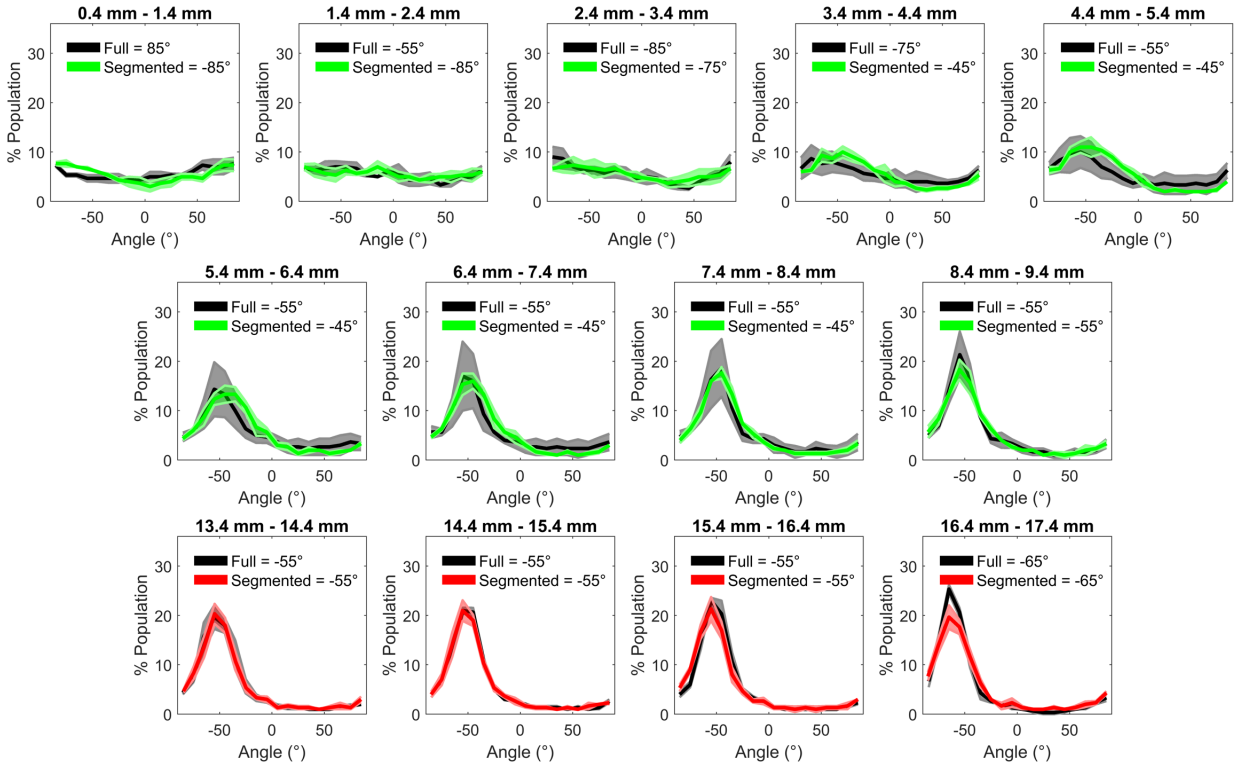

Figure 3.8: Orientation of TNF-α treated HUVECs nuclei in wells where the cells were growing only in the central region (green), only near the edge (red) or everywhere (grey). Each panel shows a different radial distance from the centre of the well. Mean data are presented as lines of best fit (obtained using seventh-order polynomials) and shaded areas show the standard error of the mean for 3 independent experiments. The modal orientation, with and without segmentation, is shown at the top of each panel. Note the absence of alignment near the well centre

3.3.3 Number of HUVECs in segmented and full wells

The number of HUVECs per mm^2 increased with radial distance under all conditions. Once again, there was no statistically difference between HUVECs grown in segmented wells and full wells, with or without TNF-α treatment, and no consistent significant effect of TNF-α (Figure 3.9 A-B).

An alternative way of quantifying HUVECs number using an immunofluorescence microscope also showed consistent result; the number of HUVECs per mm^2 at the edge (annulus with inner radius of 13.5 mm and an outer boundary

at the wall of the well) was significantly higher than that in the centre (within the circular region with radius of 10.5 mm) (Figure 3.9 C).

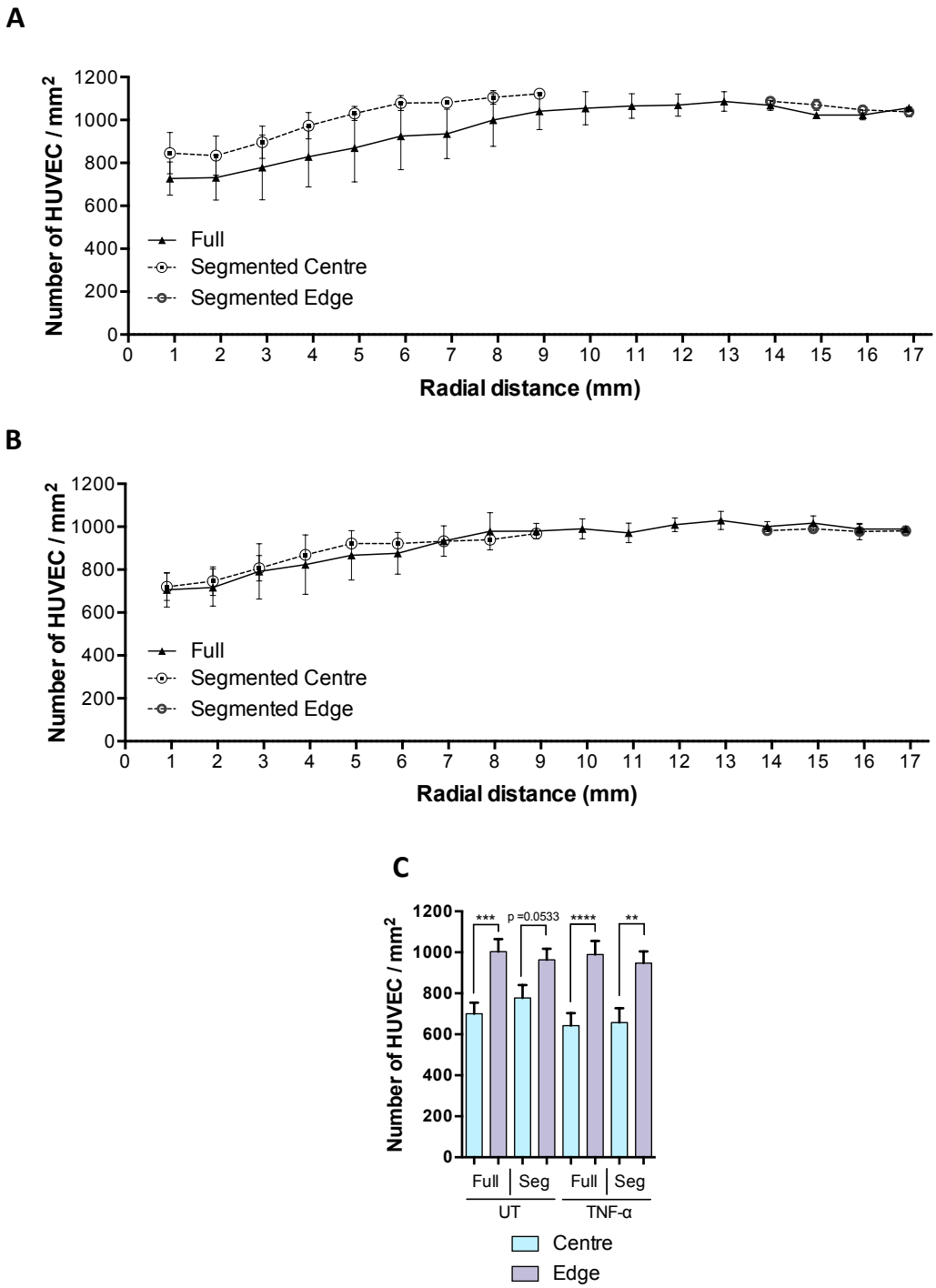

Figure 3.9: (Continued on the following page.)

Figure 3.9: Number of HUVECs per mm^2 increased with radial distance in a swirling well plate. No significant difference was observed between full and segmented wells in the number of (A) untreated and (B) TNF-α-treated HUVECs at different radial locations. (C) In both cases, there were more cells per unit area at the edge than the centre of the well. (A-B: two-way ANOVA and Bonferroni's post hoc test; n = 3, C: one-way ANOVA followed by Fisher's Least Significant Difference test, n = 6)

3.3.4 Characterisation of endothelial activation in segmented wells

Markers of endothelial activation—VCAM-1, ICAM-1, and IkBα were characterised in HUVECs grown only in the centre or at the edge of a well that were sheared using a swirling-well system. HMUF application over 1 day, compared with LMMF, suppressed VCAM-1 protein expression in a time-dependent manner; maximum suppression was observed after 4 days of shear application (Figure 3.10 A). ICAM-1 protein expression and IkBα phosphorylation were significantly reduced by 3 days and 1 day of HMUF exposure, respectively, compared with LMMF (Figure 3.10 B-C).

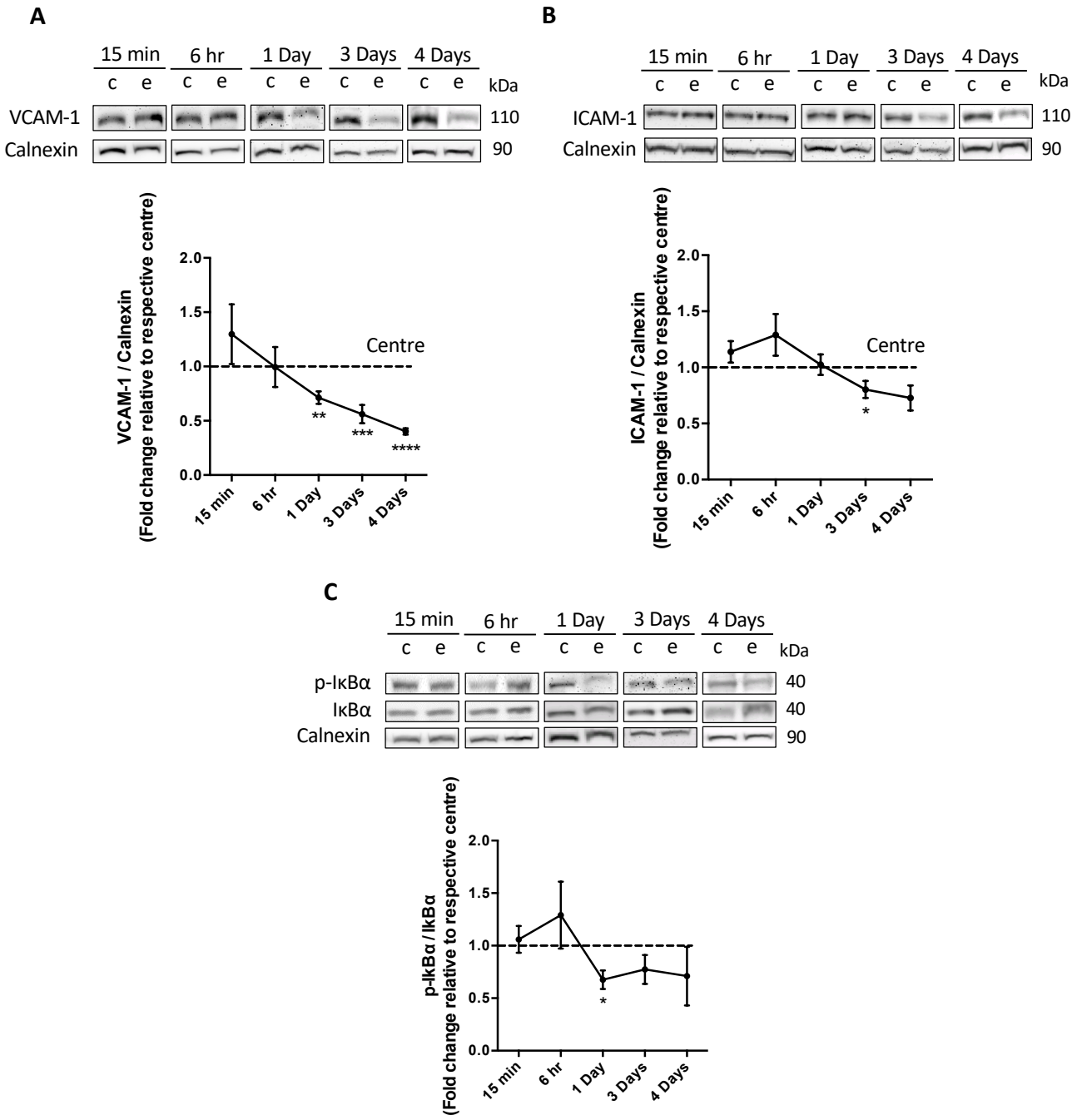

Figure 3.10: Effects of shear duration on endothelial activation. Representative Western blots and densitometry analysis of (A) VCAM-1 (B) ICAM-1, and (C) $I\kappa B\alpha$ expression in HUVECs sheared for different durations. Calnexin was used as a loading control. (c = centre, e = edge, dotted line = centre control, Unpaired two-tailed Student's t-test was performed between each edge and respective centre group; n > 3.)

Endothelial nitric oxide synthase 3 (eNOS) phosphorylation was significantly increased in HUVECs after 3 days of HMUF exposure, compared with those

subjected to LMMF (Figure 3.11).

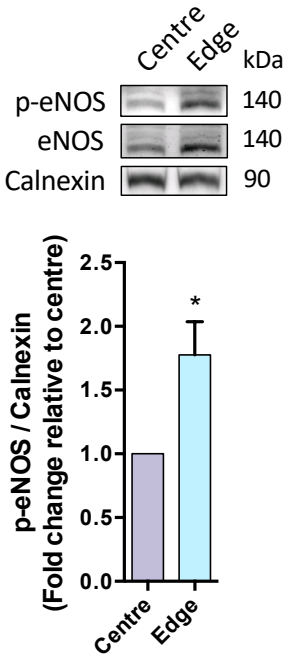

Figure 3.11: Three days of HMUF exposure increased eNOS phosphorylation in HUVECs. Representative Western blot and densitometry analysis of p-eNOS and eNOS expression in HUVECs sheared for 3 days. Calnexin was used as a loading control. (Unpaired two-tailed Student's t-test; n = 5)

3.3.5 Monocyte adhesion and endothelial adhesion molecules expression in segmented and full wells

There was a significantly higher THP-1 cell adhesion to HUVECs grown in the centre of the well than those grown at the edge under all conditions except for TNF-α-treated HUVECs grown in a full well. TNF-α treatment increased THP-1 cell adhesion to HUVECs in both regions of the well, regardless of segmentation (Figure 3.12).

In the absence of TNF-α, there was no significant effect of segmentation on the THP-1 cell adhesion to HUVECs in either the centre or the edge of the well. However, segmentation of wells containing TNF-α treated HUVECs resulted

in a significant ($p < 0.01$) increase in the monocyte adhesion at the centre but not at the edge of the well.

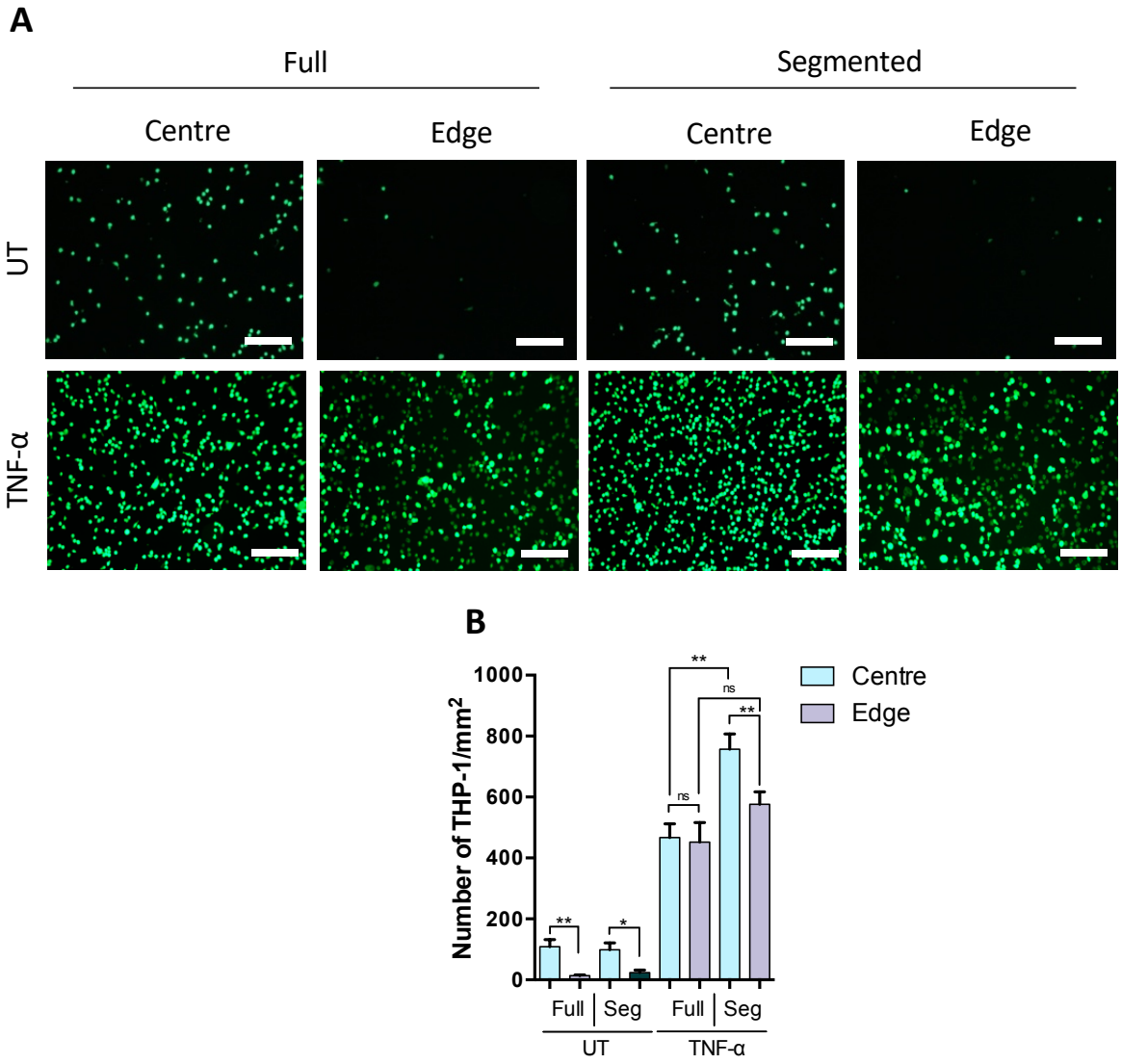

Figure 3.12: Monocyte adhesion to HUVECs grown in full wells or only at the centre or edge of segmented wells. (A) Representative images (scale bar = 200 μm) and (B) the number of Calcein AM-labelled THP-1 cells adhered on HUVECs , all shown for the centre and edge of full or segmented wells, with and without TNF-α treatment. (One-way ANOVA followed by Fisher's Least Significant Difference test, n = 7)

The number of adhered THP-1 cells in each region was normalised by the number of HUVECs in the same region to correct for the variation in HUVECs number in a different radial distance of a well, as demonstrated in Section 3.3.3.

Normalised results are presented as THP-1:HUVECs ratio, as shown in Figure 3.13. THP-1:HUVECs ratio in the centre of the well was significantly higher than that at the edge under all conditions after normalisation. Consistent with the unnormalised result, TNF-α treated HUVECs in segmented wells had a higher THP-1:HUVECs ratio than that in full wells at the centre but not at the edge of the well. Note that since segmentation had no effect on HUVECs density in either region (Figure 3.9C), this result cannot be explained by the use of normalisation.

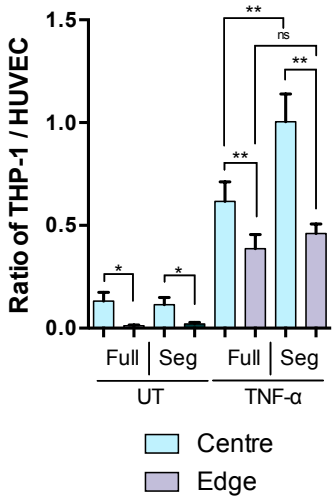

Figure 3.13: The ratio of adhered THP-1 cells to HUVECs grown in full wells or only at the centre or edge of segmented wells. (One-way ANOVA followed by Fisher's Least Significant Difference test, n = 7)

VCAM-1 and ICAM-1 are endothelial-specific cell adhesion molecules and their expression levels in HUVECs subjected to different treatments were analysed by Western blotting (Figure 3.14). Consistent with the monocyte adhesion data, segmentation of wells containing TNF-α treated HUVECs resulted in a significant increase in the expression of VCAM-1 and ICAM-1 at the centre but not at the edge of the well ($p < 0.001$, $p < 0.01$, respectively) .

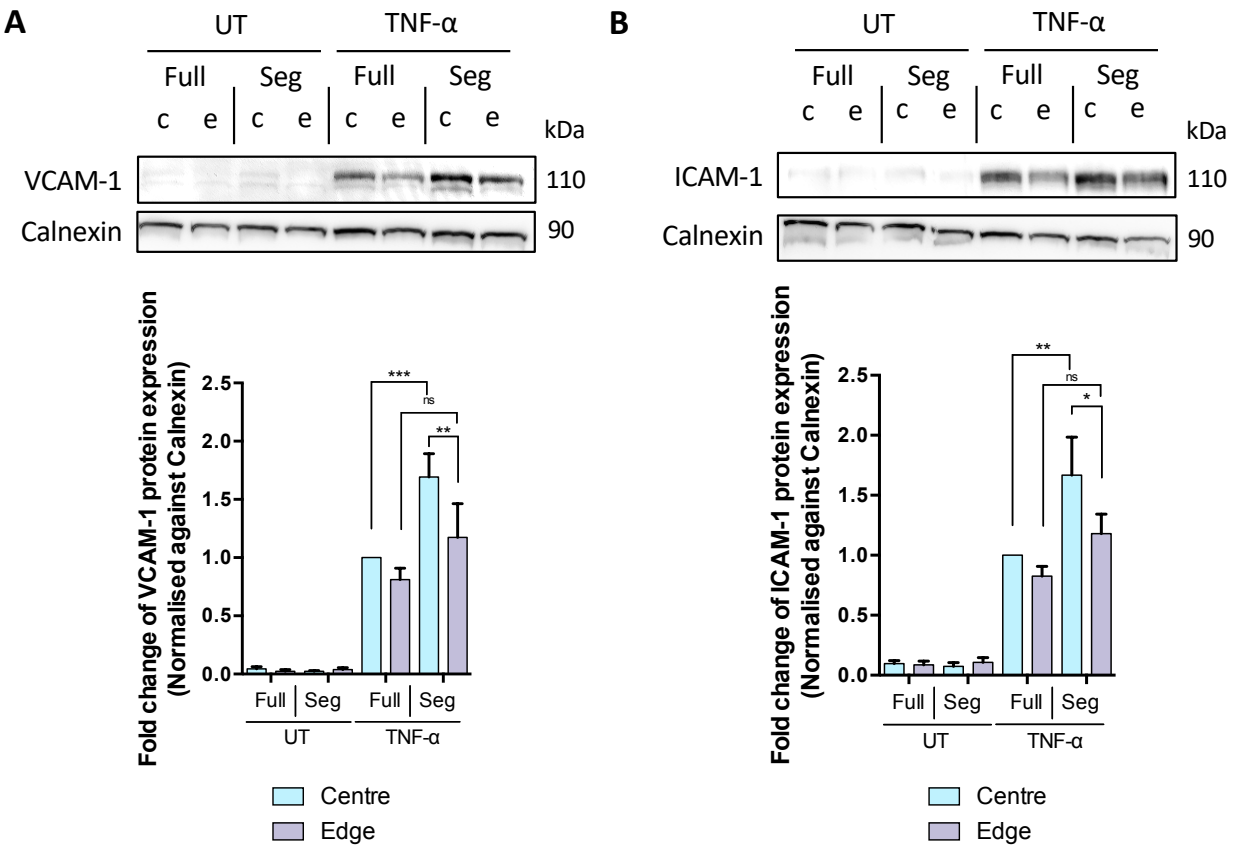

Figure 3.14: VCAM-1 and ICAM-1 expression in sheared HUVECs grown in full or segmented wells. Representative Western blots and densitometry analysis of (A) VCAM-1 and (B) ICAM-1 expression of HUVECs grown in full wells or only at the centre or edge of segmented wells, with and without TNF-α treatment. Calnexin was used as a loading control. (One-way ANOVA followed by Fisher's Least Significant Difference test, n = 5)

3.3.6 The effect of prolonged shear stress application on ECs

TNF-α-treated HUVECs exposed to HMUF for 3 days and 7 days had lower THP-1 cell adhesion than HUVECs exposed to LMMF. Interestingly, THP-1 cell adhesion to HUVECs was reduced by 7 days of HMUF exposure compared with 3 days of HMUF exposure, but there was no difference in THP-1 cell adhesion to HUVEC between 3 and 7 days of LMMF exposure (Figure 3.15).

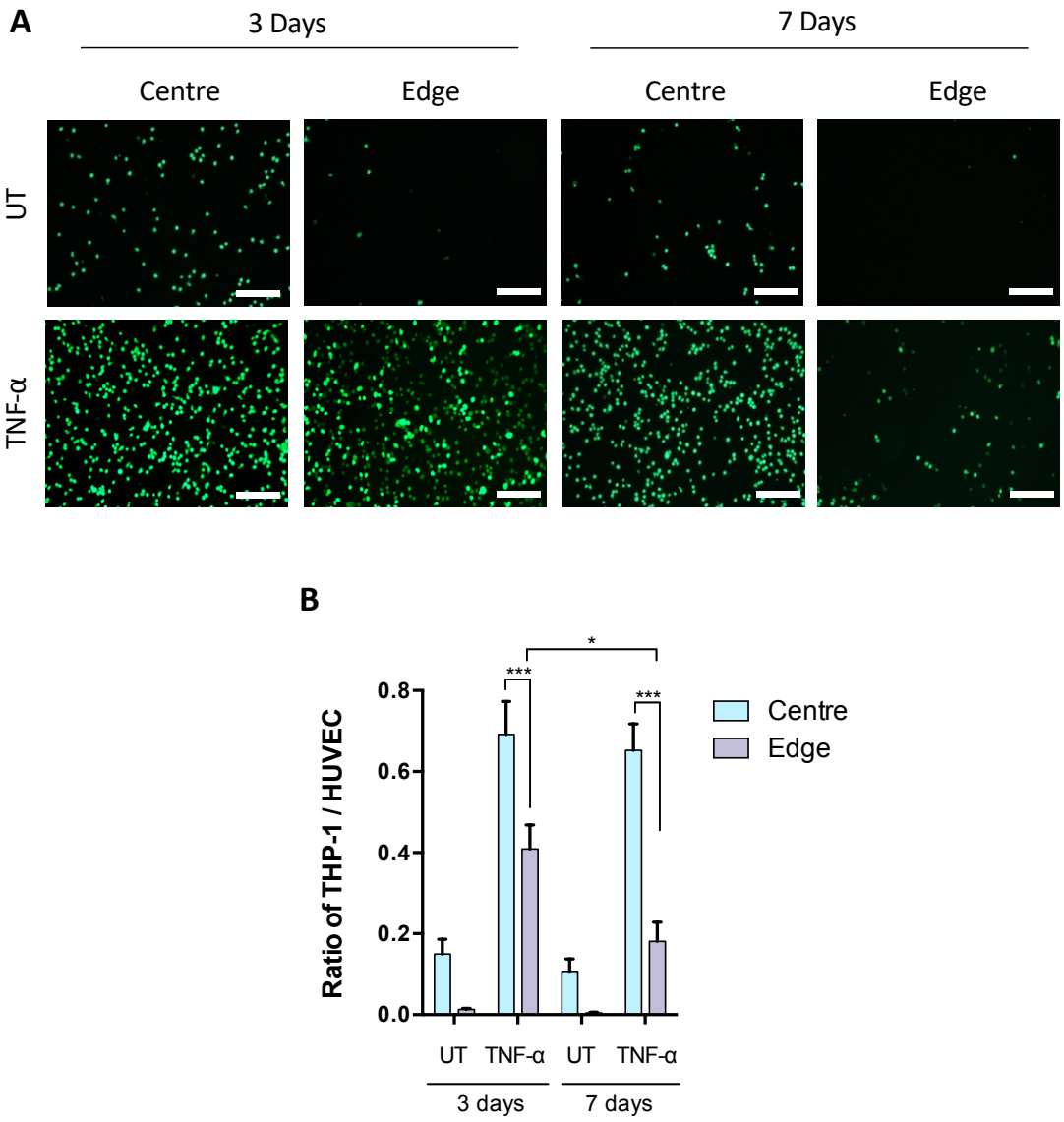

Figure 3.15: The effect of prolonged exposure to shear stress on monocyte adhesion on HUVECs grown in swirled wells. (A) Representative images of adhered Calcein AM-labelled THP-1 cells on HUVECs (scale bar = 200 μm) and (B) the ratio of THP-1 cells to HUVECs grown in swirled wells with and without TNF-α treatment and with shear applied for 3 days and 7 days. 7 days of exposure to HMUF, but not LMMF, resulted in a significantly lower THP-1 cell adhesion on TNF-α-treated HUVECs than 3 days of exposure. (One-way ANOVA followed by Fisher's Least Significant Difference test, n > 3)

3.4 Discussion

CFD characterisation of the WSS in a swirling-well system (discussed in Chapter 2) allows the comparison of the effects of LMMF and HMUF on ECs in a single well. This provides a better understanding of endothelial mechanobiology than simply comparing the effects of flow with no flow, as in early studies that employed the system (Kraiss et al., 2000; Walshe et al., 2013; Warboys et al., 2010). However, the method does have certain drawbacks. Firstly, harvesting cells for gene expression and protein analysis accurately from a specific region of a well is challenging. One way around this is to measure cell phenotype with a spatially-resolved method like microscopical techniques (Ghim et al., 2017). Secondly, ECs are known to release soluble or microparticulate mediators and this may also vary depending on the flow characteristics (Burghoff and Schrader, 2011; Sage et al., 1981; Tunica et al., 2009; Griffoni et al., 2011). Such mediators are mixed by the swirling medium and affect cells everywhere in the well, leading to decoupling between the site at which a particular shear stress profile is exerted and the sites at which its effects can be observed. The same also applies to other culture systems, even those with uniform flow properties (Plata et al., 2010).

To overcome both issues, the swirling-well system was modified to permit growth of cells only in specific regions of the well. If cells grow only in the centre, for example, they cannot be affected by mediators released at the edge of the well in response to uniaxial shear stress.

This is not the first demonstration of such segmentation method; Dardik et al. (2005) masked the unseeded part of a well with a silicone gasket to prevent cells adhesion and removed it before shear stress application. However, they observed cells proliferation and migration outwards beyond the boundaries

after 5 days of culture, which affects baseline proliferation in cells.

Cells typically adhere more avidly to hydrophilic surfaces than to hydrophobic surfaces. For this reason, multi-well cell culture plates, formed from hydrophobic polystyrene, are pre-treated by plasma oxidation. Alternatively, hydrophobic surfaces can be coated with extracellular matrix proteins such as fibronectin. In the absence of such surface modification, cells adhesion is drastically reduced but not abrogated.

In the present study, hydrophobic 6-well culture plates were coated with fibronectin at the edge or centre of the well to promote cell adhesion, and the non-fibronectin coated regions were passivated with Pluronic F-127 to prevent cell adhesion completely. The method is simple to use but effective: passivation successfully restricted cells to the fibronectin-coated regions even during prolonged culture.

As expected (Sato and Ohshima, 1994), HUVECs at the edge were elongated and aligned, whereas HUVECs in the centre exhibited a cobblestone morphology. Intriguingly, HUVECs density was higher at the edge than in the centre. Consistent with this result, Potter et al. (2011) found that aligned ECs cultured at the edge had a lower volume than nonaligned ECs cultured in the centre of a swirling well plate.

HUVECs confined to the edge or the centre of the well exhibited the same elongation, alignment and density as HUVECs at the same radial locations in wells where cells were permitted to grow everywhere. The same phenomenon was observed when the HUVECs were exposed to TNF-α and to shear (although there were minor effects of the TNF-α itself). Hence there was no evidence that these three properties were affected by the segmentation, and hence by shear-induced release and mixing of mediators.

Shear stress profiles affect vascular inflammation by modifying endothelial gene expression (Cunningham and Gotlieb, 2005; Helderman et al., 2007; Serbanovic-Canic et al., 2017). Activation of ECs and subsequent expression of cell adhesion proteins such as VCAM-1, and ICAM-1 promote the recruitment, arrest, and transmigration of circulating monocytes (Galkina and Ley, 2007; Cybulsky et al., 2001; Bourdillon et al., 2000). As discussion in Section 1.8, these steps are critical to the initiation and progression of atherosclerosis and inflammatory process (Wójciak-stothard et al., 1999). Expression of these markers can also be activated by pro-inflammatory cytokines such as TNF-α (Sprague and Khalil, 2009).

It is well understood that ECs grown in the centre of swirling wells show higher VCAM-1 and ICAM-1 protein expression than ECs at the edge (Dardik et al., 2005; Chakraborty et al., 2016). However, these studies have not characterised the expression of these markers in segmented wells over time. Our study showed that 3 days of HMUF exposure significantly reduced both VCAM-1 and ICAM-1 protein expression, which is consistent with the observation by Dardik et al. (2005), hence this time point was chosen for subsequent experiments. Although the strongest effect was observed after 4 days of shear, this time point was not chosen because some HUVECs were sheared off from the wells. This could be due to the shearing effect from swirling medium lifting HUVECs at the border of the cell colony between the centre and edge regions. We also showed that 3 days of HMUF exposure led to an increased eNOS phosphorylation, an atheroprotective marker, which agrees with other studies (Warboys et al., 2014; Filipovic et al., 2016). It is worth noting that calnexin, instead of GAPDH, was used as a loading control because shear stress has been shown to regulate GAPDH protein expression (C.M. Warboys, personal communication).

Functional assays that are commonly used in a swirling-well system are those

for permeability (Ghim et al., 2017; Mahmoud et al., 2016; Warboys et al., 2010) and migration (Mahmoud et al., 2017). There has been no report on the use of the swirling-well system for studies of leukocyte-endothelial interaction, as used here.

In this study, we performed monocyte adhesion assays on pre-sheared HUVECs monolayers in the presence or absence of TNF-α. Quantification of adhered monocytes after shear but in the absence of TNF-α showed that LMMF was more pro-inflammatory than HMUF. Our result was not affected by whether the cells were confined only to one region of the well or were seeded everywhere.

Pre-treatment with TNF-α in addition to shear increased monocyte accumulation in both regions, regardless of whether cell growth was segmented, as expected. Notably, however, in the TNF-α treated HUVECs, segmentation increased monocyte adhesion at the centre of the well but had no effect to HUVECs grown at the edge. This finding was statistically significant ($p < 0.01$) and robust, being independent of whether the data were normalised by HUVECs density or not (Figure 3.12 B and 3.13). Furthermore, expression of VCAM-1 and ICAM-1 followed the same trend: segmentation increased the expression of cell adhesion molecules by HUVECs grown in the centre of the well but had no effect on those grown at the edge (Figure 3.14). To the best of our knowledge, this is the first demonstration that segmenting the growth of cells exposed to spatially-varying shear profiles can affect the properties of those cells.

Not only is this effect novel but it has allowed the deduction of an endothelial property of potential importance in vascular pathophysiology. We interpret the results to mean that when cells were cultured both in the centre and at the edge, cells at the edge that are exposed to HMUF released a mediator that suppressed inflammation in the centre of the well, where cells were exposed to

LMMF. Such an effect would be seen when cells are cultured across the whole well, but not when they are cultured only at the centre. No effect of growth segmentation was seen at the edge of the well, where cells would be exposed to the putative mediator not only when allowed to grow everywhere but also when allowed to grow only at the edge, where the mediator is released. The effect was not observed in the absence of TNF-α, implying that the mediator influences some process resulting from the action of this cytokine.

HUVECs were also exposed to shear for up to 7 days to investigate the effect of more prolonged chronic shear stress on endothelial function. Cells were grown in the full well for this experiment because, as discussed above, HUVECs grown in segmented wells were detached after 4 days of shear application, as mentioned above. Seven days of HMUF had a stronger anti-inflammatory effect on HUVECs; this suggests that longer shear application better mimics the physiological condition for vascular cells. The method for segmenting growth of HUVECs needs to be optimised further to allow longer shear application. We could better understand the mechanobiology of ECs if prolonged shear could be applied in a segmented well.

We have demonstrated a new assay to study monocyte adhesion in a swirling-well system. This assay can be used for physiological studies and drug testing on ECs under different shear condition, and especially under the putatively atherogenic LMMF. More functional assays can be developed that use this swirling-well system, such as neutrophil adhesion and leukocyte transendothelial migration (by incorporating the Transwell® system).

The existence of an anti-inflammatory mediator that is released from cells in response to uniaxial flow clearly may be important in the pathogenesis of atherosclerosis. This new method provides a means for investigating the nature of these mediators, since it enables accurate harvesting of the cells of

interest, and allows for the collection of medium conditioned by cells exposed to well-defined flows. Shear-dependent mediators corrupting apparent relations between shear and endothelial properties can indeed be observed in cell culture. Therefore, it is necessary to segment cell growth in a swirling-well system to prevent such effects.

Chapter 4

LRG1 is a novel regulator of endothelial activation

4.1 Background

Endothelial cells (ECs) lining the inner surface of all blood vessels are important players in maintaining vascular homeostasis. In the physiological state, ECs play important roles in regulating vascular tone, vessel permeability, and leukocyte adhesion (Godo and Shimokawa, 2017). Homeostasis breaks down when the endothelium is activated, which can be triggered by factors such as pro-inflammatory cytokines, hyperglycemia, and haemodynamic shear stress (Wang et al., 2013a; Sprague and Khalil, 2009; Beckman et al., 2002). Such dysfunction of the endothelium is critical in the development of atherosclerosis—a chronic inflammatory disease that involves low density lipoprotein (LDL) transcytosis (Mundi et al., 2018; Ghim et al., 2017; Zhang et al., 2014) and monocyte recruitment (Mestas and Ley, 2008) triggered by cytokines and atherogenic flow characteristics.

The nuclear factor kappa B (NF-κB) pathway is central in the breakdown of endothelial homeostasis (Pober, 2002). Binding of tumour necrosis factor-α (TNF-α) to tumor necrosis factor receptor 1 (TNFR1) activates the NF-κB signalling cascade which requires the phosphorylation of Protein Kinase B (Akt) (Ozes et al., 1999). NF-κB activation also involves IκBα phosphorylation, leading to the translocation of NF-κB from the cytosol to the nucleus and the subsequent transcription of endothelial adhesion molecules such as vascular cellular adhesion molecule-1 (VCAM-1) and intercellular adhesion molecule-1 (ICAM-1) (Pober, 2002; Heiden et al., 2010). Binding of TNF-α to TNFR1 also induces apoptotic signalling by releasing an active form of caspase-8, which in turn cleaves and activates caspase-3 (Wang et al., 2008). Cleaved caspase-3 then targets a latent DNAse that degrades chromosomal DNA and consequently killing the cells (Sedger and Mcdermott, 2014).

Although knocking out components of the NF-κB pathway generally protects mice from atherosclerosis (Bourdillon et al., 2000; Bråne et al., 2004; Cybulsky et al., 2001), a study showed that macrophage-specific deletion of IκB kinase 2 (IKK2) led to an increase in atherosclerotic lesion formation and impaired inflammatory response (Kanters et al., 2003). This may be explained by the observation that NF-κB activation in leukocyte also plays a role in the resolution of inflammation by inducing the expression of anti-inflammatory genes and the induction of apoptosis (Lawrence et al., 2001). Thus NF-κB activation plays a role in both pro- and anti-inflammatory processes, and more understanding of the pathway is required before it could be targetted for therapeutic purposes.

Leucine-rich α-2-glycoprotein 1 (LRG1) is a novel regulator of angiogenesis, and it exerts its function by regulating the endothelial transforming growth factor-β (TGF-β) signalling pathway (Wang et al., 2013b). Besides its role

in angiogenesis, LRG1 is intimately linked to tissue inflammation. TNF-α has been shown to induce LRG1 expression in ECs (Wang et al., 2017b) and elevated LRG1 expression was observed during granulocyte differentiation (O'Donnell et al., 2002). Furthermore, elevated serum LRG1 level was reported in human patients with various inflammatory, autoimmune, and cardiovascular diseases (Xie et al., 2018; Ha et al., 2014; Serada et al., 2012; Watson et al., 2011; Yin et al., 2014; Pek et al., 2015). However, its role in endothelial activation and atherosclerosis remains to be elucidated.

This chapter aims to describe a novel role of LRG1 in endothelial activation. Given the important role of shear stress in endothelial activation as discussed in Chapter 3, LRG1 is also investigated in ECs sheared using the swirling-well system. LRG1 is a secreted glycoprotein, hence the novel method for segmenting growth of cells in a swirling-well system developed in Chapter 3 is used. We found that LRG1 expression is shear dependent, and that its expression can be induced by TNF-α via NF-κB activation. Surprisingly, our data showed that LRG1 inhibits TNF-α-induced activation of NF-κB signalling, expression of VCAM-1 and ICAM-1, and monocyte capture, firm adhesion, and transendothelial migration. Mechanistically, LRG1 exerts its function by causing the shedding of TNFR1 via the TGFβ receptor 1-SMAD2 (ALK5-SMAD2) pathway and the subsequent activation of A Disintegrin and metalloproteinase domain-containing protein 10 (ADAM10). These findings establish a novel role for LRG1 in endothelial activation and suggest that LRG1 may have a protective role in atherogenesis.

4.2 Methods and Materials

4.2.1 Cell isolation and culture

Protocol for HUVECs isolation and culture is described in Section 2.2.3.

Human aortic endothelial cells (HAECs) were obtained from Lonza (Switzerland). HAECs were cultured in flasks coated with 0.1% gelatin using EGM-2 in a humidified incubator under 95% air/5% CO_2. HAECs between passages 3–5 were used for experiments.

HUVECs were used for transfection, signalling studies, dose-dependent study of recombinant human LRG1 (rhLRG1) on monocyte adhesion, and monocyte capture assay. HAECs were used for the remaining monocyte-endothelial interaction assays and TNFR1 shedding studies.

Human acute monocytic leukaemia suspension line (THP-1 cells) were maintained as described in Section 3.2.3.

Freestyle human embryonic kidney 293 (HEK293F) were maintained in Freestyle 293F Expression Medium (both from Life Technologies, UK) on an orbital shaker orbiting at 130 rpm at 37°C in a humidified incubator under 92% air/8% CO_2.

4.2.2 Application of shear stress

ECs grown in the centre and the edge of a 6-well plate experience, respectively, low magnitude multidirectional flow (LMMF, putatively atherogenic) and high magnitude uniaxial flow (HMUF, putatively atheroprotective) when the wells

are swirled on the horizontal platform of an orbital shaker as described in Chapter 2. To ensure that cell seeding was restricted to either the centre or the edge, the wells were coated with fibronectin (Sigma-Aldrich, UK) in one region, followed by passivation of the other region with Pluronic F-127 (Sigma-Aldrich, UK) as described in Chapter 3. After seeding, the plates were left in a humidified incubator until ECs reached confluence, and then were placed on the orbital shaker (POS-300, Grant Instruments) inside the humidified incubator for another 3 days. The platform orbited in the horizontal plane with an orbital radius of 5 mm and angular velocity of 150 rpm.

4.2.3 SDS-PAGE and Western blotting

SDS-PAGE and Western blotting were performed as described in Section 3.2.11. Antibodies used in this chapter are tabulated in Table 4.1.

Antibody	Host Species	Dilution	Catalogue number	Company	Country of Origin
Primary Antibodies					
VCAM-1	Rabbit	1:2000	sc-8304	Santa Cruz Biotechnology	USA
ICAM-1	Rabbit	1:2000	sc-7891	Santa Cruz Biotechnology	USA
Phospho-Ikbα	Rabbit	1:1000	2859s	Cell Signaling Technology	USA
Ikbα	Rabbit	1:2000	sc-371	Santa Cruz Biotechnology	USA
Calnexin	Mouse	1:2000	LS-C179860	Source BioScience	UK
LRG1	Rabbit	1:2000	13224-1-AP	Proteintech	USA
GAPDH	Rabbit	1:2000	sc-25778	Santa Cruz Biotechnology	USA
6 x His	Rabbit	1:2000	a190-114a	Bethyl Laboratories	USA
Phospho-Akt	Rabbit	1:1000	9271s	Cell Signaling Technology	USA
Akt	Rabbit	1:2000	9272s	Cell Signaling Technology	USA
Cleaved Caspase 3	Rabbit	1:1000	9661s	Cell Signaling Technology	USA
TNFR1	Mouse	1:1000	sc-8436	Santa Cruz Biotechnology	USA
ADAM10	Rabbit	1:2000	14194s	Cell Signaling Technology	USA
ADAM17	Rabbit	1:2000	3976s	Cell Signaling Technology	USA
Phospho-SMAD2	Rabbit	1:1000	3108s	Cell Signaling Technology	USA
SMAD2	Rabbit	1:2000	5339s	Cell Signaling Technology	USA
Secondary Antibodies					
Mouse anti-rabbit IgG-HRP	Mouse	1:5000	sc-2357	Santa Cruz Biotechnology	USA
Goat anti-mouse IgG-HRP	Goat	1:5000	sc-2005	Santa Cruz Biotechnology	USA
Anti-Mouse IgGκ-HRP	Mouse	1:5000	sc-516102	Santa Cruz Biotechnology	USA

Table 4.1: List of antibodies used in Western blotting.

4.2.4 Quantitative reverse transcription polymerase chain reaction (qRT-PCR)

Total ribonucleic acid (RNA) was extracted from ECs using RNAzol RT (Molecular Research Centre, USA) according to the manufacturer's protocol. 1 μg of RNA was reverse transcribed into complementary DNA (cDNA) using qScript cDNA Supermix (Quanta Biosciences, USA) in a PCR thermal cycler. The transcribed cDNA was used as a template for qRT-PCR to check the gene expression using an Applied Biosystems QuantStudio 6 Flex Real-Time PCR

System (ThermoFisher Scientific, USA). The sequences of primers used are tabulated in Table 4.2. Glyceraldehyde 3-phosphate dehydrogenase (GAPDH) was used as a housekeeping gene.

Name	Gene target	Sequence of primer
LRG1	Homo sapiens leucine rich alpha-2-glycoprotein 1, mRNA	For: GATCGTGCCACTGCACTCTA Rev: GAAAGCCCATCGTGTGTTCT
VCAM-1	Homo sapiens vascular cell adhesion molecule 1, mRNA	For: GTCAATGTTGCCCCCAGAGA Rev: TGCCTGCTCCACAGGATTTT
ICAM-1	Homo sapiens intercellular adhesion molecular 1, mRNA	For: TGATGGGCAGTCAACAGCTA Rev: AGGGTAAGGTTCTTGCCCAC
GAPDH	Homo sapiens glyceraldehyde–3–phosphate dehydrogenase , mRNA	For: GGTCTCCTCTGACTTCAACA Rev: AGCCAAATTCGTTGTCATAC
ADAM10	Homo sapiens ADAM metallopeptidase domain 10,mRNA	For: AGTGCAGTGACAGGAACAGTCCTT Rev: GGACACGCCTTTGCAAGTAGCATT

For: Forward
Rev: Reverse

Table 4.2: List of primers and their sequence used in qRT-PCR.

4.2.5 Transcription factor binding sites prediction

Bioinformatics analysis was performed on the LRG1 promoter sequence to identify potential transcription factor binding sites (TFBS) on the DNA. The LRG1 gene sequence was obtained from the UCSC Genome Browser. The result showed that LRG1 gene is 4,066 bp in length and is located at chromosome 19 between 4,536,409 and 4,540,474. Excluding the untranslated regions (UTRs) on both 5' and 3' ends, the coding sequence is located between 4,537,940 – 4,540,013 on the minus strand with one 2074bp intron being encompassed. In order to identify potential TFBS, 1500 bases upstream of the genomic sequence were also included in the analysis. Four bioinformatics tools/databases were used to predict putative TFBS: PROMO, JASPAR 2016,

CONSITE and Motifmap + FIMO. This analysis was performed by Qianhe Lu, Imperial College London, UK.

4.2.6 Overexpression of LRG1 in HUVECs

LRG1 was overexpressed by transfecting pcDNA-LRG1-HIS plasmid (the plasmid was constructed by Wang et al. (2013b)) into HUVECs. Empty pcDNA3.1 plasmid was used as a control plasmid. The restriction map of pcDNA-LRG1-HIS plasmid is illustrated in Figure 4.1.

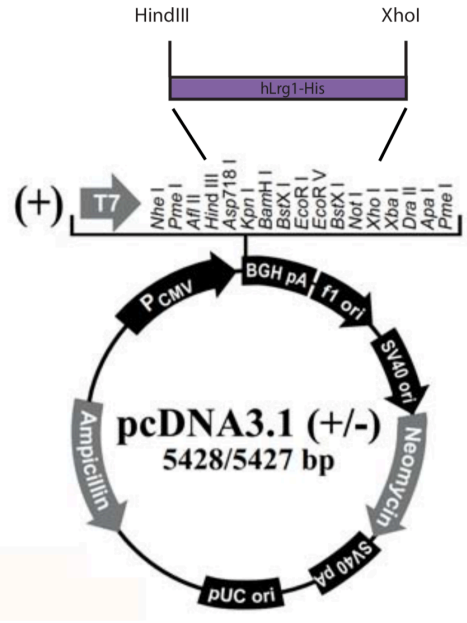

Figure 4.1: Restriction map of pcDNA-LRG1-HIS plasmid. The pcDNA-LRG1-HIS plasmid was formed by cloning the coding sequence of human LRG1 mRNA (NM_052972), carrying a Kozak consensus sequence at the 5' end and a 6 x Histidine tag at the 3' end, into the pcDNA3.1 expression vector at the HindIII/XhoI sites. The plasmid was constructed by Wang et al. (2013b). Reprinted with permission from Macmillan Publishers Ltd: Nature (Wang et al., 2013b).

Lipofectamine 3000 (ThermoFisher Scientific, UK) was used for plasmid transfection according to the manufacturer's instruction with slight modification.

Briefly, 1 μg of plasmid DNA and 2 μl of P3000 reagent were diluted in 147 μl of OptiMEM I Reduced Serum Media (ThermoFisher Scientific, UK) in one tube, while 2 μl of Lipofectamine 3000 was diluted in 148 μl of OptiMEM in another tube. After 5 minutes, contents in both tubes were mixed and incubated for another 15 minutes at room temperature to allow DNA-lipid complex formation. The complex was then added to 80% confluent HUVECs in a 6-well plate with 1.2 mL of OptiMEM medium in each well, and left for 4 h in a humidified incubator. After 4 h, the transfection medium was replaced with 2 mL of pre-warmed EGM-2 medium.

4.2.7 Production of recombinant human LRG1 protein

The LRG1 plasmid was transfected into HEK293F using Lipofectamine 3000 according to the manufacturer's protocol. Briefly, 30 μg of plasmid DNA and 60 μl of P3000 reagent were diluted in 1 mL of OptiMEM in one tube, while 60 μl of Lipofectamine 3000 was diluted in 1 mL of OptiMEM in another tube. After 5 minutes, contents in both tubes were mixed and incubated for another 15 minutes at room temperature to allow DNA-lipid complex formation. The complex was then added into a 125 mL Erlenmeyer shaker flask which contained 30 million of HEK293F at a density of 1×10^6 cells/mL. Cells were incubated for 2 days on an orbital shaker orbited at an angular velocity of 130 rpm at 37°C in a humidified incubator under 92% air/8% CO_2. The transfected cells were subcultured every 3-4 days.

G418 selective antibiotic (ThermoFisher Scientific, USA) was used to generate stable LRG1 overexpressing HEK293F cells, from which conditioned medium was collected every 3 days. Conditioned medium was pooled and concentrated by ultrafiltration using an Amicon Ultra-15 Centrifugal Unit (Merck Millipore,

USA). His buffer kit (GE Healthcare, USA) was used to prepare binding (20 mM sodium phosphate, 0.5 M NaCl, 20 mM imidazole, pH 7.4) and elution (20 mM sodium phosphate, 0.5 M NaCl, 500 mM imidazole, pH 7.4) buffers used for rhLRG1 purification. Concentrated conditioned medium was buffer-exchanged into the binding buffer and incubated with Ni-Sepharose beads (GE Healthcare, USA) overnight at 4°C on a roller, after which recombinant LRG1 (rhLRG1) was eluted from the Ni-Sepharose beads using elution buffer. Eluted rhLRG1 was buffer-exchanged into PBS. The concentration of rhLRG1 was measured by Bradford protein assay (Bio-Rad, USA). The purity of the purified rhLRG1 was evaluated by SDS-PAGE followed by Coomassie Blue staining (Bio-Rad, USA) and Western blotting.

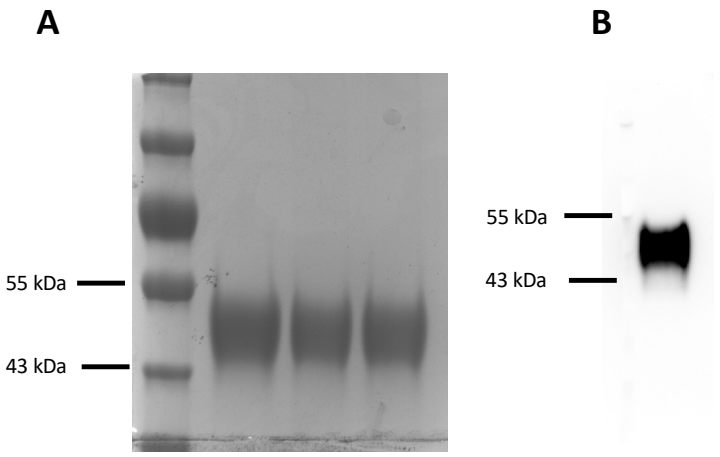

Figure 4.2: Evaluation of the purity of purified rhLRG1. The purity of purified rhLRG1 was evaluated by SDS-PAGE followed by (A) Coomassie Blue staining and (B) Western blotting.

4.2.8 Treatment with recombinant protein

TNF-α (PeproTech, UK) was used to induce endothelial activation. To investigate the effect of LRG1 on endothelial activation, ECs were pre-treated with rhLRG1 (250 μg/mL unless otherwise stated) for 24 h prior to activation with TNF-α (10 ng/mL) for another 24 h. PBS was used as a vehicle control

for both treatments. The same treatment was used for both static and shear experiments.

4.2.9 THP-1 cell capture assay

Twenty μL of HUVECs at a density of 1.5 $\times$ 10^6/mL were seeded into a microfluidic device with a straight channel (400 μm width $\times$ 100 μm height) and grown to 100% confluency in a humidified incubator. The cells were treated with 10 ng/mL TNF-α for 24 h, with or without 24 h of pre-treatment with rhLRG1 (250 μg/mL). After treatment, the device was mounted on a microscope stage-top incubator maintained at 37°C and the channel was washed twice with PBS. Using a peristaltic pump (P720, Instech Laboratories, USA), THP-1 cells at a density of 1.5 $\times$ 10^6/mL were then perfused for 15 minutes over the HUVECs monolayer at a rate that gave shear stress of 1 dyne/cm^2. The channel was subsequently washed with RPMI 1640 medium for another 10 minutes to remove any unbound cells. Phase-contrast images were taken at 10$\times$ magnification using an inverted phase-contrast microscope (Nikon Eclipse Ti, Nikon, Japan) for THP-1 cell counting. This assay was performed by Hui Min Tay and Dr Han Wei Hou, Nanyang Technological University, Singapore.

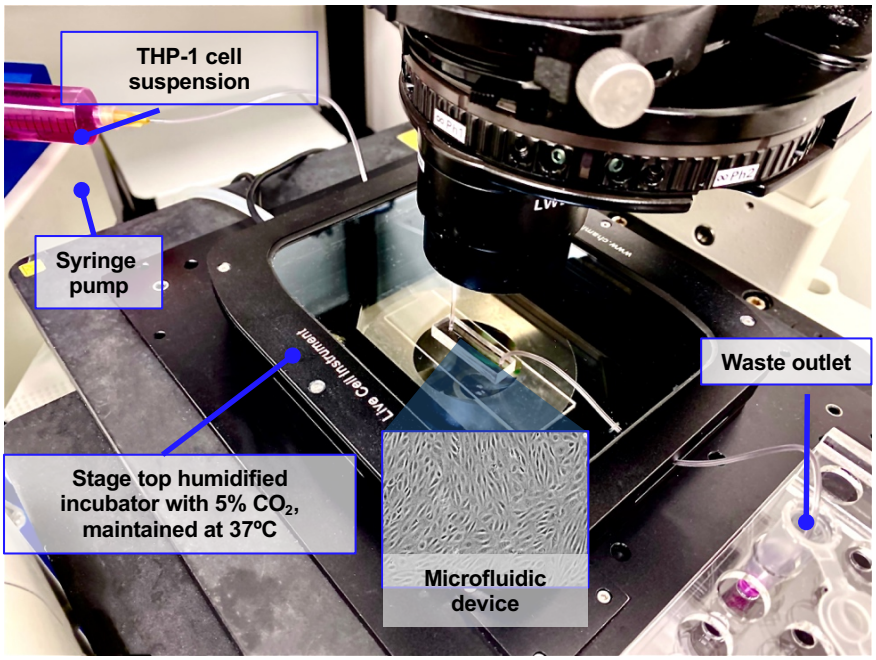

Figure 4.3: Setup of the THP-1 cell capture assay using a microfluidic chip. Photo courtesy of Hui Min Tay and Dr Han Wei Hou.

4.2.10 Fluorescent labelling of THP-1 cells with Calcein AM

THP-1 cells were labelled with Calcein AM as described in Section 3.2.9.

4.2.11 THP-1 cell adhesion assay for static experiment

One million Calcein AM-labelled THP-1 cells were applied to the monolayers of ECs in each 6-well plate and left for 1 h in a humidified incubator. Three washes with pre-warmed RPMI 1640 medium removed unbound THP-1 cells. Fluorescence from adhered THP-1 cells was measured using a plate reader (SpectraMax M5, Molecular Devices) with excitation and emission wavelengths of 495/520 nm. Relative fluorescence units (RFU) were converted to the absolute number of adhered THP-1 cells using a standard curve (Figure 4.4).

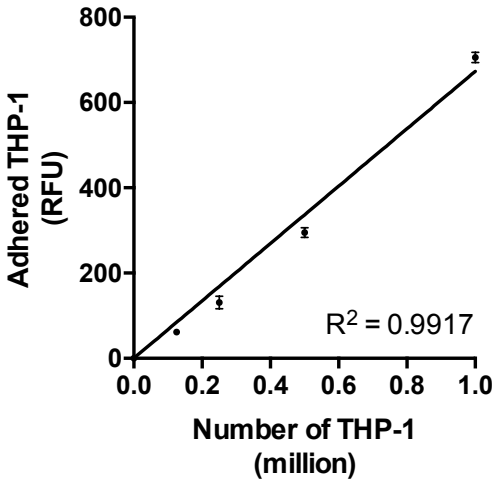

Figure 4.4: Standard curve of RFU against the number of adhered THP-1 cells.

4.2.12 Immunofluorescence staining of cleaved caspase-3

HUVECs were fixed with 4% paraformaldehyde (PFA, Sigma-Aldrich, UK) for 10 minutes, permeabilised with 0.1% Triton X-100 (Sigma-Aldrich, UK) for 5 minutes and blocked with 1% bovine serum albumin (BSA) for 1 h at room temperature. Cells were then incubated with rabbit anti-human cleaved caspase-3 antibody (#9661, Cell Signaling Technology, USA) at a 1:200 dilution in 1% BSA overnight at 4°C, followed by three washes in PBS and incubation with Alexa Fluor 488-labelled goat anti-rabbit IgG (A11008, ThermoFisher Scientific, USA) at a 1:300 dilution in PBS at room temperature for 1 h. Nuclei were stained with Hoechst 33342 (2 μg/mL, Thermofisher Scientific, USA) at a 1:1000 dilution in PBS for 15 minutes. Cleaved caspase-3 staining and nuclei were imaged with the inverted SP105F fluorescence microscope with a 20× objective, using a green fluorescent protein (GFP) filter set

(470/40 nm excitation filter, 495 nm dichroic mirror and 525/50 nm emission filter) and ultraviolet filter set (365/50 nm excitation filter, 400 nm dichroic mirror and 460/50 nm emission filter), respectively. The number of nuclei and cells with cleaved caspase-3 was quantified using a custom script written in MATLAB which distinguished stained nuclei by intensity and area thresholding. The MATLAB script was written by Dr Mean Ghim, Imperial College London, UK. The percentage of HUVECs stained with cleaved caspase-3 was calculated.

4.2.13 THP-1 cell transmigration assay

A 6.5mm-diameter Transwell® with 8 μm pore membrane was coated with 0.1% gelatin. Sixty thousand HAECs were seeded into the upper chamber of the gelatin-coated 6.5 mm-diameter Transwell® and were grown to confluence. Two hundred thousand Calcein AM-labelled THP-1 cells were resuspended in basal RPMI 1640 medium supplemented with 2% of fetal bovine serum (FBS) before being added to the top chamber of the Transwell®. Monocyte Chemoattractant Protein-1 (MCP-1) was diluted in RPMI 1640 medium supplemented with 10% FBS to reach a final concentration of 100 ng/mL, before being added to the lower chamber to serve as a chemoattractant. After 4 h incubation in a humidified incubator, the solution in the lower chamber, which contained transmigrated THP-1 cells, was collected. Transmigrated THP-1 cells remaining on the lower surface of Transwell® filter were dislodged by 5 minutes incubation with 5mM ethylenediaminetetraacetic acid (EDTA). Schematic diagram of THP-1 cell transmigration assay is shown in 4.5. Dislodged THP-1 cells were combined with the solution collected from the lower chamber earlier and centrifuged to collect a THP-1 cell pellet, which was resuspended in 100 μL of RMPI 1640 medium supplemented with 10% FBS. Resuspended THP-1

cells were transferred to a 96-well plate, and their fluorescence was measured in a plate reader. RFU were converted to the number of cells with a standard curve (Figure 4.6).

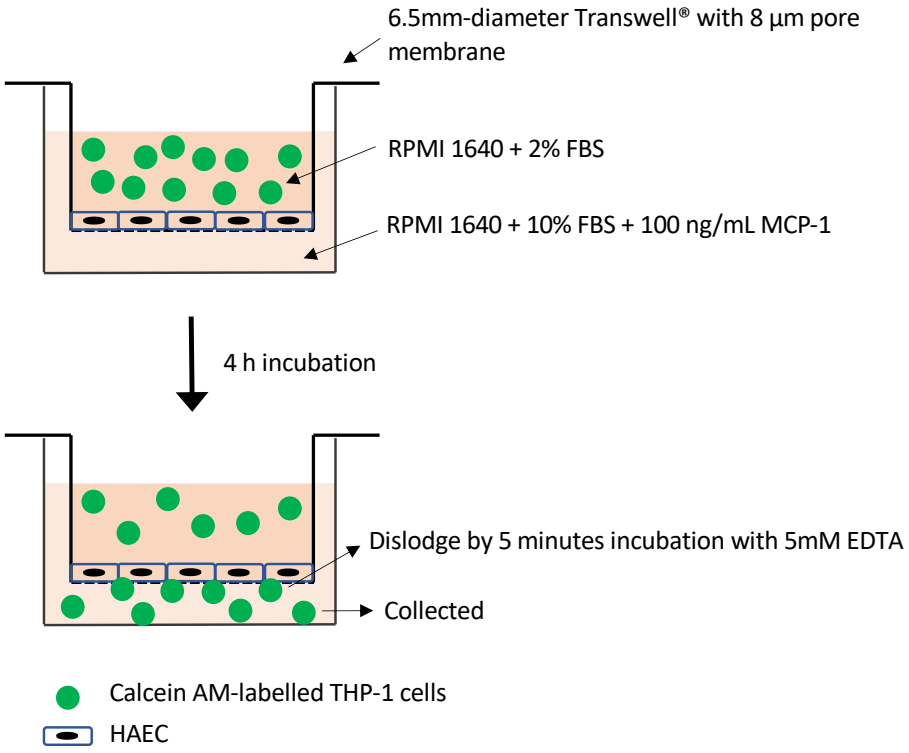

Figure 4.5: Schematic diagram of THP-1 cell transmigration assay.

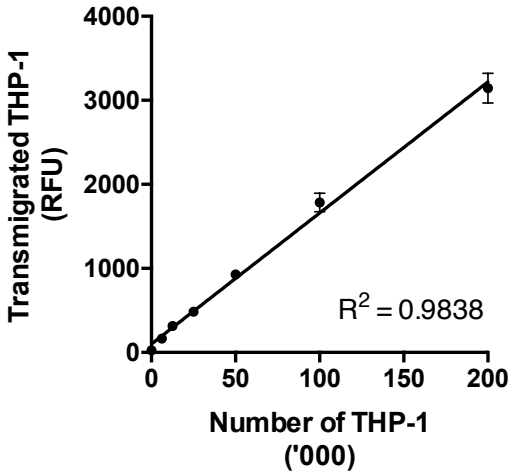

Figure 4.6: Standard curve of RFU against the number of transmigrated THP-1 cells.

4.2.14 THP-1 cell adhesion assay in a swirling-well system

THP-1 cell adhesion assay in a swirling-well system was performed as described in Section 3.2.10. HAECs were used instead of HUVECs.

4.2.15 Trypan blue exclusion assay

The trypan blue (Sigma-Aldrich, UK) exclusion assay was used to determine the viability of transfected ECs treated with TNF-α. Trypan blue solution was added to trypsinised ECs and loaded to haemocytometer to count the number of blue staining cells and the total number of cells. Culture medium was centrifuged to harvest the floating cells and the cells were counted using a haemocytometer. The percentage of dead cells was calculated and presented to show the effect of treatment on cell viability.

$$\%\ of\ dead\ cells = \frac{Non\text{-}adherent\ cells\ +\ stained\ adherent\ cells}{Non\text{-}adherent\ cells\ +\ adherent\ cells} \times 100\% \quad (4.1)$$

4.2.16 Detection of soluble tumour necrosis receptor 1 (sTNFR1) in conditioned medium

ECs were cultured in Endothelial Cell Growth Basal Medium-2 (EBM-2, Lonza, Switzerland) supplemented with 0.2% FBS for 24 h. Conditioned medium was collected and concentrated by ultrafiltration using an Amicon Ultra-15 Centrifugal Unit. Concentrated medium was subjected to Western blotting as described in section 3.2.11. Ponceau S staining was used as a loading control.

4.2.17 Inhibitor treatment

To investigate the mechanism of LRG1 activity in TNFR1 shedding, HAECs were pre-treated with inhibitors of ADAM10 (10μM, GI254023X, Sigma-Aldrich, UK), ALK1 (100nM, LDN193189, Sigma-Aldrich, UK), or ALK5 (10μM, SB431542, Stratech Scientific, UK) for 1 h, followed by treatment with 250 μg/mL of rhLRG1 for another 23 h. PBS and/or dimethyl sulfoxide (DMSO) were used as vehicle controls. HAECs were cultured in EBM-2 supplemented with 0.2% FBS for these inhibitor studies.

4.2.18 Animal work

Mouse blood was collected from 37-week old $Lrg^{-/-}$ mice and corresponding wild type controls using the terminal cardiac puncture method.

The collected blood was stored in a heparin-coated capillary tube, which were sealed with Critoseal® (Leica Biosystems, Germany) and stored upright at room temperature for 30 minutes for anticoagulation to occur. Plasma was obtained by centrifugation at 1600 g for 10 minutes and stored at –80°C. Animal experiments were performed in compliance with the guidelines of the Institutional Institutional Animal Care and Use Committee of Nanyang Technological University (A251). Dissection and blood collection were performed by Dr Rui Ning Chia, Nanyang Technological University, Singapore.

4.2.19 Enzyme-linked immunosorbent assay (ELISA)

The concentration of sTNFR1 in mouse plasma was measured using a commercial mouse sTNFR1 ELISA kit (R&D Systems, USA) according to the

manufacturer's protocol. Each sample was tested in duplicate.

4.2.20 Statistical analysis

Data are presented as mean ± standard error of the mean. Statistical analyses were performed by unpaired two-tailed Student's t-test or one-way ANOVA with Bonferroni's post hoc test using GraphPad Prism 6 (GraphPAD Software Inc., USA). The criterion for significance was $p<0.05$ (*$p<0.05$; **$p<0.01$; ***$p<0.001$; ****$p<0.0001$).

4.3 Results

4.3.1 LRG1 expression in ECs was increased by atherogenic flow and TNF-α

We exposed confluent HUVECs to two types of flow and to TNF-α. The established swirling-well system (which was developed and discussed in Chapter 2 and 3) was used to induce LMMF (putatively atherogenic flow) in the centre and HMUF (putatively atheroprotective flow) at the edge of the swirling well. Our study showed that LMMF significantly upregulated LRG1 protein levels and induced IκBα phosphorylation compared with HMUF (Figure 4.7 A-B, $p < 0.05$). Consistent with this observation, LRG1 mRNA expression in HAECs was also significantly increased by LMMF compared with HMUF (Figure 4.7 C, $p < 0.05$).

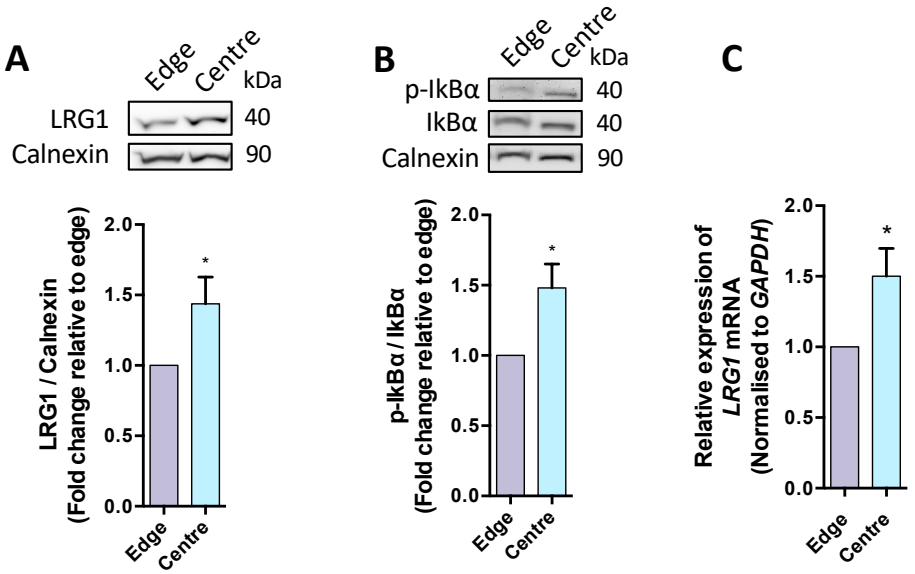

Figure 4.7: LRG1 expression in ECs was upregulated by LMMF. Representative Western blots and densitometry analysis of (A) LRG1 expression and (B) IκBα phosphorylation show that putatively atherogenic flow (centre) caused by a swirling 6-well plate upregulated the expression of LRG1 and IkBα phosphorylation in HUVECs, compared with putatively atheroprotective flow (edge). (C) LRG1 mRNA expression in HAECs was upregulated by atherogenenic flow (centre), compared with atheroprotectice flow (edge). (Unpaired two-tailed Student's t-test; n $\geq$ 5)

LRG1 protein expression in HUVECs was upregulated by TNF-α treatment (Figure 4.8 A, $p < 0.05$). Similarly, HUVECs subjected to 8 h and 12 h of TNF-α treatment showed a higher LRG1 mRNA expression than untreated control cells. No significant difference in LRG1 mRNA expression was observed after 1 h of TNF-α treatment. Similar observations were made in HAECs (Figure 4.8 C).

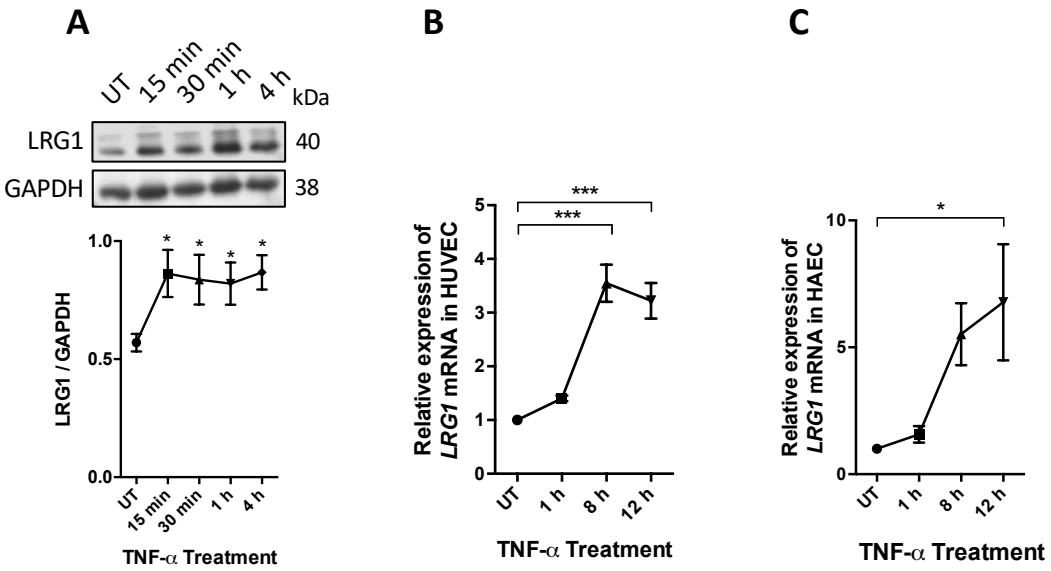

Figure 4.8: LRG1 expression in ECs was upregulated by TNF-α treatment. (A) Representative Western blot and densitometry analysis of LRG1 protein expression in HUVECs subjected to TNF-α treatment. qRT-PCT analysis of LRG1 mRNA levels in (B) HUVECs and (C) HAECs subjected to TNF-α stimulation. (One-way ANOVA followed by Bonferroni post hoc test, n $\geq$ 3)

Consistent with the upregulated expression of LRG1 in activated ECs, bioinformatic analysis of the human LRG1 promoter region led to the identification of five potential NF-κB binding sites (Figure 4.9), suggesting that LRG1 might be a direct target gene of NF-κB.

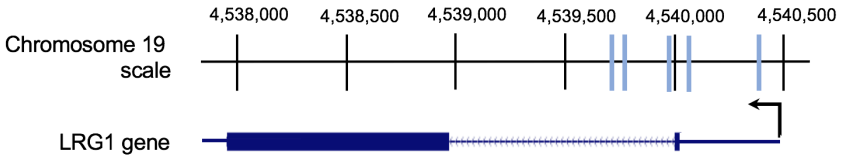

Figure 4.9: Putative NF-κB (RelA) binding sites are located within the LRG1 promoter downstream of the transcription start site. Schematic diagram shows the genomic region encompassing LRG1 locus including region upstream of transcription start site (bent arrow), untranslated region (thin blue line) and intron (thin blue line with arrow on it) are shown. Coding sequence is represented by thick blue line. Putative NF-κb (RelA) binding sites are shown as light blue bars. Five NF-κB binding sites were identified within the LRG1 promoter downstream of the transcription start site.

4.3.2 LRG1 overexpression was achieved by plasmid transfection

To investigate the functions of LRG1 in endothelial activation, we overexpressed it in HUVECs by transfecting the cells with pcDNA-LRG1-HIS plasmid. After 1 day of transfection, we observed elevated expressions of LRG1 in the conditioned medium and in the cell lysate as demonstrated by Western blot analysis and qRT-PCR analysis respectively (Figure 4.10).

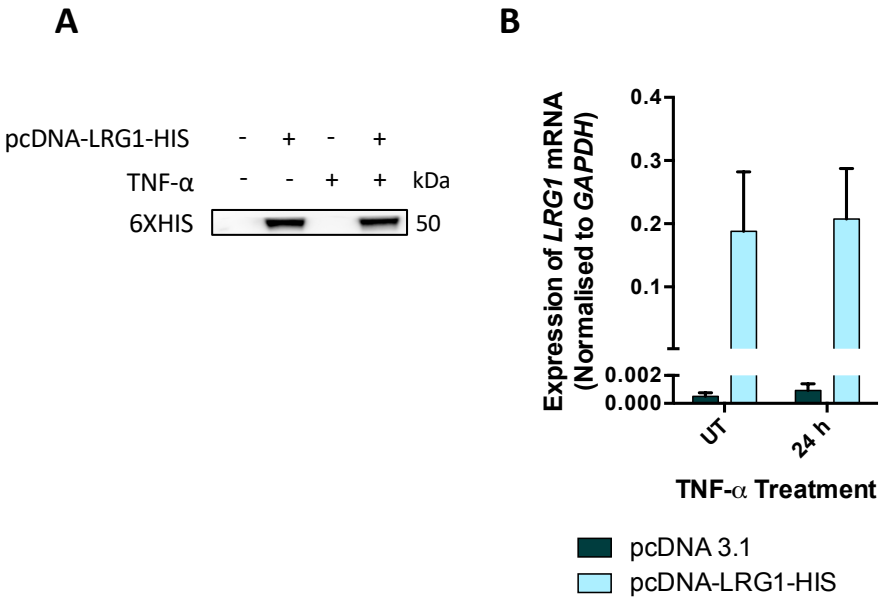

Figure 4.10: Overexpression of LRG1 in HUVECs was achieved by transfection of pcDNA-LRG1-HIS plasmid. (A) The presence of 6xHIS protein expression in conditioned medium and (B) increased LRG1 mRNA show that cells were successfully transfected with pcDNA-LRG1-HIS plasmid.

4.3.3 LRG1 overexpression suppressed TNF-α-induced endothelial activation

To study the impact of LRG1 on TNF-α-induced endothelial activation, HUVECs were treated with TNF-α 1 day after the transfection of LRG1 expres-

sion plasmid to induce endothelial activation. Our study showed a significant suppression of TNF-α-induced expression of cell adhesion molecules, VCAM-1 and ICAM-1, as well as the phosphorylation of downstream signalling transducer, IκBα, in LRG1-overexpressing HUVECs (Figure 4.11, $p < 0.05$, $p < 0.01$, $p < 0.05$, respectively).

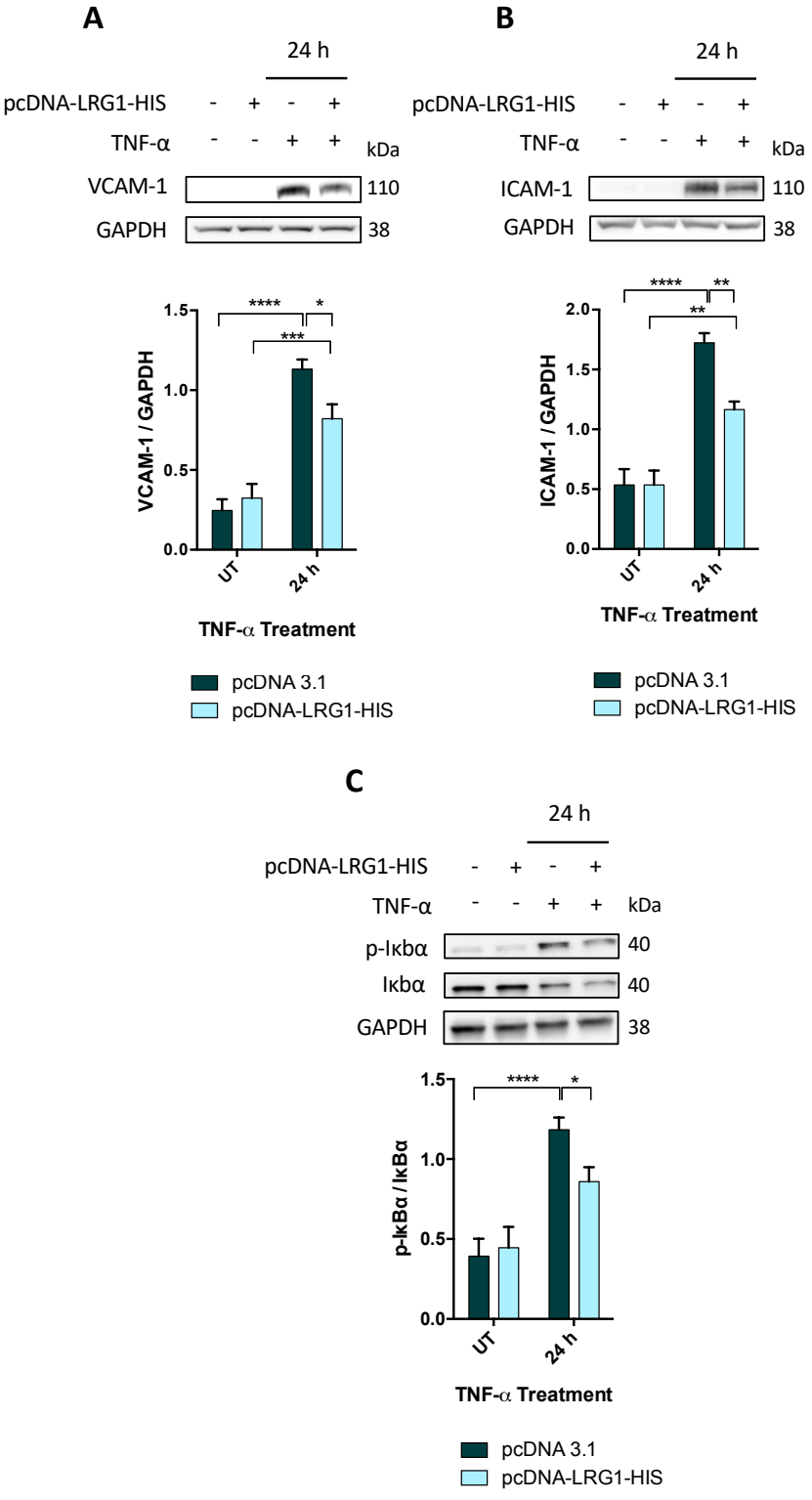

Figure 4.11: LRG1 overexpression in HUVECs suppressed TNF-α-induced endothelial activation. Representative Western blots and densitometry analysis of (A) VCAM-1, (B) ICAM-1, and (C) Ikbα phosphorylation in LRG1-overexpressing and control HUVECs subjected to TNF-α stimulation. (One-way ANOVA followed by Bonferroni post hoc test, n $\geq$ 6)

TNF-α-induced VCAM-1 mRNA level, but not ICAM-1 mRNA level, was also markedly lower in LRG1-overexpressing HUVECs (Figure 4.12).

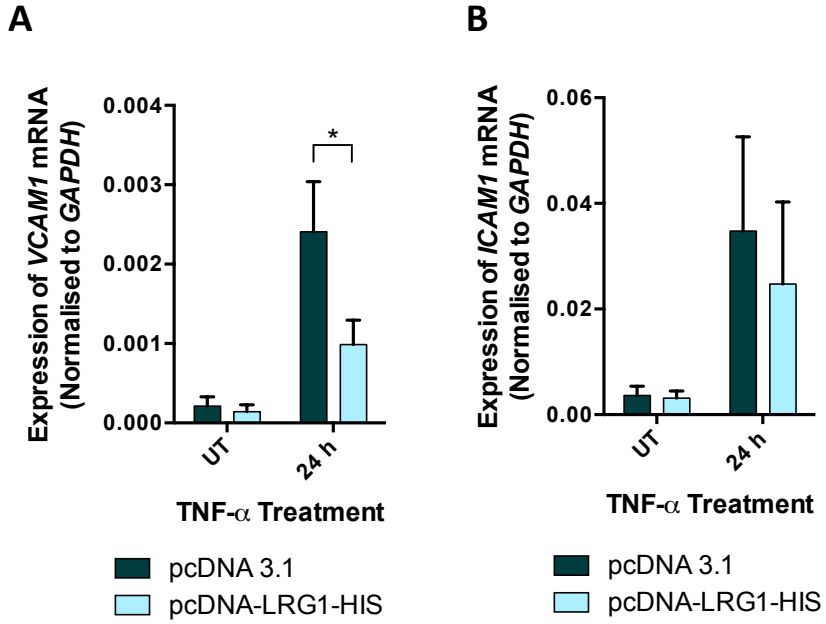

Figure 4.12: LRG1 overexpression in HUVECs suppressed VCAM-1 mRNA stimulated by TNF-α. mRNA levels of (A) VCAM-1 and (B) ICAM-1 in LRG1-overexpressing and control HUVECs stimulated by 24 h of TNF-α treatment. (One-way ANOVA followed by Bonferroni post hoc test, n = 4)

We then proceeded to check the activation of TNF-α downstream signalling transducers, IκBα and Akt, in LRG1-overexpressing HUVECs 30 minutes after TNF-α treatment. This is because signalling activation occurs within minutes after exposure to TNF-α treatment (Hoffmann et al., 2007). As expected, both the TNF-α-induced IκBα phosphorylation and Akt phosphorylation were significantly suppressed in LRG1-overexpressing HUVECs, compared with pcDNA3.1 transfected control cells (Figure 4.13, $p < 0.001$, $p < 0.05$, respectively).

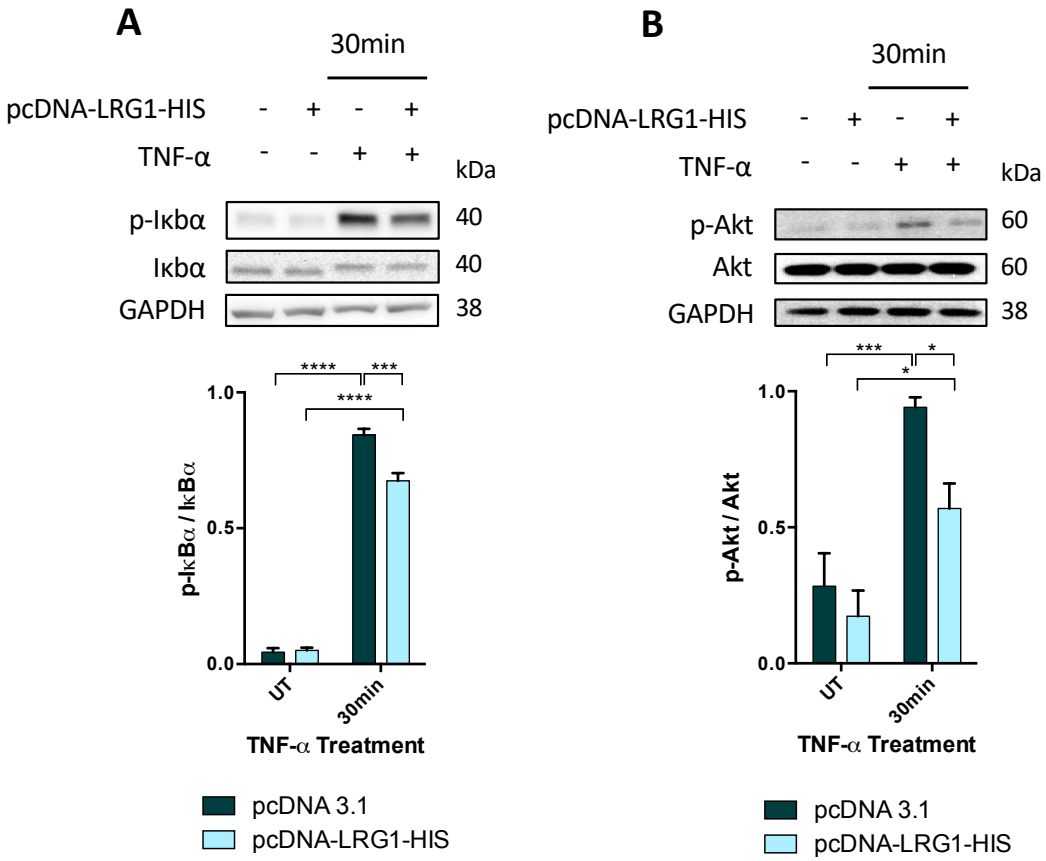

Figure 4.13: LRG1 overexpression in HUVECs suppressed TNF-α-activated IkBα and Akt. Representative Western blots and densitometry analysis of (D) Ikbα and (E) Akt phosphorylation in LRG1-overexpressing and control HUVECs stimulated by 30 minutes of TNF-α treatment. (One-way ANOVA followed by Bonferroni post hoc test, n = 5)

4.3.4 The effect of LRG1 on monocyte recruitment

Having demonstrated an inhibitory effect of LRG1 in TNF-α-induced activation of IκBα and Akt in HUVECs, we then investigated the effect of LRG1 on TNF-α- or flow-induced monocyte adhesion to ECs. Our results show that recombinant LRG1 (rhLRG1) dose-dependently suppressed TNF-α-induced THP-1 cell adhesion to HUVECs (Figure 4.14, $R^2 = 0.3403$, $p < 0.001$). The largest inhibitory effect—a 53% reduction compared with TNF-α treatment alone—was observed with 250 µg/mL of rhLRG1 treatment.

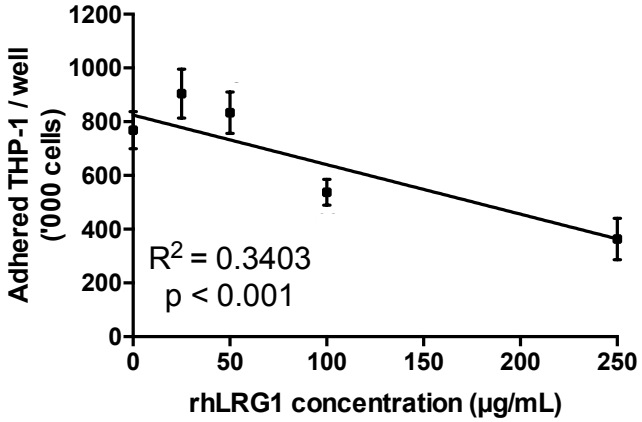

Figure 4.14: rhLRG1 treatment suppressed THP-1 cell adhesion to HUVECs activated by TNF-α in a dose-dependent manner. (Linear regression analysis, n $\geq$3)

To ensure that rhLRG1 does not induce apoptosis, HUVECs treated with different doses of rhLRG1 were stained with an antibody raised against cleaved caspase-3 a widely used marker for cell apoptosis. Our result show that rhLRG1 did not have any impact on the percentage of HUVECs expressing cleaved caspase-3 (Figure 4.15). For subsequent assays, 250 µg/mL of rhLRG1 was used.

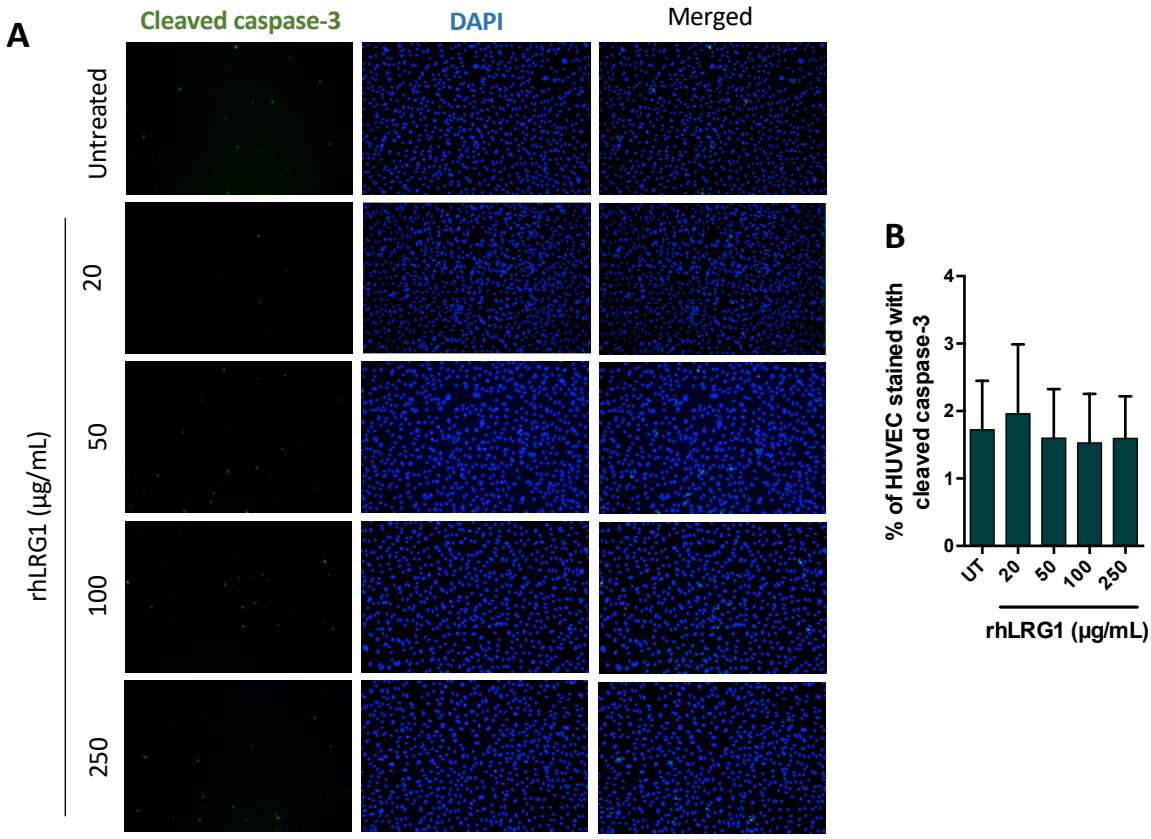

Figure 4.15: rhLRG1 did not induce apoptosis in ECs. (A) Representative images and (B) quantification of cleaved caspase-3-expressing (green) HUVECs. DAPI (blue) was used to stain cell nuclei. (One-way ANOVA followed by Bonferroni post hoc test, n = 3)

The recruitment of circulating monocyte to sub-endothelial space of the artery is a tightly regulated multi-step process, involving monocyte capture, firm adhesion, and transendothelial migration (Čejková et al., 2016). In this study, different *in vitro* assays were used to study the effect of LRG1 in these processes. rhLRG1 reduced THP-1 cell capture onto TNF-α-activated HUVECs under laminar flow in a microfluidic chip by 48%, compared with the PBS control (Figure 4.16, $p < 0.05$).

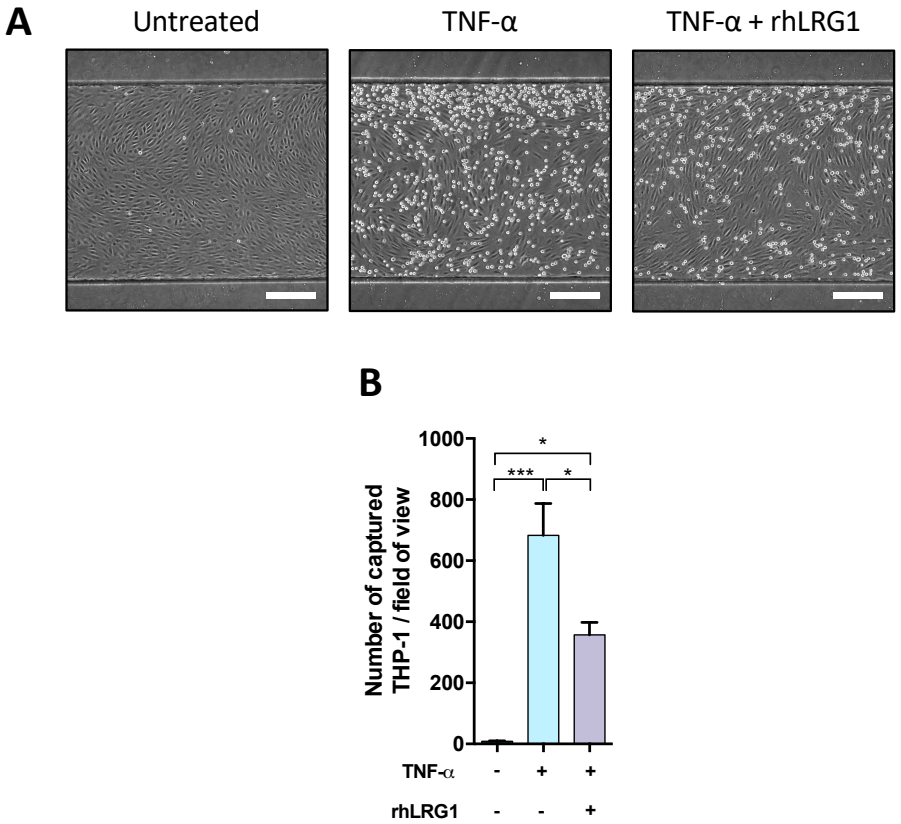

Figure 4.16: rhLRG1 treatment prevented TNF-α-induced THP-1 cell capture onto HUVECs under laminar flow in a microfluidic chip. (A) Representative images and (B) quantification of THP-1 cell captured onto HUVECs under flow in a microfluidic chip (scale bar = 100 μm). (One-way ANOVA followed by Bonferroni post hoc test, n = 4)

THP-1 cell adhesion to HAECs was also investigated under static condition. rhLRG1 treatment suppressed THP-1 cell adhesion to HAECs subjected to 6 h and 24 h of TNF-α stimulation by 26% and 24%, respectively (Figure 4.17, $p < 0.01$,$p < 0.01$, respectively).

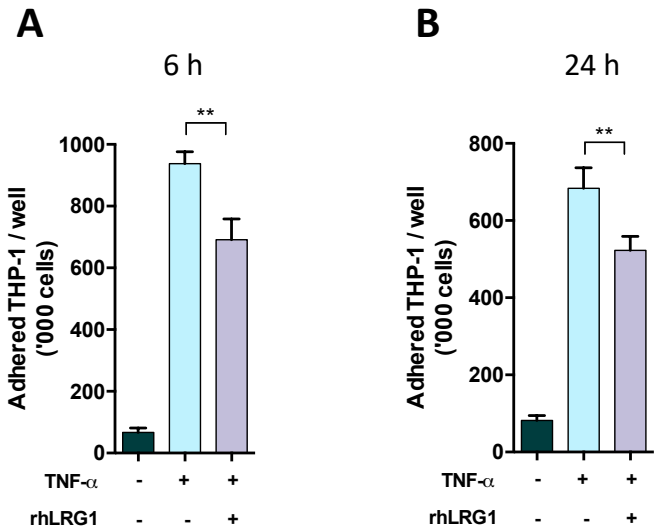

Figure 4.17: rhLRG1 treatment decreased TNF-α-induced THP-1 cell adhesion to HAECs under static condition. THP-1 cell adhesion to HAECs subjected to (A) 6 h and (B) 24 h of TNF-α treatment was significantly suppressed by rhLRG1 treatment. (One-way ANOVA followed by Bonferroni post hoc test, n $\geq$ 4)

The effect of rhLRG1 on monocyte transendothelial migration was also studied. rhLRG1 alone did not exert an effect on baseline migration; however, it prevented the TNF-α-induced migration of THP-1 cells across the HAEC monolayer (Figure 4.18, $p < 0.01$).

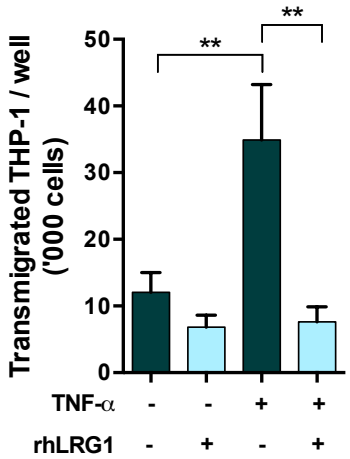

Figure 4.18: rhLRG1 treatment prevented TNF-α-induced THP-1 cell transendothelial migration through HAEC monolayers. (One-way ANOVA followed by Bonferroni post hoc test, n = 6)

Lastly, the orbital shaker method was used to study the effect of shear stress (LMMF or HMUF), TNF-α treatment, and the interplay between the two factors, on THP-1 cell adhesion to HAECs.

rhLRG1 had no effect on putatively atherogenic flow-induced THP-1 cell adhesion to HAEC. TNF-α treatment increased THP-1 cell adhesion to HAECs sheared by both flow conditions. The combination of TNF-α and putatively atherogenic flow gave greater adhesion of THP-1 cell to HAEC than the combination of TNF-α with putatively atheroprotective flow (Figure 4.19, $p < 0.0001$). rhLRG1 had no effect on THP-1 cell adhesion when TNF-α was combined with putatively atheroprotective flow but it reduced adhesion when TNF-α was combined with putatively atherogenic flow, although it did not completely eliminate the difference between both flow conditions (Figure 4.19, $p < 0.001$).

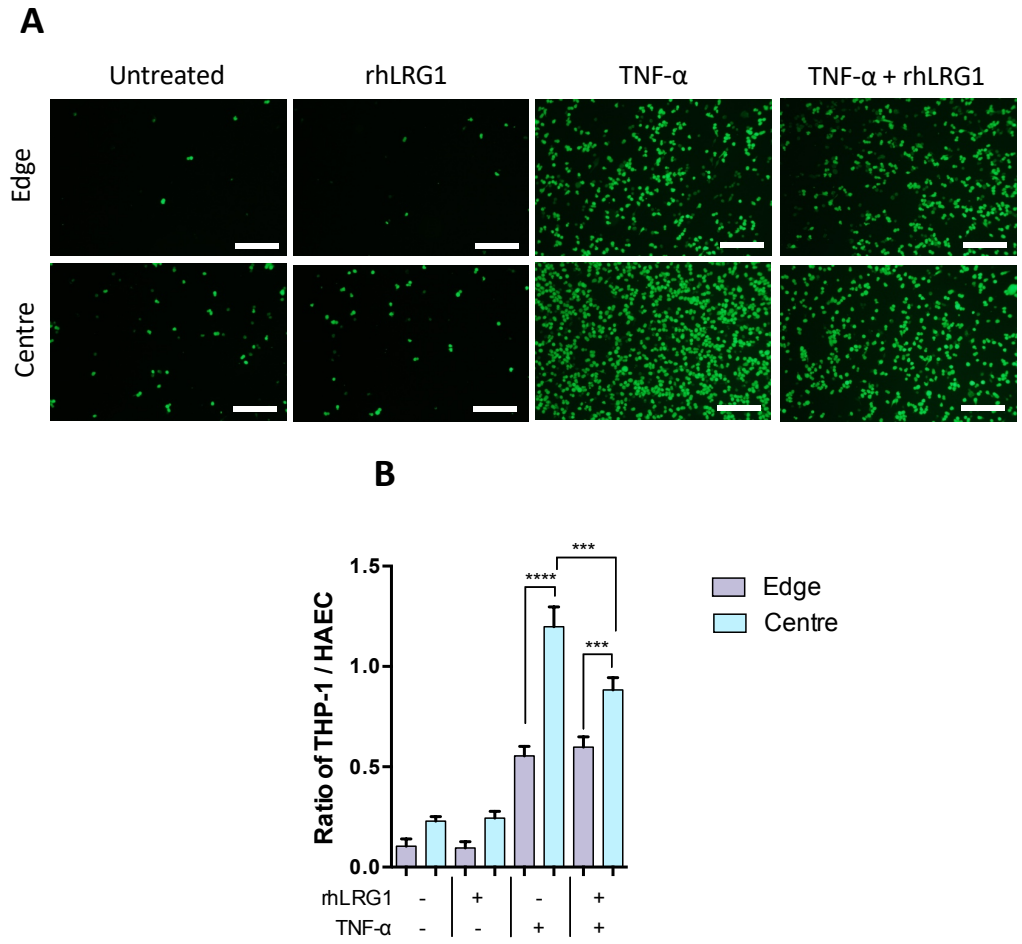

Figure 4.19: rhLRG1 significantly suppressed TNF-α-induced THP-1 cell adhesion under putatively atheroprone flow. (A) Representative images and (B) quantification of the number of Calcein-AM-stained THP-1 cells adhered to HAECs with different treatment and shear conditions using a swirling-well system (scale bar = 200 μm). Putatively atherogenic flow (centre) induced by the swirling 6-well plate increased THP-1 cell adhesion to HAECs under all treatment conditions, compared with putatively atheroprotective flow (edge). (One-way ANOVA followed by Bonferroni post hoc test, n = 5)

4.3.5 LRG1 overexpression suppressed TNF-α-induced apoptosis

Treatment with TNF-α increased the fraction of HUVECs that detached from the well plate and floated in the medium, regardless of whether LRG1 was overexpressed (Figure 4.20 A-B). TNF-α increased the number of non-viable

HUVECs, and its effect was abrogated by LRG1 overexpression (Figure 4.20 C, $p < 0.05$). Neither LRG1 overexpression or TNF-α treatment affected the total cell number (Figure 4.20 D). The percentage of TNF-α-induced dead cells was significantly reduced in LRG1-overexpressing HUVECs, compared with control (Figure 4.20 E, $p < 0.05$).

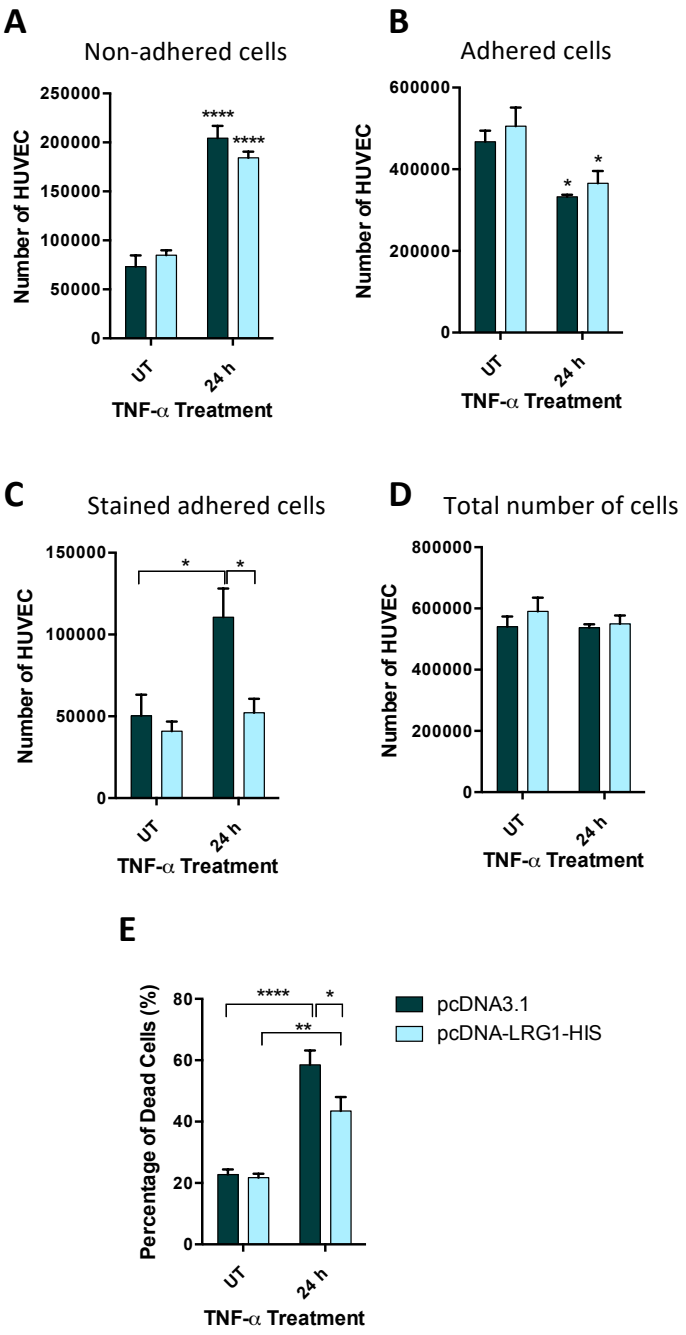

Figure 4.20: LRG1 overexpression significantly suppressed TNF-α-induced cell death compared with cells transfected with control plasmid. Number of (A) non-adhered, (B) adhered cells, (C) tryphan blue-stained adhered cells, and (D) total number of cells grown in a 6-well plate transfected with control or LRG1 plasmid, with and without TNF-α treatment. (Total number of cells = Non-adhered cells + adhered cells). (E) The percentage of dead cells in transfected HUVECs treated with TNF-α or PBS control. (One-way ANOVA followed by Bonferroni post hoc test, n = 4)

Consistent with the reduced number of non-viable cells in LRG1-overexpressing HUVECs treated with TNF-α, the level of TNF-α-induced expression of cleaved caspase-3 fragments (17/19 kDa) was significantly suppressed by the overexpression of LRG1 in HUVECs (Figure 4.21, $p < 0.05$).

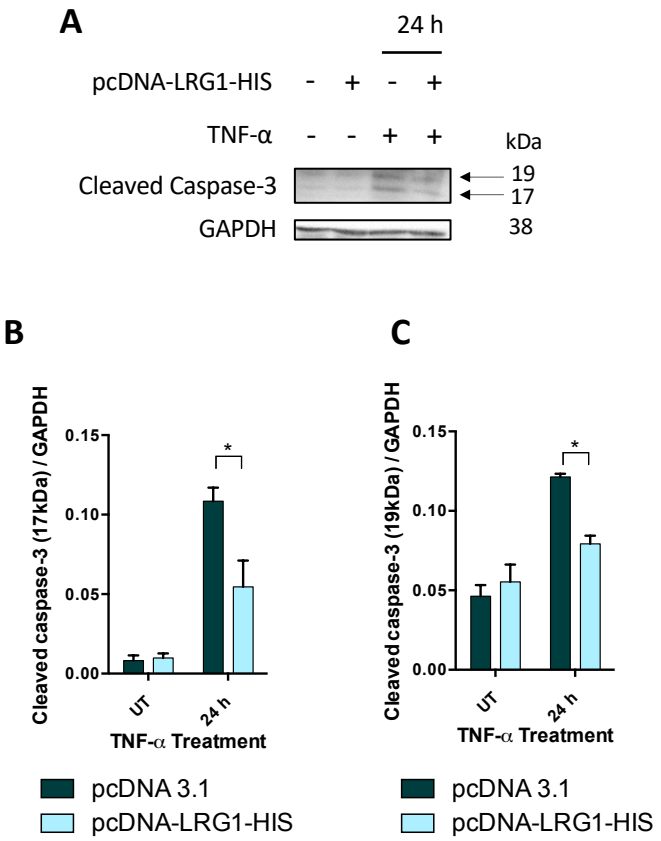

Figure 4.21: LRG1 overexpression significantly suppressed TNF-α-induced expression of cleaved caspase-3 in HUVECs. (A) Representative Western blots and (B-C) densitometry analysis of cleaved caspase-3 fragments (17 kDa and 19 kDa) expression in LRG1-overexpressing and control HUVECs stimulated by TNF-α treatment. (One-way ANOVA followed by Bonferroni post hoc test, n = 3)

4.3.6 LRG1 desensitised ECs to TNF-α by causing TNFR1 shedding via ALK5-SMAD2 pathway

Having established an inhibitory effect of LRG1 on endothelial TNF-α signalling and TNF-α-induced endothelial activation and apoptosis, we went on to explore the underlying molecular mechanisms of LRG1 action. Data presented in previous sections are consistent with LRG1 exerting its effect by modulating a receptor for TNF-α: NF-κB translocation, Akt phosphorylation, and activation of the apoptotic pathway can all be triggered by the same upstream receptor, TNFR1 (Sedger and Mcdermott, 2014).

Our study demonstrated a lower TNFR1 expression in the lysate of LRG1-overexpressing HUVECs but a higher level of sTNFR1 in the medium conditioned by LRG1-overexpressing HUVECs, compared with pcDNA3.1-transfected control HUVECs (Figure 4.22, $p < 0.05$, $p < 0.05$).

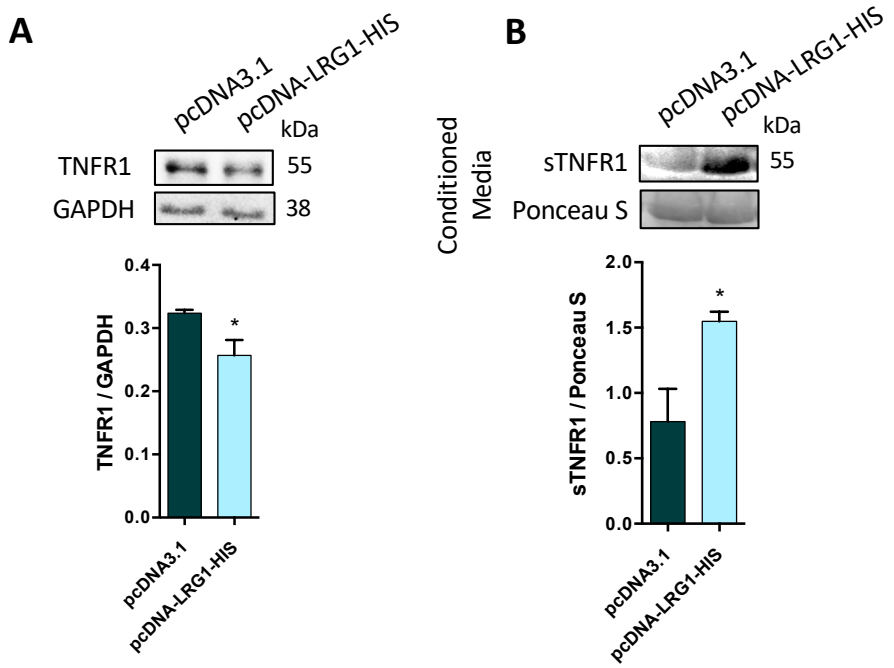

Figure 4.22: LRG1 overexpression resulted in TNFR1 shedding in HUVECs. Representative Western blots and densitometry analysis of (A) TNFR1 expression in LRG1-overexpressing and control HUVECs and (B) soluble TNFR1 level in their conditioned medium. (Unpaired two-tailed Student's t-test, n = 4)

LRG1 was previously reported to interact with different type I TGFβ receptors—ALK1 and ALK5 (Wang et al., 2013b). To understand whether LRG1-mediated TNFR1 shedding is dependent on TGFβ signalling, HAECs were treated with rhLRG1 in the presence or absence of either an ALK5 (SB431542) or an ALK1 (LDN193189) specific inhibitor.

Our study showed that SB431542 treatment (Figure 4.23 A, $p < 0.05$), but not LDN193189 treatment (Figure 4.24, $p > 0.05$), suppressed the rhLRG1-induced shedding of TNFR1. Intriguingly, we showed that rhLRG1 was able to induce SMAD2 phosphorylation in HAECs (Figure 4.23 B, $p < 0.0001$), suggesting that rhLRG1 exerted its effect on TNFR1 shedding via the ALK5-SMAD2 pathway; p-SMAD2 was absent in the presence of SB431542, with or without rhLRG1 (Figure 4.23 B).

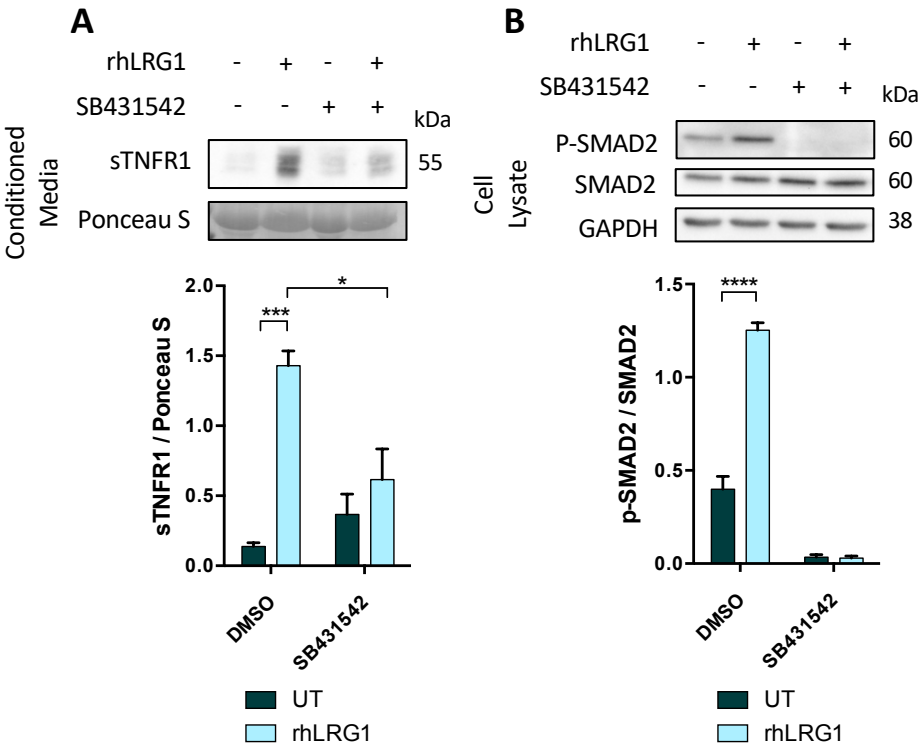

Figure 4.23: rhLRG1 caused TNFR1 shedding via the ALK5-SMAD2 pathway. Representative Western blots and densitometry analysis of (A) sTNFR1 level in the conditioned medium of HAECs and (B) SMAD2 phosphorylation in HAECs treated with rhLRG1 (or PBS as a control), and in some cases also with the ALK5 inhibitor, SB431542. rhLRG1 significantly increased the concentration of sTNFR1 in conditioned medium, and its activity was significantly reduced in the presence of the ALK5 inhibitor. rhLRG1 also increased SMAD2 activation, and the effect was diminished by the ALK5 inhibitor. (One-way ANOVA followed by Bonferroni post hoc test, n = 3)

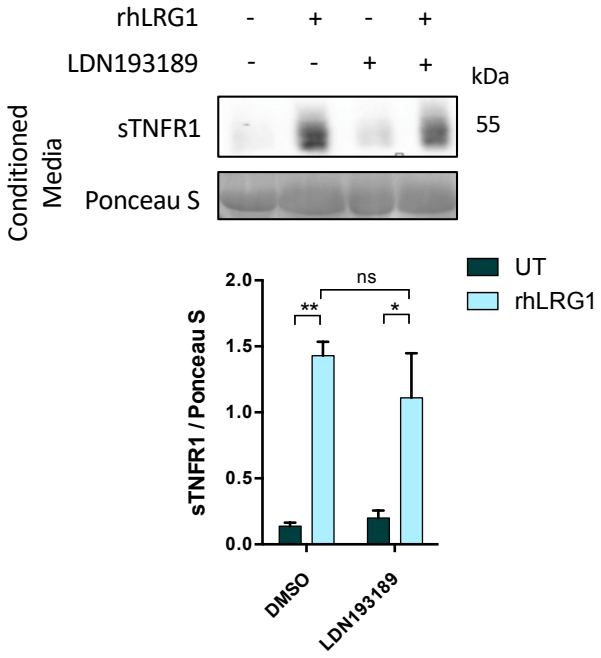

Figure 4.24: ALK1 inhibition did not influence the increase in TNFR1 shedding caused by rhLRG1. Representative Western blots and densitometry analysis of sTNFR1 level in the medium conditioned by HAECs treated with rhLRG1 (or PBS as a control), and in some cases also with the ALK1 inhibitor, LDN193189. rhLRG1 significantly increased the concentration of sTNFR1 in conditioned medium, and its activity was unaffected by ALK1 inhibitor treatment. (One-way ANOVA followed by Bonferroni post hoc test, n = 3)

4.3.7 LRG1-mediated TNFR1 shedding is dependent on ADAM10 activation

ADAM10 and ADAM17 are two key enzymes involved in TNFR1 shedding from the cell surface (Yang et al., 2015, 2017; Fischer et al., 2015). We found that the active form of ADAM10 protein and its mRNA were upregulated in HUVECs transfected with pcDNA-LRG1-HIS plasmid, compared with HUVECs transfected with control plasmid (Figure 4.25, $p < 0.01$ and $p < 0.05$). LRG1 overexpression did not affect ADAM17 expression (Figure 4.26).

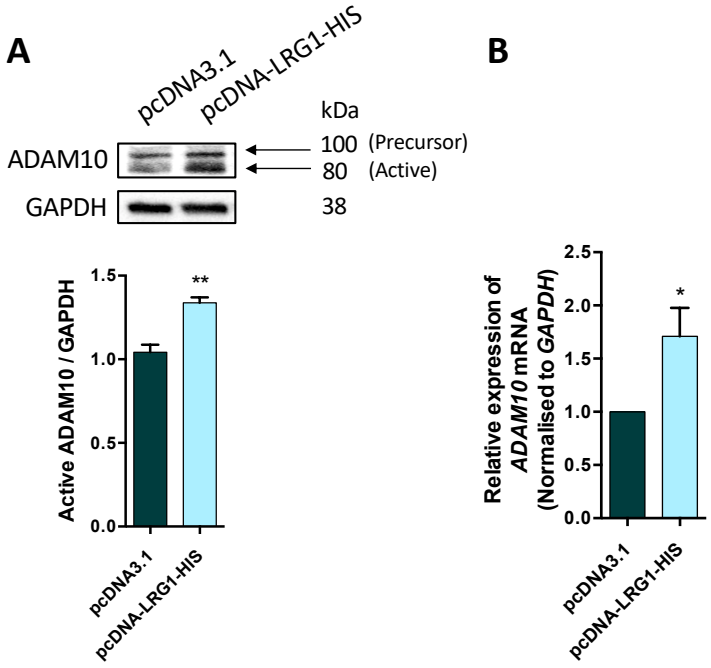

Figure 4.25: LRG1 overexpression significantly increased the expression of active ADAM10. (A) Representative Western blots and densitometry analysis and (B) qRT-PCR analysis of the expression of ADAM10 in LRG1-overexpressing and control HUVECs. (Unpaired two-tailed Student's t-test, n $\geq$ 3)

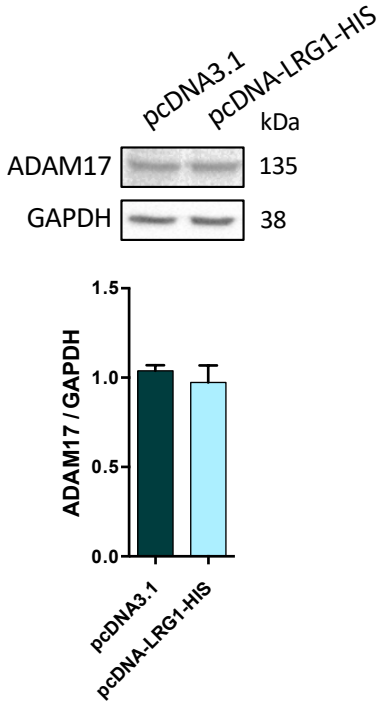

Figure 4.26: LRG1 overexpression had no effect on ADAM17 expression. Representative Western blots and densitometry analysis of ADAM17 expression in LRG1-overexpressing and control HUVECs.

To understand the role of ADAM10 in LRG1-mediated TNFR1 shedding, HAECs were treated with GI254023X, a potent ADAM10 inhibitor. Consistent with our previous observation, rhLRG1 significantly increased the concentration of sTNFR1 in HAECs conditioned medium, compared with conditioned medium from cells treated with the PBS-treated control cells. This promoting effect of rhLRG1 on TNFR1 shedding was significantly attenuated in the presence of GI254023X (Figure 4.27, $p < 0.01$).

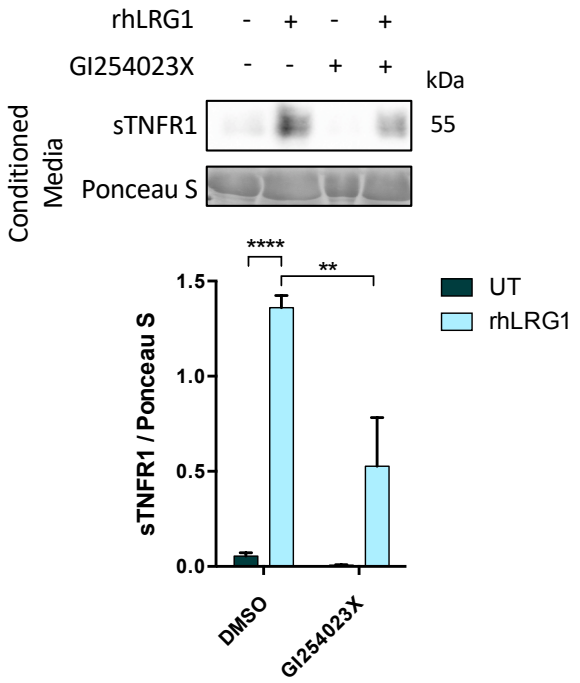

Figure 4.27: rhLRG1 induced TNFR1 shedding in a ADAM10-dependent manner Representative Western blot and densitometry analysis of sTNFR1 level in the conditioned medium of HAECs treated with rhLRG1 (or PBS as a control), and in some cases also with the ADAM10 inhibitor GI254023X. rhLRG1 significantly increased the concentration of sTNFR1 in conditioned medium, and its activity was significantly reduced in the presence of ADAM10 inhibitor. (One-way ANOVA followed by Bonferroni post hoc test, n = 4)

4.3.8 Plasma concentration of sTNFR1 was reduced in *Lrg1*$^{-/-}$ mice

Causality between LRG1 and TNFR1 shedding was investigated *in vivo* by measuring the concentration of sTNFR1 in the plasma of *Lrg1*$^{-/-}$ and wild type control mice. 37-week old *Lrg1*$^{-/-}$ mice had 33% lower plasma sTNFR1 concentrations than wild type mice (Figure 4.28, $p < 0.01$).

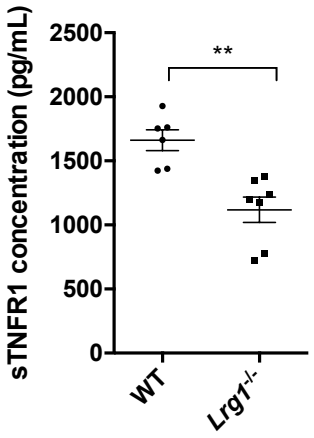

Figure 4.28: *Lrg1*$^{-/-}$ mice expressed lower plasma level of sTNR1 than wild type control. ELISA measurement revealed that the concentration of sTNFR1 in the plasma of 37-week-old *Lrg1*$^{-/-}$ mice was significantly lower than that in wild type counterparts. (Unpaired two-tailed Student's t-test, n $\geq$ 6)

4.4 Discussion

In this chapter, we revealed a novel role of LRG1 in the regulation of endothelial activation. LRG1 is intimately linked to inflammatory and autoimmune diseases (Xie et al., 2018; Ha et al., 2014; Serada et al., 2012; Watson et al., 2011; Yin et al., 2014; Pek et al., 2015), with higher LRG1 level reported in the serum of patients than healthy controls. To understand the role of LRG1 in inflammation and endothelial activation, we exposed cultured ECs to two known inducers of endothelial activation—putatively atherogenic flow (Ghim et al., 2017) and TNF-α (Collins, 1994).

We induced LMMF (putatively atherogenic flow) and HMUF (putatively atheroprotective flow) using a swirling-well system (as discussed in Chapters 2 and 3). LRG1 expression was upregulated after three days of LMMF exposure in HUVECs, compared with HMUF. White et al. (2011) have also shown that LRG1

gene expression was regulated by shear stress, but they only investigated normal versus pathologically-elevated unidirectional shear stress which is relevant only to stenotic arteries (GEO DataSet GDS3868). Instead, LMMF should be used as it is known to be responsible for the initiation of atherosclerotic lesions (Peiffer et al., 2013a).

TNF-α treatment upregulated LRG1 expression in ECs. This result is consistent with the work of Wang et al. (2017b), which also showed the upregulation and secretion of LRG1 in HUVECs after TNF-α treatment. Since both LMMF and TNF-α can induce endothelial activation through NF-κB activation, we proceeded to investigate the possibility of NF-κB-dependent induction of LRG1 expression. Indeed, bioinformatic analysis identified 5 potential NF-κB binding sites within the LRG1 promoter region. Liu (2019) has confirmed this in-silico data using Chromatin Immunoprecipitation (ChIP) assay; TNF-α promotes the binding of NF-κB to the LRG1 promoter region in human dermal microvascular endothelial cells. These data suggest that the upregulation of LRG1 in activated ECs is mediated by the NF-κB pathway.

To understand the functional consequence of elevated LRG1 expression in activated ECs, we either transfected ECs with a LRG1-expressing plasmid or subjected ECs to the treatment of rhLRG1. Our study demonstrated a strong inhibitory effect of LRG1 in shear- or TNF-α-induced endothelial activation. To the best of our knowledge, this is the first report showing that LRG1 has a regulatory role in endothelial activation. LRG1 reduced IκBα and Akt phosphorylation after 30 minutes of TNF-α treatment, and reduced the expression of VCAM-1 and ICAM-1 (both of which are the downstream of NF-κB pathway). Regulation of vascular adhesion molecules is thought to play a critical role in atherogenesis. For instance, mice with VCAM-1 mutation (Cybulsky et al., 2001) and ICAM-1 deficiency (Bourdillon et al., 2000) have decreased

atherosclerosis compared with control mice.

Vascular adhesion molecules are important players that mediate monocyte capture, adhesion, and subsequent transendothelial migration (Gerhardt and Ley, 2015). These processes are critical in atherosclerosis and other inflammatory diseases (Mestas and Ley, 2008). We found that rhLRG1 reduced monocyte capture on ECs under flow conditions, adhesion to ECs under static conditions, and transendothelial migration. rhLRG1 was also shown to suppress putatively atherogenic flow-induced monocyte adhesion to ECs. Interestingly, the effect of rhLRG1 on shear-induced monocyte adhesion was not observed without TNF-α treatment; it is possible that the effect of rhLRG1 can only be observed in high magnitude endothelial activation. These findings imply that LRG1 upregulation in human disease might reduce monocyte-endothelial interactions and monocyte infiltration into the subendothelial space of arteries.

TNF-α activates the NF-κB pathway by binding to TNFR1 (Fischer et al., 2015). Akt phosphorylation and the caspase-3-dependent apoptotic pathway are also induced by this receptor (Sedger and Mcdermott, 2014). All three were suppressed by LRG1, so we tested the hypothesis that LRG1 interfered with NF-κB signalling via TNFR1. We showed that the overexpression of LRG1 in HUVECs resulted in TNFR1 shedding into the overlying medium, suggesting that the inhibitory effect of LRG1 in TNF-α-induced ECs activation is mediated by the shedding of TNFR1. Shedding of TNFR1 from cell membrane desensitises cells to TNF-α ligands and soluble TNFR1 acts as an antagonist to circulating TNF-α (Giai et al., 2013). TNFR1 shedding is an important process in immunomodulation; knock-in mice with mutated non-cleavable TNFR1 are more susceptible to inflammation and autoimmune disorders (Xanthoulea et al., 2004). Patients with a rare genetic disease—TNF receptor-associated periodic syndrome (TRAPS) exhibit non-cleavable TNFR1; this is partially

responsible for their prolonged and unprovoked episodes of fever and inflammation of multiple organs (McDermott et al., 1999).

LRG1 was previously shown to interact with ALK1 and ALK5 receptors (Wang et al., 2013b), hence we examined their possible role in the effect of LRG1 on TNFR1 shedding. Inhibition of ALK5, but not ALK1, partially attenuated the effect of LRG1. The fact that the LRG1-mediated TNFR1 shedding was not fully abrogated by ALK5 inhibition implies the presence of other mechanisms. We also demonstrated that LRG1 alone can activate SMAD2 signalling in HAECs; ALK5-SMAD2 signalling has been shown to promote cell homeostasis (Goumans et al., 2009).

We further showed that the shedding of TNFR1 induced by LRG1 was mediated by ADAM10, an enzyme known to cause TNFR1 shedding in other contexts (Yang et al., 2015, 2017): LRG1-overexpressing HUVECs exhibited an increase in ADAM10 activation, and inhibition of ADAM10 partially abrogated the effect of LRG1 on TNFR1 shedding. We did not observe any changes in ADAM17, another key enzyme commonly involved in TNFR1 shedding.

The role of LRG1 in TNFR1 shedding was further investigated using *Lrg*1 knockout ($Lrg1^{-/-}$) mice. The concentration of sTNFR1 depends in part on TNFR1 shedding (Hawari et al., 2004). The reduction of plasma sTNFR1 in $Lrg1^{-/-}$ mice compared with wild type mice is consistent with the mechanism discussed above: absence of LRG1 resulted in partial impairment in TNFR1 shedding. It is, however, noteworthy that the concentration of sTNFR1 in $Lrg1^{-/-}$ was not reduced to zero, suggesting that there are other pathways responsible for TNFR1 shedding.

The NF-κB pathway has long been proposed as a therapeutic target in inflammatory and autoimmune diseases, but complete inhibition of TNF-α using a

neutralising reagent has resulted in disease exacerbation, risk of infections, and other side effects related to immune regulation and tissue regeneration (reviewed by Fischer et al. (2015)). Hence, attention has been redirected to the modulation of TNFR1. In light of the role of LRG1 in TNFR1 shedding, the potential therapeutic role of LRG1, including in atherosclerosis, should be investigated further.

In conclusion, this chapter presented compelling evidence for the novel role of LRG1 in endothelial activation. LRG1 expression is triggered by TNF-α and atherogenic flow, through the transcriptional activity of NF-κB. We have also showed that LRG1 is a novel suppressor of endothelial activation, including NF-κB activity and monocyte recruitments, by the shedding of TNFR1 via ALK5-SMAD2 signalling and ADAM10 activation. A model for the actions of LRG1 in endothelial activation is shown in Figure 4.29. Our understanding of LRG1 in endothelial activation might provide a new avenue for therapeutic discovery in inflammatory and autoimmune diseases.

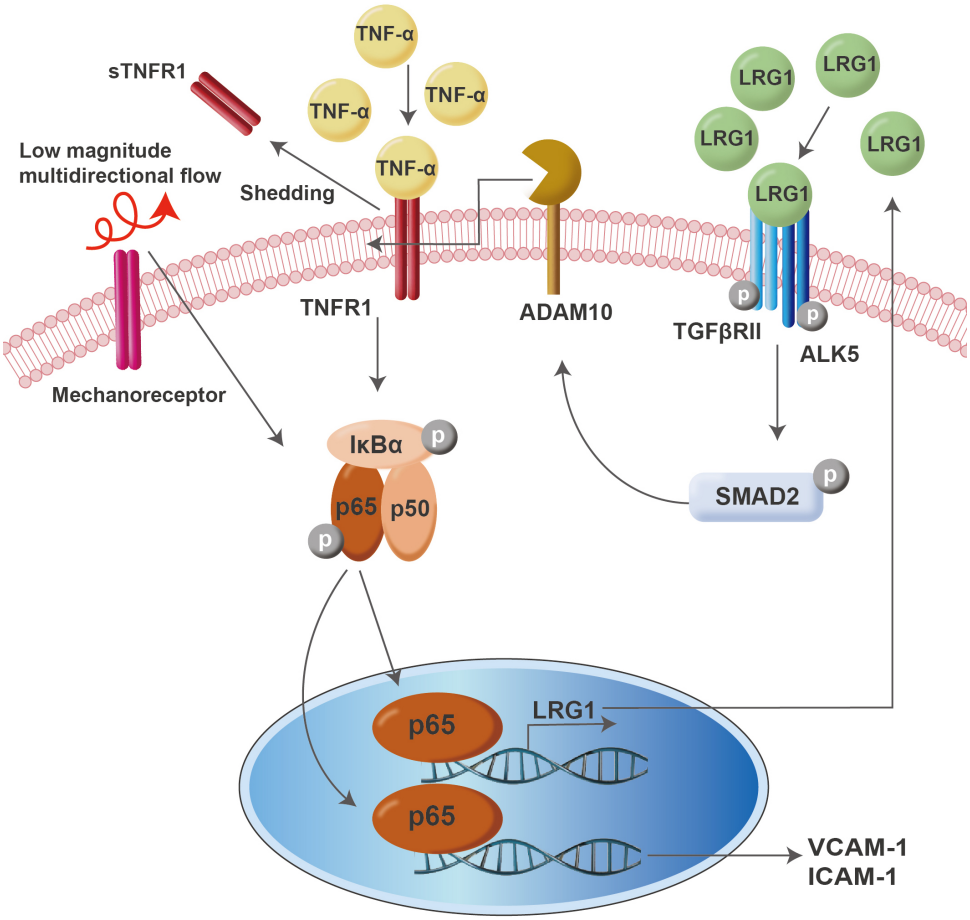

Figure 4.29: Working model of LRG1 activity in endothelial activation

Chapter 5

LRG1 in human atherosclerosis

5.1 Background

The previous chapter demonstrated a novel role of leucine-rich α-2-glycoprotein 1 (LRG1) in endothelial activation. LRG1 inhibits endothelial activation and monocyte recruitment by the shedding of tumour necrosis receptor 1 (TNFR1) mediated by ALK5-SMAD2 signalling and A Disintegrin and metalloproteinase domain-containing protein 10 (ADAM10) activation. However, our understanding of LRG1 in endothelial activation is limited to cultured ECs and a brief study of knockout mice.

Although many studies have shown that LRG1 is increased in the serum of patients with disease (Xie et al., 2018; Ha et al., 2014; Serada et al., 2012; Watson et al., 2011; Yin et al., 2014; Pek et al., 2015), there has been no study to investigate the expression of LRG1 in atherosclerotic tissues. The direct association of LRG1 and sTNFR1 expression in human diseases has not been investigated either.

This chapter will examine the clinical relevance of the *in vitro* data presented in Chapter 4. To do that, we collaborated with clinical partners from Harefield Hospital and Manchester Metropolitan University to obtain human clinical samples and examine the expression of LRG1 in these samples. We found that LRG1 is highly expressed in ECs of stenotic arteries, and is upregulated in the serum of critical limb ischemia (CLI) patients. We also established a correlation between LRG1 and sTNR1 expressions in the serum of CLI patients. These findings support our mechanistic understanding of LRG1 in endothelial activation, and imply that LRG1 may play a significant role in atherogenesis.

5.2 Methods and Materials

5.2.1 Collection of blood samples from CLI patients

Peripheral blood samples were collected from patients with CLI and CLI with diabetes on the day before their lower limb amputation (n=11/group). Peripheral blood samples were also collected from 11 healthy control participants. Clinical characteristics of healthy control participants and CLI patients are summarised in Table 5.1.

Characteristics	Healthy control	CLI	CLI + Diabetes
Age, Mean	40.0 ± 4.9	65.0 ± 15.3	71.6 ± 13.0
Gender (M/F) %	55/45	73/27	91/9
Number of patients	11	11	11

± Standard error mean

Table 5.1: Clinical characteristics of CLI patients.

Blood samples were centrifuged to isolate serum for analysis. All human

blood was obtained with informed consent and procedures were in accordance with institutional guidelines and the Declaration of Helsinki (Ethical reference: 14/NW/1062, approved by Manchester Metropolitan University Internal Ethics Approval Committee). Serum samples were collected, processed, and provided by Dr Fiona Wilkinson and Dr Ria Weston from Manchester Metropolitan University, UK.

5.2.2 Collection of coronary artery samples

Five-μm-thick sections of formalin-fixed, paraffin-embedded left anterior descending epicardial coronary arteries from deceased organ donors (non-stenotic, n=3), deceased patients with ischemic heart disease (stenotic, n=2) and dilated cardiomyopathy (stenotic, n=4) were obtained from Harefield Hospital, UK. Coronary arteries were obtained from a historical biobank of specimen collected prior to September 2006 and the implementation of the Human Tissue Act in the UK. Tissue was collected and stored with the permission of the patients who had expressed no objection to tissues removed during the course of their surgery being used for research and teaching purposes. Coronary arteries were harvested by Professor Sir Magdi Yacoub, processed by Dr Padmini Sarathchandra, and provided by Dr Adrian Chester, from Harefield Hospital, UK.

5.2.3 Elastic Van Gieson (EVG) staining of coronary artery sections

After deparaffinisation and rehydration, the coronary artery sections were immersed in Miller's elastin stain for 2 h at room temperature, followed by three

washes with deionised (DI) water. After the washing steps, sections were immersed in Van Giesson stain for 5 minutes at room temperature to stain elastic fibres (dark purple), collagen (pink to red), and muscle (yellow). Stained sections were rinsed with DI water before graded methanol dehydration followed by Histo-Clear. Slides were mounted using DPX mountant (Sigma-Aldrich, UK) before imaging. EVG staining was performed by Dr Padmini Sarathchandra, Harefield Hospital, UK.

5.2.4 Immunohistochemical staining of coronary artery sections

Deparaffinisation was performed by immersing slides three times in Histo-Clear (National Diagnostics, USA), twice in 100% ethanol, once in 90% ethanol, once in 70% ethanol, followed by rehydration in DI water (each step was performed for 5 minutes). Antigens were retrieved by soaking the slide in heated citrate buffer (pH 6, Sigma-Aldrich, UK) for 30 minutes at 100°C. After cooling and rinsing with DI water, the sections were incubated with 3% hydrogen peroxide (Sigma-Aldrich, UK) for 10 minutes to block endogenous peroxidase activity. The sections were equilibrated with Tris-buffered Saline (TBS) for 5 minutes. Nonspecific binding was blocked by incubating the sections with 10% goat serum (Sigma-Aldrich, UK) in TBS for 45 minutes. The sections were incubated with rabbit anti-LRG1 primary antibody (13224-1-AP, Proteintech, USA) at a 1:400 dilution in TBS diluent overnight at 4°C, followed by mouse anti-rabbit horseradish peroxidase-conjugated secondary antibodies (sc-2357, Santa Cruz Biotechnology, USA) at a 1:200 dilution in TBS diluent for 1 h at room temperature. The slides were then incubated in a substrate reagent containing diaminobenzidine (DAB+, Agilent, USA) for 5 minutes. Nuclei were counter-stained in Gill's Haematoxylin (Sigma-Aldrich, UK) for

30 s, followed by quick incubation with 1% acid alcohol (Sigma-Aldrich, UK) to produce crisp nuclear boundaries. Slides were mounted using Canada Balsam (Sigma-Aldrich, UK) after sequential dehydration steps. Buffers and reagents used in the immunohistochemical staining are summarised in Table 5.2. The percentage of EC stained with LRG1 was calculated.

Buffers	Components		Remarks
1M Tris	Tris	60.57 g	Adjust pH to 7.4
	DI water	Top up to 500 ml	
Tris-buffered saline buffer	1M Tris	50 ml	
(TBS)	NaCl	9g	
	DI water	Top up to 1 L	
TBS diluent	Bovine serum albumin	0.5 g	
	TBS buffer	50 ml	
1% acid alcohol	70% Ethanol	990 ml	
	Concentrated hydrochloric acid	10 ml	

Table 5.2: List of buffers and reagents used in immunohistochemical staining.

5.2.5 Enzyme-linked immunosorbent assay (ELISA)

The concentration of LRG1 and soluble TNFR1 (sTNFR1) in human serum was measured using a commercial human LRG1 ELISA (IBL, Japan) and a human sTNFR1 ELISA kit (R&D Systems, USA) according to the manufacturer's protocol. Each sample was tested in duplicate.

5.2.6 Statistical analysis

Data are presented as mean ± standard error of the mean. Statistical analyses were performed by unpaired two-tailed Student's t-test or one-way ANOVA with Bonferroni's post-hoc test using GraphPad Prism 6 (GraphPAD Software

Inc., USA). The criterion for significance was $p<0.05$ (*$p<0.05$; **$p<0.01$; ***$p<0.001$; ****$p<0.0001$).

5.3 Results

5.3.1 LRG1 was highly expressed in endothelial cells of stenotic arteries

Non-stenotic coronary artery sections from deceased organ donors (n=3) and stenotic coronary artery sections from deceased donors with ichemic heart disease (n=2) and dilated cardiomyopathy (n=4) were stained with an anti-LRG1 antibody. They were also stained with Elastic van Gieson to visualise the degree of stenosis of the artery (Figure 5.1 A). The percentage of LRG1-expressing ECs in stenotic arteries was 3-fold higher than that in non-stenotic control samples (Figure 5.1 B, $p < 0.001$).

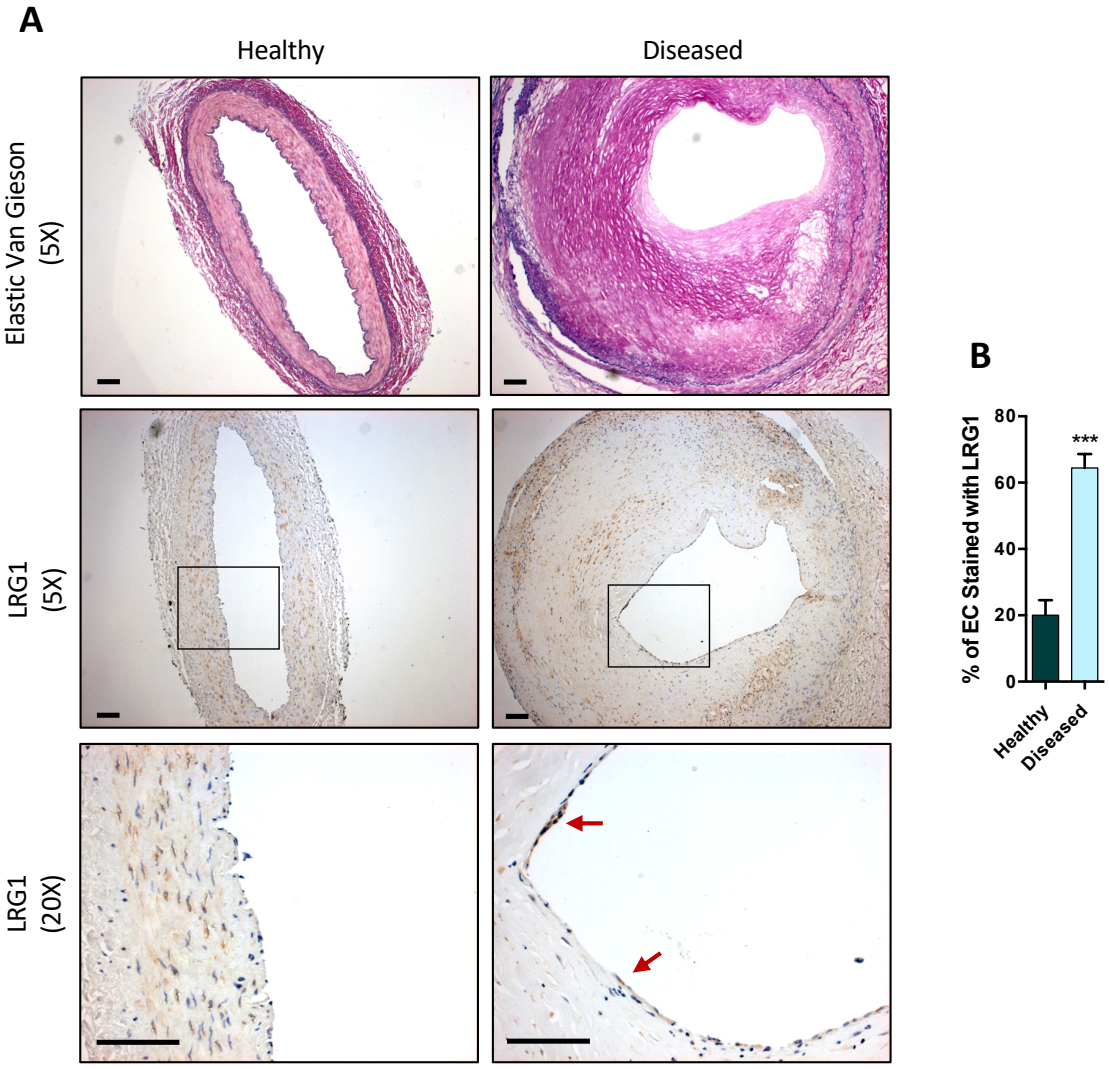

Figure 5.1: LRG1 was highly expressed in endothelial cells of stenotic arteries. (A) Elastic Van Gieson (EVG) and immunohistochemical staining of LRG1 in non-stenotic and stenotic coronary artery sections. (Scale bar = 100 μm) (B) Percentage of ECs stained with LRG1 in stenotic coronary arteries was significantly higher than non-stenotic coronary arteries. (Unpaired two-tailed Student's t-test; n $\geq$ 3)

5.3.2 Serum concentration of LRG1 was significantly higher in CLI patients

Serum LRG1 concentration in 22 patients with CLI, of which 11 were diagnosed with diabetes, was analysed and compared with that of 11 healthy subjects.

The clinical characteristics of these patients are summarised in Table 5.1. The LRG1 concentration in the serum of CLI patients and diabetic CLI patients were significantly higher than that in healthy controls [42.34 ± 6.09 µg/mL and 38.73 ± 3.51 µg/mL versus 11.44 ± 1.35 µg/mL, $p < 0.0001$ and $p < 0.001$, respectively]. There was no significant difference in the serum concentration of LRG1 between the two groups of CLI patients (Figure 5.2 A). The ability of LRG1 to differentiate CLI patients from healthy control was analysed using receiver operating curve (ROC) analysis. The area under curve (AUC) yielded results of 0.9339 and 0.9917 for CLI patients and diabetic CLI patients, respectively, compared with healthy controls (Figure 5.2 B, $p < 0.001$ and $p < 0.0001$, respectively).

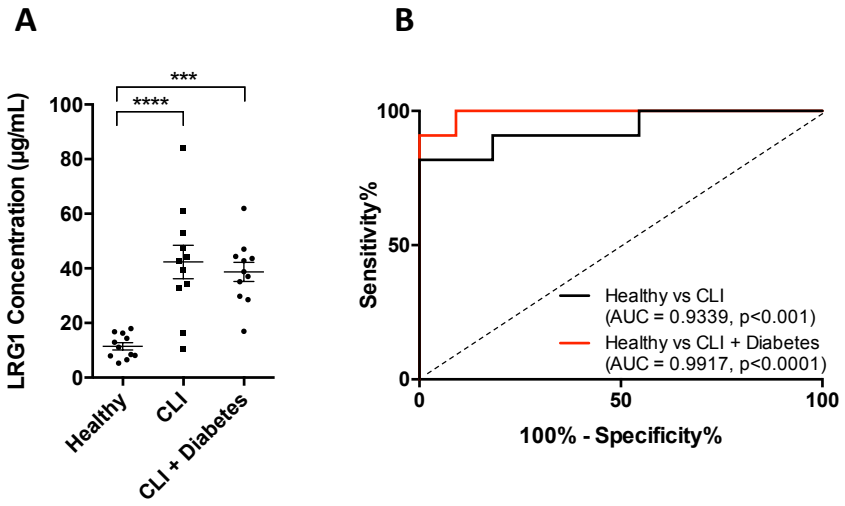

Figure 5.2: Serum LRG1 was significantly higher in patients with CLI. (A) ELISA measurement of LRG1 concentration in healthy control and CLI patients (with or without diabetes). (B) ROC curve analysis for the ability of serum LRG1 to differentiate between healthy control and CLI patients, and between healthy control and CLI patients with diabetes. (One-way ANOVA followed by Bonferroni post hoc test, n = 11/group)

5.3.3 Serum concentration of sTNFR1 was positively correlated with LRG1 in CLI patients

Our *In vitro* and mouse data suggest a link between LRG1 and TNFR1 shedding. To test whether the association is true in human subjects, we analysed serum sTNFR1 concentration in CLI patients, diabetic CLI patients, and healthy control patients. Our data revealed a significantly higher sTNFR1 level in serum of CLI patients, irrespective of the presence of diabetes, than that in serum of healthy controls [3.048 $\pm$ 0.436 µg/mL and 3.519 $\pm$ 0.419 µg/mL versus 1.128 $\pm$ 0.084 µg/mL, $p < 0.01$ and $p < 0.001$, respectively]. There was no significant difference in serum sTNFR1 concentration between the two groups of CLI patients (Figure 5.3 A). The ability of sTNFR1 concentrations to differentiate CLI patients from healthy controls was analysed using ROC analysis. The Area Under Curve (AUC) yielded results of 0.9503 and 1 between healthy controls and CLI patients or diabetic CLI patients, respectively (Figure 5.3 B, $p < 0.001$ and $p < 0.0001$, respectively).

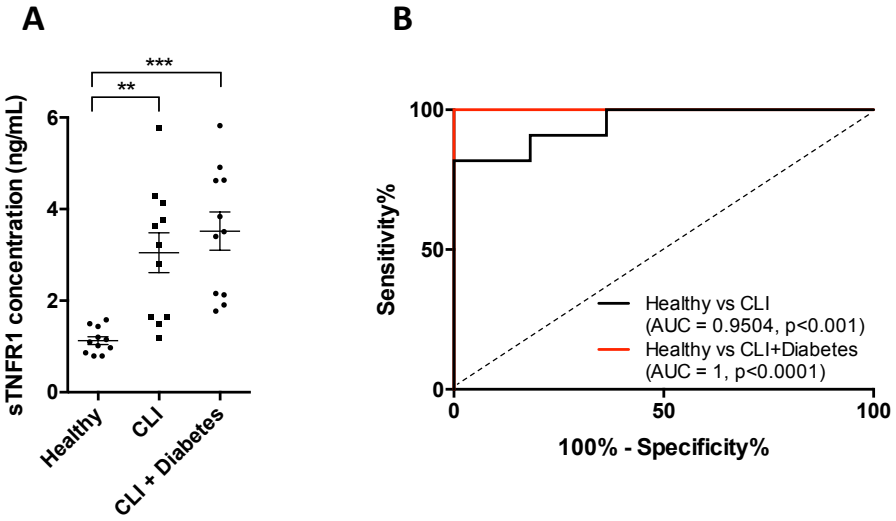

Figure 5.3: Soluble TNFR1 was significantly higher in the serum of CLI patients. A) ELISA measurement of sTNFR1 concentration in healthy control and CLI patients (with and without diabetes). (B) ROC curve analysis for the ability of serum sTNFR1 to differentiate between healthy control and CLI, and between healthy control and CLI with diabetes. (One-way ANOVA followed by Bonferroni post hoc test, n = 11/group)

Furthermore, there was a significant positive correlation between the expression of LRG1 and sTNFR1 in human serum (Figure 5.4, $R^2 = 0.601$, $p < 0.0001$).

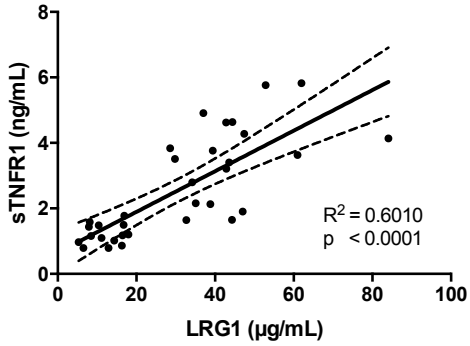

Figure 5.4: Serum concentration of LRG1 was significantly correlated with sTNFR1. (Linear regression analysis, n = 33; Dashed lines indicate the 95% confidence intervals for the regression line.)

5.4 Discussion

LRG1 expression has been found to be highly expressed in human liver (Uhlén et al., 2015) and cancerous tumours (Zhang et al., 2018; Andersen et al., 2010). Wang et al. (2013b) found that the retinal vasculature expressed LRG1, and that expression was upregulated during pathological remodelling. However, the expression of LRG1 in atherosclerotic tissues has not previously been characterised.

In our study, endothelial LRG1 expression was higher in stenotic arteries than non-stenotic arteries, suggesting a role for LRG1 in cardiovascular homeostasis and disease. This observation is consistent with the findings described in Chapter 4, which shown that the LRG1 expression is induced in activated ECs. Preliminary observations of high LRG1 expression in the medial layer and thickened intima of an artery (Figure A.1 and A.2) suggest that it is worth investigating the role of LRG1 in other cell types during atherogenesis.

Elevated serum LRG1 levels are intimately associated with various diseases, including different types of cancers (Zhang et al., 2018; Andersen et al., 2010; Furukawa et al., 2015), inflammatory bowel disease (Serada et al., 2012), joint disorders (Ha et al., 2014), and cardiovascular diseases (Xie et al., 2018; Watson et al., 2011; Yin et al., 2014). Recently, Pek et al. (2015) have demonstrated that type 2 diabetes (T2D) patients with peripheral arterial disease (PAD) had higher plasma LRG1 concentrations than T2D patients without PAD, and higher LRG1 is a predictor of arterial stiffness and endothelial dysfunction. On the other hand, Bos et al. (2017) saw a reduction in LRG1 expression in familial hypercholesterolemia (FH) patients with high atherosclerotic burden, compared with FH patients without atherosclerotic burden; LRG1 expression was not detected in FH patients who had a symptomatic coronary artery dis-

ease.

We observed a significantly higher serum LRG1 in patients with CLI, an advanced stage of PAD. CLI results from a progressive narrowing or blockage of arteries supporting the limb as a consequence of atherosclerosis (Santilli and Santilli, 1999). Intriguingly, there is no difference in serum LRG1 levels between CLI patients with diabetes and without diabetes suggesting the increase in circulating LRG1 is specifically associated with CLI. LRG1 has been proposed as a biomarker for various diseases (Ha et al., 2014; Serada et al., 2012; Watson et al., 2011; Yin et al., 2014; Bos et al., 2017). Our ELISA data and ROC analysis suggest that LRG1 might also be a biomarker for CLI; further investigation with a larger cohort is required.

The clinical relevance of the role of LRG1 on TNFR1 shedding, which has been described in Chapter 4, was investigated using serum samples of CLI patients. CLI patients expressed significantly higher serum concentrations of sTNFR1, which is consistent with another study on coronary atherosclerosis (Kim et al., 2017). We observed a positive correlation between the concentration of LRG1 and sTNFR1 in human serum; together with the mechanistic study of LRG1 on TNFR1 shedding described in Chapter 4, we speculate that the upregulation of serum LRG1 in inflammatory diseases like atherosclerosis might have an important role in modulating endothelial activation via the shedding of TNFR1.

In conclusion, results presented in this chapter can be interpreted together with the data described in Chapter 4. The upregulation of LRG1 in the ECs of stenotic arteries and the serum of CLI patients is likely to be a result of endothelial activation; then the upregulated LRG1 expression modulates endothelial activation, which might suggest a negative feedback mechanism, by the shedding of TNFR1 via ALK5-SMAD2 signalling and ADAM10 activation.

Chapter 6

Conclusion and future work

This chapter contains a summary of the key findings presented in this thesis and recommendations for future work to further our understanding of endothelial cell mechanobiology and the role of LRG1 in atherogenesis.

6.1 Summary of key findings

The swirling-well system is capable of generating a complex flow environment whilst permitting high throughput and chronic exposure of ECs to flow (Warboys et al., 2019). Chapter 2 described a CFD simulation of the flow behaviour in a swirling 6-well. This was necessary as specific parameters of the system used in this thesis had not been simulated before. WSS metrics—TAWSS, OSI, transWSS—were calculated at the base of the well. The data demonstrated that the centre and the edge of the well experience low magnitude multidirectional flow (LMMF, putatively atherogenic) and high magnitude uniaxial flow (HMUF, putatively atheroprotective), respectively; this closely mimics the pathological and physiological flow in human arteries (Giddens et al., 1993;

Gimbrone et al., 2000). Besides serving as a reference to those who are using the swirling-well system with the same parameters, the comprehensive understanding of the flow behaviour guided the design of experiments described in subsequent chapters.

As discussed in Section 1.9, mixing of soluble mediators released from sheared ECs (Burghoff and Schrader, 2011) masks the regional specific effect of shear on EC behaviour in the swirling well. This disadvantage has been resolved by the novel coating method described in Chapter 3. Regions of interest were coated with fibronectin, while the remaining surfaces were passivated with Pluronic F-127. This restricted cell growth only to the fibronectin-coated segments.

The coating method was evaluated by investigating the morphology of sheared HUVECs. Sheared HUVECs in full and segmented wells exhibited similar morphology: there was no evidence that the growth segmentation affects cell properties and morphology. HMUF significantly suppressed endothelial activation and the expression of EC adhesion molecules. An atheroprotective marker, eNOS phosphorylation, was also shown to be activated by HMUF.

The growth segmentation demonstrated that ECs release anti-inflammatory mediator(s) when exposed to HMUF. In TNF-α-treated HUVECs, segmentation increased monocyte adhesion in the centre but not at the edge of the well. This result suggests that HMUF at the edge of the well triggers the release of an anti-inflammatory mediator that suppresses endothelial activation in the centre of the well, where HUVECs were exposed to LMMF. When no cells were grown at the edge of the well, higher monocyte adhesion occurred at the centre of a segmented well.

Shear stress-mediated release of soluble mediators from ECs may be important in atherogenesis; however, the process is still poorly understood. Hence, the use

of this improved swirling-well system should be promoted as it enables accurate harvesting of the cells of interest and collection of the medium conditioned by cells exposed to a specific flow. It is necessary to segment cell growth to prevent the general mixing of soluble mediators that can corrupt apparent relations between shear and endothelial properties.

The improved swirling-well system was then adopted in the investigation of the expression of LRG1 in activated ECs. In Chapter 4, a novel role of LRG1 in endothelial activation was established. TNF-α and LMMF (generated using the improved swirling-well system) induce LRG1 expression in ECs through the transcriptional activity of NF-κB. It was also demonstrated that LRG1 suppressed endothelial NF-κB signalling, adhesion molecules expression, and monocyte recruitment to ECs. Mechanistically, LRG1 exerted its anti-inflammatory function by the shedding of TNFR1 through the ALK5-SMAD2 pathway and the activation of ADAM10.

Chapter 5 investigated the expression of LRG1 in sections of the stenotic coronary arteries and the concentration of LRG1 in the serum of critical limb ischemia (CLI) patients. LRG1 was highly expressed in ECs of stenotic arteries and found at elevated concentration in the serum of CLI patients. These results are consistent with the *in vitro* data discussed in Chapter 4: higher LRG1 expression was observed in activated ECs. A positive correlation was also observed between the concentration of LRG1 and sTNFR1 in human serum, which reaffirmed that LRG1 plays an important role in TNFR1 shedding.

As discussed in Section 1.10, LRG1 is highly expressed in the serum of patients with various diseases (Serada et al., 2010; Kimura et al., 2017; Rainer et al., 2017; Xuan et al., 2019; Pek et al., 2015; Watson et al., 2011) and its expression can be triggered by TNF-α in endothelial cells (Wang et al., 2017b). Results presented in Chapter 4 and 5 not only provided more evidence that

LRG1 is triggered in activated ECs, but also revealed a novel functional and molecular mechanism of LRG1 in endothelial activation. LRG1 has been proposed as a biomarker in various diseases due to its altered expression, but our understanding of LRG1 in endothelial activation suggest that the molecule is not merely a biomarker; it might have an important role in the pathogenesis of various diseases like atherosclerosis.

6.2 Future work

The findings presented in this thesis have opened new perspectives on endothelial mechanobiology and identified a novel role of LRG1 in endothelial activation. The role of LRG1 in the pathogenesis of diseases should be investigated further, and its therapeutic potential should be explored. Several recommendations for future work are outlined in this section that could further advance our understanding of the role of biomechanical factors and LRG1 in endothelial activation and atherogenesis.

6.2.1 Identification of soluble mediators in sheared endothelial cells

As shown in Chapter 3, segmenting cell growth using the coating method revealed the secretion of anti-inflammatory mediators. Although Burghoff and Schrader (2011) have investigated the nature of secretome by ECs under shear stress, they did not investigate the effects of multidirectional flow or chronic shear (>24 h). Multidirectional flow is an emerging and potentially important factor in atherogenesis (Peiffer et al., 2013a). Moreover, the results shown in Section 3.3.6 highlighted the importance of prolonged shear stress application

in the study of endothelial mechanobiology. Hence, the improved swirling-well system is a better platform that can induce complex and chronic multidirectional flow for the identification of soluble mediators.

Using the coating method, medium conditioned by ECs exposed to LMMF and HMUF can be collected. Proteomic approaches can be used to identify the nature of soluble mediators in the medium conditioned by sheared ECs. It would also be beneficial to perform metabolomics analysis of the conditioned medium, and genomics and transcriptomics analysis of the ECs exposed to LMMF and HMUF. Results from these integrated -omics analyses would provide unprecedented insights into the role of chronic LMMF in atherogenesis.

6.2.2 Understand endothelial cell biology with prolonged application of shear

HUVECs were unable to remain attached to segmented wells for more than 4 days of shear. This issue needs to be overcome in order to study the effect of even more prolonged shear application (7 days). One potential route is to test whether human aortic endothelial cells (HAECs) can remain attached after more prolonged shear application than HUVECs. Other possibilities involve altered substrate or medium composition. For example, cells may attach better in M199 than in DMEM (M.A. Schwartz, personal communication).

Other ECs phenotype such as proliferation, migration, endothelial to mesenchymal transition (EndMT), and permeability should be investigated after prolonged shear application. Warboys et al. (2010) have shown that acute and chronic exposure to shear stress has opposite effects on EC permeability. Hence, following the same logic, prolonged exposure to LMMF and HMUF might uncover new phenotypic observations which could not otherwise be dis-

covered with acute laminar or oscillatory shear application. ECs exposed to prolonged LMMF or HMUF and their conditioned medium should be analysed with integrative -omics to understand the effect of prolonged shear stress on ECs.

6.2.3 Further investigate the role of LRG1 in atherogenesis

Atherosclerosis is a complex disease that involves not only ECs, but also monocytes and smooth muscle cells (SMCs). Although a novel role of LRG1 in endothelial activation has been presented in this thesis, the role of LRG1 in atherogenesis is still unknown. A comprehensive understanding of the role of LRG1 in different cell types and atherogenesis is required, and may help to provide a new avenue for therapeutic discovery in atherosclerosis.

Oxidised LDL (ox-LDL) is a key molecule responsible for atherogenesis (Li and Mehta, 2005). In light of the role of LRG1 in the regulation of endothelial activation, it may also have a role in preventing ox-LDL-induced endothelial dysfunction. It would be interesting to incubate ECs with ox-LDL, with or without the treatment of recombinant LRG1, to study the effect of LRG1 in ox-LDL-induced endothelial dysfunction.

High LRG1 expression was observed in the medial layer and thickened intima of the coronary arteries (Figure A.1 and A.2). Foam cell formation and SMC migration are two key processes that contribute to intimal thickening (Basatemur et al., 2019; Woollard and Geissmann, 2010). The role of LRG1 in macrophage differentiation, foam cell formation, and SMC activation should therefore be investigated.

Angiogenesis (microvessel formation), a process that can be stimulated by plaque hypoxia, in an atherosclerotic plaque increases the risk of plaque rupture (Sluimer and Daemen, 2009). As discussed in Section 1.10, LRG1 promotes the angiogenic pathway (Wang et al., 2013b) and Hypoxia-inducible factor 1 subunit alpha (HIF-1α) activation (Zhang et al., 2016a). It is possible that high expression of LRG1, although shown to be beneficial in the regulation of endothelial activation, might be detrimental due to its pro-angiogenic role. LRG1 potentially has a paradoxical role in atherogenesis. The use of a transgenic animal model, specifically the apolipoprotein E (ApoE)/LRG1 double knockout mice ($ApoE^{-/-}Lrg^{-/-}$), could resolve this paradox. $ApoE^{-/-}$ mice are susceptible to developing atherosclerosis when fed a high-fat diet. Endothelial activation, lesion formation, foam cells formation, and SMCs activation can be investigated in such animals.

Bibliography

A. Allam, R. Thompson, L. Wann, M. Miyamoto, and G. Thomas. Computed Tomographic Assessment of Atherosclerosis in Ancient Egyptian Mummies To. *Journal of American Medical Association*, 302(19), 2009.

P. Alpresa. *Fluid Dynamics of Orbitally Shaken Shallow Fluid Layers*. PhD thesis, 2017.

P. Alpresa, S. Sherwin, P. Weinberg, and M. Reeuwijk. Orbitally shaken shallow fluid layers. I. Regime classification. *Physics of Fluids*, 30(032107), 2018.

R. Amer, L. Tiosano, and J. Pe'er. Leucine-Rich a -2-Glycoprotein-1 (LRG-1) Expression in Retinoblastoma. *Investigative Opthalmology & Visual Science*, 59:685–692, 2018.

R. Anada, K. Wong, J. Jayapalan, O. Hashim, and D. Ganesan. Panel of serum protein biomarkers to grade the severity of traumatic brain injury. *Electrophoresis*, 39(18):2308–2315, 2018.

J. Andersen, K. Boylan, R. Jemmerson, M. Geller, B. Misemer, K. Harrington, S. Weivoda, B. Witthuhn, P. Argenta, R. Vogel, and A. Skubitz. Leucine-rich alpha-2-glycoprotein-1 is upregulated in sera and tumors of ovarian cancer patients. *Journal of Ovarian Research*, 3(21), 2010.

T. Asakura and T. Karino. Flow Patterns and Spatial Distribution of Atherosclerotic Lesions in Human. *Circulation Research*, 66(4):1045–1067, 1990.

D. Baeriswyl, I. Prionisti, T. Peach, G. Tsolkas, K. Chooi, J. Vardakis, S. Morel, M. Diagbouga, P. Bijlenga, S. Cuhlmann, P. Evans, B. Kwak, Y. Ventikos, and R. Krams. Disturbed flow induces a sustained, stochastic NF-κB activation which may support intracranial aneurysm growth in vivo. *Scientific Reports*, 9(1):1–14, 2019.

G. Basatemur, H. Jørgensen, M. Clarke, M. Bennett, and Z. Mallat. Vascular smooth muscle cells in atherosclerosis. *Nature Reviews Cardiology*, 16(12): 727–744, 2019.

J. Beckman, M. Creager, and P. Libby. Diabetes and Atherosclerosis: Epidemiology, Pathophysiology, and Management. *The Journal of the American Medical Association*, 287(19):2570–2581, 2002.

R. E. Berson, M. Purcell, and M. K. Sharp. Computationally determined shear on cells grown in orbiting culture dishes. In *Oxygen Transport to Tissue XXIX*, pages 189–198. 2008.

K. Birukov, A. Birukova, S. Dudek, A. Verin, M. Crow, X. Zhan, N. DePaola, and J. Garcia. Shear stress-mediated cytoskeletal remodeling and cortactin translocation in pulmonary endothelial cells. *American Journal of Respiratory Cell and Molecular Biology*, 26(4):453–464, 2002.

A. Bond, S. Iftikhar, A. Bharath, and P. Weinberg. Morphological evidence for a change in the pattern of aortic wall shear stress with age. *Arteriosclerosis, Thrombosis, and Vascular Biology*, 31(3):543–550, 2011.

S. Bos, M. Phillips, G. Watts, A. Verhoeven, E. Sijbrands, and N. Ward. Novel protein biomarkers associated with coronary artery disease in statin-treated patients with familial hypercholesterolemia. *Journal of Clinical Lipidology*, 11(3):682–693, 2017.

M. Bourdillon, R. Poston, C. Covacho, E. Chignier, G. Bricca, and J. McGregor. ICAM-1 Deficiency Reduces Atherosclerotic Lesions in Double-Knockout Mice (ApoE -/-/ICAM-1 -/-) Fed a Fat or a Chow Diet. *Arteriosclerosis, Thrombosis, and Vascular Biology*, 20:2630–2635, 2000.

K. Boylan, J. Andersen, L. Anderson, L. Higgins, and A. Skubitz. Quantitative proteomic analysis by iTRAQ®for the identification of candidate biomarkers in ovarian cancer serum. *Proteome Science*, 8(31):1–9, 2010.

L. Bråne, L. Hovgaard, M. Nitulescu, E. Bengtsson, J. Nilsson, and S. Jovinge. Inhibition of Tumor Necrosis Factor-α Reduces Atherosclerosis in Apolipoprotein E Knockout Mice. *Arteriosclerosis, Thrombosis, and Vascular Biology*, 24:2137–2142, 2004.

M. Brockhaus, H. Schoenfeld, E. Schlaeger, W. Hunziker, W. Lesslauer, and H. Loetscher. Identification of two types of tumor necrosis factor receptors on human cell lines by monoclonal antibodies. *Proceedings of the National Academy of Sciences of the United States of America*, 87(4):3127–3131, 1990.

S. Burghoff and J. Schrader. Secretome of human endothelial cells under shear stress. *Journal of Proteome Research*, 10(3):1160–1169, 2011.

C. G. Caro, J. M. Fitz-Gerald, and R. C. Schroter. Atheroma and arterial wall shear. Observation, correlation and proposal of a shear dependent mass transfer mechanism for atherogenesis. *Proceedings of the Royal Society of London. Series B. Biological sciences*, 177:109–159, 1971.

M. Cavalcante, J. Torres-Romero, M. Lobo, F. Moreno, L. Bezerra, D. Lima, J. Matos, R. Moreira, and A. Monteiro-Moreira. A panel of glycoproteins as candidate biomarkers for early diagnosis and treatment evaluation of B-cell acute lymphoblastic leukemia. *Biomarker Research*, 4(1):1–8, 2016.

S. Čejková, I. Králová-Lesná, and R. Poledne. Monocyte adhesion to the endothelium is an initial stage of atherosclerosis development. *Cor et Vasa*, 58(4):e419–e425, 2016.

R. Chaerkady, P. Thuluvath, M. Kim, A. Nalli, P. Vivekanandan, J. Simmers, M. Torbenson, and A. Pandey. 18O labeling for a quantitative proteomic analysis of glycoproteins in hepatocellular carcinoma. *Clinical Proteomics*, 4(3-4):137–155, 2008.

A. Chakraborty, S. Chakraborty, V. Jala, B. Haribabu, M. Sharp, and R. Berson. Effects of biaxial oscillatory shear stress on endothelial cell proliferation and morphology. *Biotechnology and Bioengineering*, 109(3):695–707, 2012.

A. Chakraborty, S. Chakraborty, V. Jala, J. Thomas, M. Sharp, R. Berson, and B. Haribabu. Impact of Bi-Axial Shear on Atherogenic Gene Expression by Endothelial Cells. *Annals of Biomedical Engineering*, 44(10):3032–3045, 2016.

D. Chappell, S. Varner, R. Nerem, R. Medford, and R. Alexander. Oscillatory shear stress stimulates adhesion molecule expression in cultured human endothelium. *Circulation research*, 82:532–539, 1998.

B. Chen, Y. Li, Y. Zhao, K. Chen, S. Li, J. Lao, S. Yuan, J. Shyy, and S. Chien. DNA microarray analysis of gene expression in endothelial cells in response to 24-h shear stress. *Physiological Genomics*, 7:55–63, 2001.

Y. Chen, X. Liu, J. Wu, H. Ren, J. Wang, Z. Ding, and Y. Jiang. Proteomic analysis of cerebrospinal fluid in amyotrophic lateral sclerosis. *Experimental and Therapeutic Medicine*, 11(6):2095–2106, 2016.

K. J. Cheung, K. Tilleman, D. Deforce, I. Colle, and H. Van Vlierberghe. The HCV serum proteome: A search for fibrosis protein markers. *Journal of Viral Hepatitis*, 16(6):418–429, 2009.

J. Chiu, C. Chen, P. Lee, C. Yang, H. Chuang, S. Chien, and S. Usami. Analysis of the effect of disturbed flow on monocytic adhesion to endothelial cells. *Journal of Biomechanics*, 36(12):1883–1895, 2003.

J. Choi, H. Liu, D. Shin, G. Yu, J. Hwang, E. Kim, and J. Yun. Proteomic and cytokine plasma biomarkers for predicting progression from colorectal adenoma to carcinoma in human patients. *Proteomics*, 13:2361–2374, 2013.

S. Choi, J. Lim, Y. Kim, M. Song, W. Jung, J. Seo, J. Lee, and D. Sul. Plasma proteomic analysis of patients infected with H1N1 influenza virus. *Proteomics*, 14:1933–1942, 2014.

D. Chokchaichamnankit, K. Watcharatanyatip, P. Subhasitanont, C. Weeraphan, S. Keeratichamroen, N. Sritana, N. Kantathavorn, P. Ayudthaya, K. Saharat, J. Chantaraamporn, C. Verathamjamras, N. Phoolcharoen,

K. Wiriyaukaradecha, N. Paricharttanakul, W. Udomchaiprasertkul, T. Sricharunrat, C. Auewarakul, J. Svasti, and C. Srisomsap. Urinary biomarkers for the diagnosis of cervical cancer by quantitative label-free mass spectrometry analysis. *Oncology Letters*, 17(6):5453–5468, 2019.

P. Chong, Y. Sakai, H. Torisu, T. Tanaka, K. Furuno, Y. Mizuno, S. Ohga, T. Hara, and R. Kira. Leucine-rich alpha-2 glycoprotein in the cerebrospinal fluid is a potential inflammatory biomarker for meningitis. *Journal of the Neurological Sciences*, 392:51–55, 2018.

R. Codina, A. Vanasse, A. Kelekar, V. Vezys, and R. Jemmerson. Cytochrome c-induced lymphocyte death from the outside in: Inhibition by serum leucine-rich alpha-2-glycoprotein-1. *Apoptosis*, 15:139–152, 2010.

R. Collins, R. Velji, N. Guevara, M. J. Hicks, L. Chan, and A. Beaudet. P-selectin or intercellular adhesion molecule (ICAM)-1 deficiency substantially protects against atherosclerosis in apolipoprotein E-deficient mice. *Journal of Experimental Medicine*, 191(1):189–194, 2000.

T. Collins. NF-κB and IκBα: An Inducible Regulatory System in Endothelial Activation. *Journal of Experimental Medicine*, 179:503–512, 1994.

C. Cummings, J. Walder, A. Treeful, and R. Jemmerson. Serum leucine-rich alpha-2-glycoprotein-1 binds cytochrome c and inhibits antibody detection of this apoptotic marker in enzyme-linked immunosorbent assay. *Apoptosis*, 11:1121–1129, 2006.

K. Cunningham and A. Gotlieb. The role of shear stress in the pathogenesis of atherosclerosis. *Laboratory Investigation*, 85:9–23, 2005.

M. Cybulsky, P. Connelly, D. Milstone, M. Cybulsky, K. Iiyama, H. Li, S. Zhu, M. Chen, M. Iiyama, V. Davis, P. Connelly, and D. Milstone. A major role for VCAM-1 , but not ICAM-1 , in early atherosclerosis. *The Journal of Clinical Investigation*, 107(10):1255–1262, 2001.

A. Dardik, L. Chen, J. Frattini, H. Asada, F. Aziz, F. Kudo, and B. Sumpio. Differential effects of orbital and laminar shear stress on endothelial cells. *Journal of Vascular Surgery*, 41(5):869–880, 2005.

M. E. DeBakey, G. M. Lawrie, and D. H. Glaeser. Patterns of atherosclerosis and their surgical significance. *Annals of Surgery*, 201(2):115–131, 1985.

R. Dekker, S. Soest, R. Fontijin, S. Salamanca, P. Groot, E. VanBavel, H. Pannekoek, and A. Horrevoets. Plano Nacional de Pós-Graduação 2005-2010 ea reforma da educação superior do governo Lula. *Blood*, 100(5):1689–1698, 2002.

L. Druhan, A. Lance, S. Li, A. Price, J. Emerson, S. Baxter, J. Gerber, and B. Avalos. Leucine Rich α-2 Glycoprotein : A Novel Neutrophil Granule Protein and Modulator of Myelopoiesis. *PLoS ONE*, 12(1):1–13, 2017.

W. Enos, R. Holmes, and J. Beyer. Coronary Disease Among United States Soldiers Killed in Korea. *JAMA : the journal of the American Medical Association*, 152(12):1090–1092, 1953.

W. Enos, J. Beyer, and R. Holmes. Pathogenesis of coronary disease in american soldiers killed in korea. *Journal of the American Medical Association*, 158(11):912–914, 1955.

Y. Fang, D. Wu, and K. Birukov. Mechanosensing and mechanoregulation of endothelial cell functions. *Comprehensive Physiology*, 9(2):873–904, 2019.

R. Feaver, B. Gelfand, and B. Blackman. Human haemodynamic frequency harmonics regulate the inflammatory phenotype of vascular endothelial cells. *Nature Communications*, 4:1–11, 2013.

S. Feng, N. Bowden, M. Fragiadaki, C. Souilhol, S. Hsiao, M. Mahmoud, S. Allen, D. Pirri, B. Ayllon, S. Akhtar, A. A. Roger Thompson, H. Jo, C. Weber, V. Ridger, A. Schober, and P. Evans. Mechanical activation of hypoxia-inducible factor 1a drives endothelial dysfunction at atheroprone sites. *Arteriosclerosis, Thrombosis, and Vascular Biology*, 37(11):2087–2101, 2017.

S. Ferrero, D. Gillott, V. Remorgida, P. Anserini, N. Ragni, and J. Grudzinskas. Increased expression of one isoform of leucine-rich alpha-2-glycoprotein in peritoneal fluid of women with uterine leiomyomas. *Archives of Gynecology and Obstetrics*, 279:365–371, 2009.

N. Filipovic, K. Ghimire, I. Saveljic, Z. Milosevic, and C. Ruegg. Computational modeling of shear forces and experimental validation of endothelial cell responses in an orbital well shaker system. *Computer Methods in Biomechanics and Biomedical Engineering*, 19(6):581–590, 2016.

R. Fischer, R. Kontermann, and O. Maier. Targeting sTNF/TNFR1 Signaling as a New Therapeutic Strategy. *Antibodies*, 4:48–70, 2015.

C. Fish-Low, L. Than, K. Ling, Q. Lin, and Z. Sekawi. Plasma proteome profiling reveals differentially expressed lipopolysaccharide-binding protein among leptospirosis patients. *Journal of Microbiology, Immunology and Infection*, In Press, 2019.

I. Fleming, B. Fisslthaler, M. Dixit, and R. Busse. Role of PECAM-1 in the shear-stress-induced activation of Akt and the endothelial nitric oxide synthase (eNOS) in endothelial cells. *Journal of Cell Science*, 118(18):4103–4111, 2005.

I. Fleming, B. Kwak, and M. Meens. *The endothelial cell*, volume 1. 2017.

J. Florian, J. Kosky, K. Ainslie, Z. Pang, R. Dull, and J. Tarbell. Heparan sulfate proteoglycan is a mechanosensor on endothelial cells. *Circulation research*, 93(10), 2003.

D. Fry. Certain Chemorheologic Considerations Regarding the Blood Vascular Interface with Particular Reference to Coronary Artery Disease. *Circulation*, 40(5s4):38–57, 1969.

K. Furukawa, K. Kawamoto, H. Eguchi, M. Tanemura, T. Tanida, Y. Tomimaru, H. Akita, N. Hama, H. Wada, S. Kobayashi, Y. Nonaka, S. Takamatsu, S. Shinzaki, T. Kumada, S. Satomura, T. Ito, S. Serada, T. Naka, M. Mori, Y. Doki, E. Miyoshi, and H. Nagano. Clinicopathological Significance of Leucine-Rich α 2-Glycoprotein-1 in Sera of Patients With Pancreatic Cancer. *Pancreas*, 44(1):93–98, 2015.

E. Galkina and K. Ley. Vascular Adhesion Molecules in Atherosclerosis. *Arteriosclerosis, Thrombosis, and Vascular Biology*, 27:2104–2112, 2007.

Y. Gao, J. Zhou, Z. Xie, J. Wang, C. Ho, Y. Zhang, and Q. Li. Mechanical strain promotes skin fibrosis through LRG-1 induction mediated by ELK1 and ERK signalling. *Communications Biology*, 2(359), 2019.

G. García-Cardeña, J. Comander, K. Anderson, B. Blackman, and M. Gimbrone. Biomechanical activation of vascular endothelium as a determinant of its functional phenotype. *Proceedings of the National Academy of Sciences of the United States of America*, 98(8):4478–4485, 2001.

T. Gerhardt and K. Ley. Monocyte trafficking across the vessel wall. *Cardiovascular Research*, 107(3):321–330, 2015.

B. Ghafouri, A. Carlsson, S. Holmberg, A. Thelin, and C. Tagesson. Biomarkers of systemic inflammation in farmers with musculoskeletal disorders; A plasma proteomic study. *BMC Musculoskeletal Disorders*, 17(206):1–11, 2016.

M. Ghim, P. Alpresa, S. Yang, S. Braakman, S. Gray, S. Sherwin, M. Reeuwijk, and P. Weinberg. Visualization of three pathways for macromolecule transport across cultured endothelium and their modification by flow. *American Journal of Physiology-Heart and Circulatory Physiology*, 313(5):H959–H973, 2017.

M. C. Ghim. *Effects of multidirectional flow on cultured endothelium.* PhD thesis, 2016.

C. Giai, C. Gonzalez, C. Ledo, A. Garofalo, M. Di Genaro, D. Sordelli, and M. Gomez. Shedding of tumor necrosis factor receptor 1 induced by protein a decreases tumor necrosis factor alpha availability and inflammation during systemic Staphylococcus aureus infection. *Infection and Immunity*, 81(11): 4200–4207, 2013.

D. Giddens, C. Zarins, and S. Glagov. The role of fluid mechanics in the localization and detection of atherosclerosis. *Journal of biomechanical engineering*, 115:588–594, 1993.

M. Gimbrone, J. Topper, T. Nagel, K. Anderson, and G. Garcia-Cardeña. Endothelial dysfunction, hemodynamic forces, and atherosclerosis. *Annals of the New York Academy of Sciences*, 902(1):230–240, 2000.

G. Glorieux, W. Mullen, F. Duranton, S. Filip, N. Gayrard, H. Husi, E. Schepers, N. Neirynck, J. Schanstra, J. Jankowski, H. Mischak, À. Argilés, R. Vanholder, A. Vlahou, and J. Klein. New insights in molecular mechanisms involved in chronic kidney disease using high-resolution plasma proteome analysis. *Nephrology Dialysis Transplantation*, 30:1842–1852, 2015.

S. Godo and H. Shimokawa. Endothelial Functions. *Arteriosclerosis, Thrombosis, and Vascular Biology*, 37(9):e108–e114, 2017.

M. Goumans, Z. Liu, and P. Ten Dijke. TGF-β signaling in vascular biology and dysfunction. *Cell Research*, 19(1):116–127, 2009.

C. Griffoni, S. Di Molfetta, L. Fantozzi, C. Zanetti, P. Pippia, V. Tomasi, and E. Spisni. Modification of proteins secreted by endothelial cells during modeled low gravity exposure. *Journal of Cellular Biochemistry*, 112:265–272, 2011.

Y. Ha, E. Kang, S. Lee, S. Lee, Y. Park, J. Song, and S. Choi. Usefulness of Serum Leucine-Rich Alpha-2 Glycoprotein as a Disease Activity Biomarker in Patients with Rheumatoid Arthritis. *Journal of Korean Medical Sciences*, 29(9):1199–1204, 2014.

C. Hahn and M. Schwartz. Mechanotransduction in vascular physiology and atherogenesis. *Nature Reviews Molecular Cell Biology*, 10(1):53–62, 2009.

M. Haidekker, C. White, and J. Frangos. Analysis of temporal shear stress gradients during the onset phase of flow over a backward-facing step. *Journal of Biomechanical Engineering*, 123(5):455–463, 2001.

K. Hase, A. Kanda, I. Hirose, K. Noda, and S. Ishida. Systemic factors related to soluble (pro)renin receptor in plasma of patients with proliferative diabetic retinopathy. *PLoS ONE*, 12(12), 2017.

T. Hashida, T. Nakada, M. Satoh, K. Tomita, R. Kawaguchi, F. Nomura, and S. Oda. Proteome analysis of hemofilter adsorbates to identify novel substances of sepsis: a pilot study. *Journal of Artificial Organs*, 20(2): 132–137, 2017.

F. Hawari, F. Rouhani, X. Cui, Z. Yu, C. Buckley, M. Kaler, and S. Levine. Release of full-length 55-kDa TNF receptor 1 in exosome-like vesicles : A mechanism for generation of soluble cytokine receptors. *Proceedings of the National Academy of Sciences of the United States of America*, 101(5):1297–1302, 2004.

X. He and D. Ku. Pulsatile flow in the human left coronary artery bifurcation: Average conditions. *Journal of Biomechanical Engineering*, 118:74–82, 1996.

K. Heiden, S. Cuhlmann, L. Luong, M. Zakkar, and P. Evans. Role of nuclear factor κB in cardiovascular health and disease. *Clinical Science*, 118:593–605, 2010.

F. Helderman, D. Segers, R. De Crom, B. Hierck, R. Poelmann, P. Evans, and R. Krams. Effect of shear stress on vascular inflammation and plaque development. *Current Opinion in Lipidology*, 18:527–533, 2007.

K. Heo, H. Lee, P. Nigro, T. Thomas, N. Le, E. Chang, C. McClain, C. Reinhart-King, M. King, B. Berk, K. Fujiwara, C. Woo, and J. Abe. PKCζ mediates disturbed flow-induced endothelial apoptosis via p53 SUMOylation. *Journal of Cell Biology*, 193(5):867–884, 2011.

W. Herrington, B. Lacey, P. Sherliker, J. Armitage, and S. Lewington. Epidemiology of Atherosclerosis and the Potential to Reduce the Global Burden of Atherothrombotic Disease. *Circulation Research*, 118(4):535–546, 2016.

H. Himburg and M. Friedman. Correspondence of low mean shear and high harmonic content in the porcine iliac arteries. *Journal of Biomechanical Engineering*, 128(6):852–856, 2006.

C. Hirt and B. Nichols. Volume of Fluid (VOF) Method for the Dynamics of Free Boundaries. *Journal of Computational Physics*, 39:201–225, 1981.

A. Hoffmann, A. Levchenko, M. Scott, and D. Baltimore. The IκB–NF-κB Signaling Module : Temporal Control and Selective Gene Activation. *Science*, 298(11):1241–1245, 2007.

H. Honda, M. Fujimoto, S. Miyamoto, N. Ishikawa, S. Serada, N. Hattori, S. Nomura, N. Kohno, A. Yokoyama, and T. Naka. Sputum leucine-rich alpha-2 glycoprotein as a marker of airway inflammation in asthma. *PLoS ONE*, 11(9):1–12, 2016.

H. Honda, M. Fujimoto, S. Serada, H. Urushima, T. Mishima, H. Lee, T. Ohkawara, N. Kohno, N. Hattori, A. Yokoyama, and T. Naka. Leucine-rich α-2 glycoprotein promotes lung fibrosis by modulating TGF-β signaling in fibroblasts. *Physiological reports*, 5(24):1–13, 2017.

Q. Hong, L. Zhang, J. Fu, D. Verghese, K. Chauhan, G. Nadkarni, Z. Li, W. Ju, M. Kretzler, G. Cai, X. Chen, V. D'Agati, S. Coca, D. Schlondorff, J. He, and K. Lee. LRG1 promotes diabetic kidney disease progression by enhancing TGF-b–induced angiogenesis. *Journal of the American Society of Nephrology*, 30(4):546–562, 2019.

T. Hsiai, S. Cho, P. Wong, M. Ing, A. Salazar, A. Sevanian, M. Navab, L. Demer, and C. Ho. Monocyte recruitment to endothelial cells in response to oscillatory shear stress. *FASEB Journal*, 17(12):1648–1657, 2003.

B. Hunt and K. Jurd. Endothelial cell activation. *British Medical Journal*, 316 (5):1328–1332, 1998.

Y. Huo, A. Hafezi-Moghadam, and K. Ley. Role of vascular cell adhesion molecule-1 and fibronectin connecting segment-1 in monocyte rolling and adhesion on early atherosclerotic lesions. *Circulation Research*, 87(2):153–159, 2000.

Y. Huo, C. Weber, S. B. Forlow, M. Sperandio, J. Thatte, M. Mack, S. Jung, D. Littman, and K. Ley. The chemokine KC, but not monocyte chemoattractant protein-1, triggers monocyte arrest on early atherosclerotic endothelium. *Journal of Clinical Investigation*, 108(9):1269–1271, 2001.

J. Ishizaki, A. Takemori, K. Suemori, T. Matsumoto, Y. Akita, K. Sada, Y. Yuzawa, K. Amano, Y. Takasaki, M. Harigai, Y. Arimura, H. Makino, M. Yasukawa, N. Takemori, H. Hasegawa, Y. Murakawa, E. Muso, A. Komatsuda, S. Ito, T. Fujii, A. Kawakami, I. Nakaya, T. Saito, T. Ito, N. Hirawa, M. Yamamura, M. Nakano, K. Nitta, M. Ogura, T. Naniwa, S. Ozaki, J. Hirahashi, N. Ogawa, T. Hosoya, T. Wada, S. Horikoshi, Y. Kawaguchi, T. Hayashi, M. Yoshida, T. Watanabe, D. Inaguma, K. Tsuruya, N. Homma, T. Takeuchi, N. Nakagawa, S. Takeda, R. Katabuchi, M. Iwano, T. Atsumi, S. Fujimoto, S. Banno, T. Sugihara, M. Kobayashi, K. Yamagata, S. Homma, H. Dobashi, N. Tsuboi, A. Ishizu, and H. Sugiyama. Targeted proteomics reveals promising biomarkers of disease activity and organ involvement in antineutrophil cytoplasmic antibody-associated vasculitis. *Arthritis Research and Therapy*, 19(218), 2017.

M. Ivancic, B. Megna, Y. Sverchkov, M. Craven, M. Reichelderfer, P. Pickhardt, M. Sussman, and G. Kennedy. Noninvasive Detection of Colorectal Carcinomas Using Serum Protein Biomarkers. *Journal of Surgical Research*, 246:160–169, 2020.

E. A. Jaffe, R. L. Nachman, C. G. Becker, and C. R. Miinick. Culture of Human Endothelial Cells Derived from Umbilical Veins. *The Journal of Clinical Investigation*, 52:2745–2756, 1973.

W. Jiang, T. Ma, C. Zhang, X. Tang, Q. Xu, X. Meng, and T. Ma. Identification of urinary candidate biomarkers of cisplatin-induced nephrotoxicity in patients with carcinoma. *Journal of Proteomics*, 210, 2020.

Z. Jin, H. Ueba, T. Tanimoto, A. Lungu, M. Frame, and B. Berk. Ligand-independent activation of vascular endothelial growth factor receptor 2 by fluid shear stress regulates activation of endothelial nitric oxide synthase. *Circulation Research*, 93(4):354–363, 2003.

T. Kakisaka, T. Kondo, T. Okano, K. Fujii, K. Honda, M. Endo, A. Tsuchida, T. Aoki, T. Itoi, F. Moriyasu, T. Yamada, H. Kato, T. Nishimura, S. Todo, and S. Hirohashi. Plasma proteomics of pancreatic cancer patients by multi-dimensional liquid chromatography and two-dimensional difference gel electrophoresis (2D-DIGE): Up-regulation of leucine-rich alpha-2-glycoprotein in pancreatic cancer. *Journal of Chromatography B*, 852:257–267, 2007.

E. Kanters, M. Pasparakis, M. Gijbels, M. Vergouwe, I. Partouns-Hendriks, R. Fijneman, B. Clausen, I. Forster, M. Kockx, K. Rajewsky, G. Kraal, M. Hofker, and M. Winther. Inhibition of NF-κB activation in macrophages increases atherosclerosis in LDL receptor-deficient mice. *The Journal of Clinical Investigation*, 112(8):1176–1185, 2003.

M. Karin. How NF- kB is activated : the role of the IkB kinase (IKK) complex. *Oncogene*, 18:6867–6874, 1999.

M. Karin and Y. Ben-neriah. Phosphorylation meets ubiquitination: the control of NF-κB activity. *Annual Review of Immunology*, 18:621–663, 2000.

A. Kentsis, Y. Lin, K. Kurek, M. Calicchio, Y. Wang, F. Monigatti, F. Campagne, R. Lee, B. Horwitz, H. Steen, and R. Bachur. Discovery and Validation of Urine Markers of Acute Pediatric Appendicitis Using High-Accuracy Mass Spectrometry. *Annals of Emergency Medicine*, 55(1):62–70, 2010.

A. Kentsis, S. Ahmed, K. Kurek, E. Brennan, G. Bradwin, H. Steen, and R. Bachur. Detection and diagnostic value of urine leucine-rich α-2-glycoprotein in children with suspected acute appendicitis. *Annals of Emergency Medicine*, 60(1), 2012.

H. Kim, J. Lee, J. An, J. Kim, W. Lim, J. Seo, W. Chung, Y. Oh, Y. Kim, C. Lim, J. Zo, M. Kim, and S. Kim. Soluble Tumor Necrosis Factor Receptors and Arterial Stiffness in Patients With Coronary Atherosclerosis. *American Journal of Hypertension*, 30(3):313–318, 2017.

Y. Kimura, M. Yanagimachi, Y. Ino, M. Aketagawa, M. Matsuo, A. Okayama, H. Shimizu, K. Oba, I. Morioka, T. Imagawa, T. Kaneko, S. Yokota, H. Hirano, and M. Mori. Identification of candidate diagnostic serum biomarkers for Kawasaki disease using proteomic analysis. *Scientific Reports*, 7(March): 1–12, 2017.

T. Kita, N. Kume, M. Minami, K. Hayashida, T. Murayama, H. Sano, H. Moriwaki, H. Kataoka, E. Nishi, H. Horiuchi, H. Arai, and M. Yokode. The role of oxidized LDL in atherosclerosis. *Annals New York Academy of Sciences*, 47(1):199–206, 2001.

B. Kobe and J. Deisenhofer. Proteins with leucine-rich repeats. *Current opinion in structural biology*, 5:409–416, 1995.

M. Koch, G. Mitulovic, E. Hanzal, W. Umek, S. Seyfert, T. Mohr, H. Koelbl, and R. Laterza. Urinary proteomic pattern in female stress urinary incontinence: a pilot study. *International Urogynecology Journal*, 27(11):1729–1734, 2016.

L. Kraiss, A. Weyrich, N. Alto, D. Dixon, T. Ennis, V. Modur, T. McIntyre, S. Prescott, and G. Zimmerman. Fluid flow activates a regulator of translation, p70/p85 S6 kinase, in human endothelial cells. *American Journal of Physiology - Heart and Circulatory Physiology*, 278:1537–1544, 2000.

L. Kraiss, N. Alto, D. Dixon, T. McIntyre, A. Weyrich, and G. Zimmerman. Fluid flow regulates E-selectin protein levels in human endothelial cells by inhibiting translation. *Journal of Vascular Surgery*, 37(1):161–168, 2003.

D. N. Ku, D. P. Giddens, C. K. Zarins, and S. Glagov. Pulsatile flow and atherosclerosis in the human carotid bifurcation. Positive correlation between plaque location and low and oscillating shear stress. *Arteriosclerosis*, 5(3):293–302, 1985.

J. Ladd, T. Busald, M. Johnson, Q. Zhang, S. Pitteri, H. Wang, D. Brenner, P. Lampe, R. Kucherlapati, Z. Feng, R. Prentice, and S. Hanash. Increased plasma levels of the APC-interacting protein MAPRE1, LRG1, and IGFBP2 preceding a diagnosis of colorectal cancer in women. *Cancer Prevention Research*, 5(4):655–664, 2012.

T. Lawrence, D. Gilroy, P. Colville-Nash, and D. Willoughby. Possible new role for NF-κB in the resolution of inflammation. *Nature Medicine*, 7(12): 1291–1297, 2001.

H. Lee, M. Fujimoto, T. Ohkawara, H. Honda, S. Serada, Y. Terada, and T. Naka. Leucine rich α-2 glycoprotein is a potential urinary biomarker for renal tubular injury. *Biochemical and Biophysical Research Communications*, 498(4):1045–1051, 2018.

M. Levesque and R. Nerem. The elongation and orientation of cultured endothelial cells in response to shear stress. *Journal of Biomechanical Engineering*, 107(4):341–347, 1985.

M. Levesque, D. Liepsch, S. Moravec, and R. M. Nerem. Correlation of endothelial cell shape and wall shear stress in a stenosed dog aorta. *Arteriosclerosis*, 6(2):220–229, 1986.

K. Ley, E. Lundgren, E. Berger, and K. E. Arfors. Shear-dependent inhibition of granulocyte adhesion to cultured endothelium by dextran sulfate. *Blood*, 73(5):1324–1330, 1989.

D. Li and J. Mehta. Oxidized LDL, a critical factor in atherogenesis. *Cardiovascular Research*, 68(3):353–354, 2005.

X. Li, M. Miyajima, R. Mineki, H. Taka, K. Murayama, and H. Arai. Analysis of potential diagnostic biomarkers in cerebrospinal fluid of idiopathic normal pressure hydrocephalus by proteomics. *Acta Neurochirurgica*, 148:859–864, 2006.

X. Li, M. Miyajima, C. Jiang, and H. Arai. Expression of TGF-βs and TGF-β type II receptor in cerebrospinal fluid of patients with idiopathic normal pressure hydrocephalus. *Neuroscience Letters*, 413:141–144, 2007.

Y. Li, Y. Zhang, F. Qiu, and Z. Qiu. Proteomic identification of exosomal LRG1: A potential urinary biomarker for detecting NSCLC. *Electrophoresis*, 32(15):1976–1983, 2011.

P. Libby. Current Concepts of the Pathogenesis of the Acute Coronary Syndromes. *Circulation*, 104:365–372, 2001.

C. Lin, Y. Chen, W. Liu, H. Chou, Y. Chang, S. Lin, J. Li, S. Jian, Y. Lee, and H. Chan. Proteomic identification of plasma biomarkers in uterine leiomyoma. *Molecular BioSystems*, 8:1136–1145, 2012.

M. Lindén, S. Lind, C. Mayrhofer, U. Segersten, K. Wester, Y. Lyutvinskiy, R. Zubarev, P. Malmström, and U. Pettersson. Proteomic analysis of urinary biomarker candidates for nonmuscle invasive bladder cancer. *Proteomics*, 12 (1):135–144, 2012.

C. Liu. *Roles of leucine-rich alpha-2- glycoprotein 1 in normal and diabetic wound healing*. PhD thesis, Nanyang Technological University, 2019.

C. Liu, S. Lim, M. Teo, M. Tan, M. Kulkarni, B. Qiu, A. Li, S. Lal, C. dos Remedios, N. Tan, W. Wahli, M. Ferenczi, W. Song, W. Hong, and X. Wang. Collaborative Regulation of LRG1 by TGF-β1 and PPAR-β/δ Modulates Chronic Pressure Overload–Induced Cardiac Fibrosis. *Circulation: Heart Failure*, 12, dec 2019.

J. Liu, S. Pek, K. Ang, S. Tavintharan, and S. Lim. Plasma leucine-rich α-2-glycoprotein 1 predicts rapid eGFR decline and albuminuria progression in type 2 diabetes mellitus. *Journal of Clinical Endocrinology and Metabolism*, 102(10):3683–3691, 2017.

Y. Liu, X. Luo, H. Hu, R. Wang, Y. Sun, R. Zeng, and H. Chen. Integrative Proteomics and Tissue Microarray Profiling Indicate the Association between Overexpressed Serum Proteins and Non-Small Cell Lung Cancer. *PLoS ONE*, 7(12), 2012.

A. Lusis. Atherosclerosis. *Nature*, 407(9):233–241, 2000.

J. Lynch, J. Fay, M. Meehan, K. Bryan, K. Watters, D. Murphy, and R. Stallings. MiRNA-335 suppresses neuroblastoma cell invasiveness by direct targeting of multiple genes from the non-canonical TGF-β signalling pathway. *Carcinogenesis*, 33(5):976–985, 2012.

M. Mahmoud, H. Kim, R. Xing, S. Hsiao, A. Mammoto, J. Chen, J. Serbanovic-Canic, S. Feng, N. Bowden, R. Maguire, M. Ariaans, S. Francis, P. Weinberg, K. Van Der Heiden, E. Jones, T. Chico, V. Ridger, and P. Evans. TWIST1 integrates endothelial responses to flow in vascular dysfunction and atherosclerosis. *Circulation Research*, 119(3):450–462, 2016.

M. Mahmoud, J. Serbanovic-Canic, S. Feng, C. Souilhol, R. Xing, S. Hsiao, A. Mammoto, J. Chen, M. Ariaans, S. Francis, K. Van Der Heiden, V. Ridger, and P. Evans. Shear stress induces endothelial-to-mesenchymal transition via the transcription factor Snail. *Scientific Reports*, 7(3375), 2017.

P. Májek, Z. Reicheltová, J. Suttnar, J. Čermák, and J. Dyr. Plasma protein alterations in the refractory anemia with excess blasts subtype 1 subgroup of myelodysplastic syndrome. *Proteome Science*, 10(31), 2012.

P. Majek, Z. Riedelova-Reicheltova, J. Suttnar, K. Pecankova, J. Cermak, and J. Dyr. Proteome changes in the plasma of myelodysplastic syndrome patients with refractory anemia with excess blasts subtype 2. *Disease Markers*, 2014, 2014.

P. Majek, K. Pecankova, J. Cermak, and J. Dyr. Plasma Protein Biomarker Candidates for Myelodysplastic Syndrome Subgroups. *BioMed Research International*, 2015, 2015.

M. McDermott, I. Aksentijevich, J. Galon, E. McDermott, B. William Ogunkolade, M. Centola, E. Mansfield, M. Gadina, L. Karenko, T. Pettersson, J. McCarthy, D. Frucht, M. Aringer, Y. Torosyan, A. Teppo, M. Wilson, H. Mehmet Karaarslan, Y. Wan, L. Todd, G. Wood, R. Schlimgen, T. Kumarajeewa, S. Cooper, J. Vella, C. Amos, J. Mulley, K. Quane, M. Molloy, A. Ranki, R. Powell, G. Hitman, J. O'Shea, and D. Kastner. Germline mutations in the extracellular domains of the 55 kDa TNF receptor, TNFR1, define a family of dominantly inherited autoinflammatory syndromes. *Cell*, 97(1):133–144, 1999.

R. P. McEver. Selectins: Lectins that initiate cell adhesion under flow. *Current Opinion in Cell Biology*, 14(5):581–586, 2002.

N. Merna, A. Wong, V. Barahona, P. Llanos, B. Kunar, B. Palikuqi, M. Ginsberg, S. Rafii, and S. Rabbany. Laminar shear stress modulates endothelial luminal surface stiffness in a tissue-specific manner. *Microcirculation*, 25(5): 1–10, 2018.

J. Mestas and K. Ley. Monocyte-Endothelial Cell Interactions in the Development of Atherosclerosis. *Trends in Cardiovascular Medicine*, 18(6):228–232, 2008.

E. Miyauchi, T. Furuta, S. Ohtsuki, M. Tachikawa, Y. Uchida, H. Sabit, W. Obuchi, T. Baba, M. Watanabe, T. Terasaki, and M. Nakada. Identification of blood biomarkers in glioblastoma by SWATH mass spectrometry and quantitative targeted absolute proteomics. *PLoS ONE*, 13(3):1–22, 2018.

Y. Mohamied, E. Rowland, E. Bailey, E. Sherwin, M. Schwartz, and P. Weinberg. Change of Direction in the Biomechanics of Atherosclerosis. *Annals of Biomedical Engineering*, 43(1):16–25, 2014.

J. Moonen, E. Lee, M. Schmidt, M. Maleszewska, J. Koerts, L. Brouwer, T. Van Kooten, M. Van Luyn, C. Zeebregts, G. Krenning, and M. Harmsen. Endothelial-to-mesenchymal transition contributes to fibro-proliferative vascular disease and is modulated by fluid shear stress. *Cardiovascular Research*, 108(3):377–386, 2015.

M. Moss and D. Minond. Recent Advances in ADAM17 Research: A Promising Target for Cancer and Inflammation. *Mediators of Inflammation*, 2017, 2017.

A. Mu, B. Lim, O. Hashim, and A. Shuib. Identification of O-glycosylated proteins that are aberrantly excreted in the urine of patients with early stage ovarian cancer. *International Journal of Molecular Sciences*, 14:7923–7931, 2013.

W. Muller, S. Weigl, X. Deng, and D. Phillips. PECAM-1 is required for transendothelial migration of leukocytes. *Journal of Experimental Medicine*, 178(2):449–460, 1993.

S. Mundi, M. Massaro, E. Scoditti, M. Carluccio, V. Hinsbergh, M. Iruela-arispe, and R. Caterina. Endothelial permeability , LDL deposition , and cardiovascular risk factors — a review. *Cardiovascular Research*, 114:35–52, 2018.

T. Nagel, N. Resnick, C. Dewey, and M. Gimbrone. Vascular endothelial cells respond to spatial gradients in fluid shear stress by enhanced activation of transcription factors. *Arteriosclerosis, Thrombosis, and Vascular Biology*, 19(8):1825–1834, 1999.

H. Nakajima, S. Serada, M. Fujimoto, T. Naka, and S. Sano. Leucine-rich α-2 glycoprotein is an innovative biomarker for psoriasis. *Journal of Dermatological Science*, 86:170–174, 2017.

M. Nakajima, M. Miyajima, I. Ogino, M. Watanabe, H. Miyata, K. L. Karagiozov, H. Arai, Y. Hagiwara, T. Segawa, K. Kobayashi, and Y. Hashimoto. Leucine-rich α-2-glycoprotein is a marker for idiopathic normal pressure hydrocephalus. *Acta Neurochirurgica*, 153:1339–1346, 2011.

M. Nambu, T. Masuda, S. Ito, K. Kato, T. Kojima, H. Daiko, Y. Ito, K. Honda, and S. Ohtsuki. Leucine-rich alpha-2-glycoprotein 1 in serum is a possible biomarker to predict response to preoperative chemoradiotherapy for esophageal cancer. *Biological and Pharmaceutical Bulletin*, 42(10):1766–1771, 2019.

R. M. Nerem, M. J. Levesque, and J. F. Cornhill. Vascular endothelial morphology as an indicator of the pattern of blood flow. *Journal of Biomechanical Engineering*, 103(3):172–176, 1981.

A. Ng, J. Eisenberg, R. Heath, A. Huett, C. Robinson, G. Nau, and R. Xavier. Human leucine-rich repeat proteins: A genome-wide bioinformatic categorization and functional analysis in innate immunity. *Proceedings of the National Academy of Sciences of the United States of America*, 108(Suppl. 1): 4631–4638, 2011.

L. O'Donnell, L. Druhan, and B. Avalos. Molecular characterization and expression analysis of leucine- rich α2-glycoprotein, a novel marker of granulocytic differentiation. *Journal of Leukocyte Biology*, 72:478–485, 2002.

E. Orwoll, J. Wiedrick, J. Jacobs, E. Baker, P. Piehowski, V. Petyuk, Y. Gao, T. Shi, R. Smith, D. Bauer, S. Cummings, C. Nielson, and J. Lapidus. High-throughput serum proteomics for the identification of protein biomarkers of mortality in older men. *Aging Cell*, 17:1–12, 2018.

G. Ostermann, K. Weber, A. Zernecke, A. Schröder, and C. Weber. JAM-I is a ligand of the $\beta 2$ integrin LFA-I involved in transendothelial migration of leukocytes. *Nature Immunology*, 3(2):151–158, 2002.

O. Ozes, L. Mayo, J. Gustin, S. Pfeffer, L. Pffeffer, and D. Donner. NF-kB activation by tumour necrosis factor requires the Akt serine-threonine kinase. *Nature*, 401:82–85, 1999.

L. Pan, Z. Hong, L. Yu, Y. Gao, R. Zhang, H. Feng, L. Su, and G. Wang. Shear stress induces human aortic endothelial cell apoptosis via interleukin-1 receptor-associated kinase 2-induced endoplasmic reticulum stress. *Molecular Medicine Reports*, 16(5):7205–7212, 2017.

J. Park, Y. Choi, J. Namkung, S. Yi, H. Kim, J. Yu, Y. Kim, M. Kwon, W. Kwon, D. Oh, S. Kim, S. Jeong, W. Han, K. Lee, J. Heo, J. Park, J. Park, S. Kim, C. Kang, W. Lee, S. Lee, S. Han, T. Park, J. Jang, and Y. Kim. Diagnostic performance enhancement of pancreatic cancer using proteomic multimarker panel. *Oncotarget*, 8(54):93117–93130, 2017.

A. Passerini, D. Polacek, C. Shi, N. Francesco, E. Manduchi, G. Grant, W. Pritchard, S. Powell, G. Chang, C. Stoeckert, and P. Davies. Coexisting proinflammatory and antioxidative endothelial transcription profiles in a disturbed flow region of the adult porcine aorta. *Proceedings of the National Academy of Sciences of the United States of America*, 101(8):2482–2487, 2004.

V. Peiffer, S. Sherwin, and P. Weinberg. Computation in the rabbit aorta of a new metric - the transverse wall shear stress - to quantify the multidirectional character of disturbed blood flow. *Journal of Biomechanics*, 46(15):2651–2658, 2013a.

V. Peiffer, S. Sherwin, and P. Weinberg. Does low and oscillatory wall shear stress correlate spatially with early atherosclerosis? A systematic review. *Cardiovascular Research*, 99:242–250, 2013b.

S. Pek, S. Tavintharan, X. Wang, S. Lim, K. Woon, L. Yeoh, X. Ng, J. Liu, and C. Sum. Elevation of a Novel Angiogenic Factor, Leucine-Rich-α2-Glycoprotein (LRG1), Is Associated With Arterial Stiffness, Endothelial Dysfunction, and Peripheral Arterial Disease in Patients With Type 2 Diabetes. *The Journal of Clinical Endocrinology and Metabolism*, 100(4):1586–1593, 2015.

A. Plata, S. Sherwin, and R. Krams. Endothelial nitric oxide production and transport in flow chambers: The importance of convection. *Annals of Biomedical Engineering*, 38(9):2805–2816, 2010.

J. Pober. Endothelial activation: intracellular signaling pathways. *Arthritis Research*, 4(Suppl 3):109–116, 2002.

J. S. Pober. Cytokine-mediated activation of vascular endothelium:Physiology and Pathology. *American Journal of Pathology*, 133(3):426–433, 1988.

C. Potter, M. Lundberg, L. Harrington, C. Warboys, T. Warner, R. Berson, A. Moshkov, J. Gorelik, P. Weinberg, and J. Mitchell. Role of shear stress in endothelial cell morphology and expression of cyclooxygenase isoforms. *Arteriosclerosis, Thrombosis, and Vascular Biology*, 31:384–391, 2011.

C. Potter, S. Schobesberger, M. Lundberg, P. Weinberg, J. Mitchell, and J. Gorelik. Shape and compliance of endothelial cells after shear stress in vitro or from different aortic regions: Scanning ion conductance microscopy study. *PLoS ONE*, 7(2):1–5, 2012.

S. Preibisch, S. Saalfeld, and P. Tomancak. Globally optimal stitching of tiled 3D microscopic image acquisitions. *Bioinformatics*, 25(11):1463–1465, 2009.

J. Qiao, J. Tripathi, N. Mishra, Y. Cai, S. Tripathi, X. Wang, S. Imes, M. Fishbein, S. Clinton, P. Libby, A. Lusis, and T. Rajavashisth. Role of macrophage colony-stimulating factor in atherosclerosis: Studies of osteopetrotic mice. *American Journal of Pathology*, 150(5):1687–1699, 1997.

T. H. Rainer, L. Y. Leung, C. P. Chan, Y. K. Leung, N. M. Cheng, P. B. Lai, Y. S. Cheung, and C. A. Graham. Circulating human leucine-rich α-2-glycoprotein 1 mRNA and protein levels to detect acute appendicitis in patients with acute abdominal pain. *Clinical Biochemistry*, 50(9):485–490, 2017.

C. Ramos, Y. Huo, U. Jung, S. Ghosh, D. Manka, I. Sarembock, and K. Ley. Direct Demonstration of P-Selectin– and VCAM-1–Dependent Mononuclear Cell Rolling in Early Atherosclerotic Lesions of Apolipoprotein E–Deficient Mice. *Circulation Research*, 84:1237–1244, 1999.

J. Robert, B. Weber, L. Frese, M. Emmert, D. Schmidt, A. Von Eckardstein, L. Rohrer, and S. Hoerstrup. A three-dimensional engineered artery model for in vitro atherosclerosis research. *PLoS ONE*, 8(11), 2013.

R. Ross, J. Glomset, and L. Harker. Response to injury and atherogenesis. *American Journal of Pathology*, 86(3):675–684, 1977.

H. Sage, P. Pritzl, and P. Bornstein. Secretory phenotypes of endothelial cells in culture: comparison of aortic, venous, capillary, and corneal endothelium. *Arteriosclerosis*, 1(6):427–442, 1981.

M. Salek, P. Sattari, and R. Martinuzzi. Analysis of fluid flow and wall shear stress patterns inside partially filled agitated culture well plates. *Annals of Biomedical Engineering*, 40(3):707–728, 2011.

M. Salö, B. Roth, P. Stenström, E. Arnbjörnsson, and B. Ohlsson. Urinary biomarkers in pediatric appendicitis. *Pediatric Surgery International*, 32(8): 795–804, 2016.

N. S. Sandanayake, J. Sinclair, F. Andreola, M. H. Chapman, A. Xue, G. J. Webster, A. Clarkson, A. Gill, I. D. Norton, R. C. Smith, J. F. Timms, and S. P. Pereira. A combination of serum leucine-rich α-2-glycoprotein 1, CA19-9 and interleukin-6 differentiate biliary tract cancer from benign biliary strictures. *British Journal of Cancer*, 105(9):1370–1378, 2011.

J. Santilli and S. Santilli. Chronic critical limb ischemia: Diagnosis, treatment and prognosis. *American Family Physician*, 59(7):1899–1908, 1999.

J. Sarvari, Z. Mojtahedi, Y. Kuramitsu, M. Fattahi, A. Ghaderi, K. Nakamura, and N. Erfani. Comparative proteomics of sera from HCC patients with different origins. *Hepatitis Monthly*, 14(1):1–6, 2014.

M. Sato and N. Ohshima. Flow-induced changes in shape and cytoskeletal structure of vascular endothelial cells. *Biorheology*, 31(2):143–153, 1994.

A. Schenkel, Z. Mamdouh, and W. Muller. Locomotion of monocytes on endothelium is a critical step during extravasation. *Nature Immunology*, 5(4): 393–400, 2004.

H. Schnittler, R. Franke, U. Akbay, C. Mrowietz, and D. Drenckhahn. Improved in vitro rheological system for studying the effect of fluid shear stress on cultured cells. *The American journal of physiology*, 265:C289–298, 1993.

L. Sedger and M. Mcdermott. TNF and TNF-receptors : From mediators of cell death and inflammation to therapeutic giants – past , present and future. *Cytokine and Growth Factor Reviews*, 25:453–472, 2014.

R. Sen and D. Baltimore. Inducibility of κ immunoglobulin enhancer-binding protein NF-κB by a posttranslational mechanism. *Cell*, 47(6):921–928, 1986.

S. Serada, M. Fujimoto, A. Ogata, F. Terabe, T. Hirano, H. Iijima, S. Shinzaki, T. Nishikawa, T. Ohkawara, K. Iwahori, N. Ohguro, T. Kishimoto, and T. Naka. iTRAQ-based proteomic identification of leucine-rich α-2 glycoprotein as a novel infl ammatory biomarker in autoimmune diseases. *Annals of the Rheumatic Diseases*, 69(4):770–774, 2010.

S. Serada, M. Fujimoto, F. Terabe, H. Iijima, S. Shinzaki, S. Matsuzaki, T. Ohkawara, R. Nezu, S. Nakajima, T. Kobayashi, S. Plevy, T. Takehara, and T. Naka. Serum Leucine-rich Alpha-2 Glycoprotein Is a Disease Activity Biomarker in Ulcerative Colitis. *Inflammatory Bowel Diseases*, 18(11): 2169–2179, 2012.

J. Serbanovic-Canic, A. De Luca, C. Warboys, P. Ferreira, L. Luong, S. Hsiao, I. Gauci, M. Mahmoud, S. Feng, C. Souilhol, N. Bowden, J.-P. Ashton, H. Walczak, D. Firmin, R. Krams, J. Mason, D. Haskard, S. Sherwin,

V. Ridger, T. Chico, and P. Evans. Zebrafish model for functional screening of flow-responsive genes. *Arteriosclerosis, Thrombosis, and Vascular Biology*, 37(1), 2017.

E. Shinozaki, K. Tanabe, T. Akiyoshi, T. Tsuchida, Y. Miyazaki, N. Kojima, M. Igarashi, M. Ueno, M. Suenaga, N. Mizunuma, K. Yamaguchi, K. Nakayama, S. Iijima, and T. Yamaguchi. Serum leucine-rich alpha-2-glycoprotein-1 with fucosylated triantennary N-glycan: A novel colorectal cancer marker. *BMC Cancer*, 18(406):1–9, 2018.

S. Shinzaki, K. Matsuoka, H. Iijima, S. Mizuno, S. Serada, M. Fujimoto, N. Arai, N. Koyama, E. Morii, M. Watanabe, T. Hibi, T. Kanai, T. Takehara, and T. Naka. Leucine-rich Alpha-2 glycoprotein is a serum biomarker of mucosal healing in ulcerative colitis. *Journal of Crohn's and Colitis*, 11 (1):84–91, 2017.

R. Shirai, F. Hirano, N. Ohkura, K. Ikeda, and S. Inoue. Up-regulation of the expression of leucine-rich α2-glycoprotein in hepatocytes by the mediators of acute-phase response. *Biochemical and Biophysical Research Communications*, 382:776–779, 2009.

J. Sluimer and M. Daemen. Immune activation and inflammation in HIV-1 infection :. *Journal of Pathology2*, 218:7–29, 2009.

C. Smith, I. Batruch, J. Bauça, H. Kosanam, J. Ridley, M. Bernardini, F. Leung, E. Diamandis, and V. Kulasingam. Deciphering the peptidome of urine from ovarian cancer patients and healthy controls. *Clinical Proteomics*, 11 (23), 2014.

M. Sng, J. Chan, Z. Teo, T. Phua, E. Tan, J. Wee, N. Koh, C. Tan, J. Chen, M. Pal, B. Tong, Y. Tnay, X. Ng, P. Zhu, S. Chiba, X. Wang, W. Wahli, and N. Tan. Selective deletion of PPARβ/δ in fibroblasts causes dermal fibrosis by attenuated LRG1 expression. *Cell Discovery*, 4(15), 2018.

A. Sprague and R. Khalil. Inflammatory cytokines in vascular dysfunction and vascular disease. *Biochemical Pharmacology*, 78:539–552, 2009.

S. Staubach, M. Pekmez, and F. Hanisch. Differential proteomics of urinary exovesicles from classical galactosemic patients reveals subclinical kidney insufficiency. *Journal of Proteome Research*, 15(6):1754–1761, 2016.

D. Sun, Y. Shi, L. Wang, Y. Lv, Q. Han, Z. Wang, and G. Dai. Leucine-rich alpha-2-glycoprotein-1, relevant with microvessel density, is an independent survival prognostic factor for stage III colorectal cancer patients: A retrospective analysis. *Oncotarget*, 8(39):66550–66558, 2017.

C. P. Suresh, A. Saha, M. Kaur, R. Kumar, N. K. Dubey, T. Basak, V. Tanwar, G. Bhardwaj, S. Sengupta, V. Batra, and A. Upadhyay. Differentially expressed urinary biomarkers in children with idiopathic nephrotic syndrome. *Clinical and Experimental Nephrology*, 20:273–283, 2016.

M. Thi, J. Tarbell, S. Weinbaum, and D. Spray. The role of the glycocalyx in reorganization of the actin cytoskeleton under fluid shear stress: A "bumper-car" model. *Proceedings of the National Academy of Sciences of the United States of America*, 101(47):16483–16488, 2004.

J. Thomas, A. Chakraborty, M. K. Sharp, and R. E. Berson. Spatial and temporal resolution of shear in an orbiting petri dish. *Biotechnology Progress*, 27(2):460–465, 2011.

R. Thompson, A. Allam, G. Lombardi, L. S. Wann, M. L. Sutherland, J. Sutherland, M. Soliman, B. Frohlich, D. Mininberg, J. Monge, C. Vallodolid, S. Cox, G. Abd El-Maksoud, I. Badr, M. Miyamoto, A. El-Halim Nur El-Din, J. Narula, C. Finch, and G. Thomas. Atherosclerosis across 4000 years of human history: The Horus study of four ancient populations. *The Lancet*, 381(9873):1211–1222, 2013.

N. Townsend, P. Bhatnagar, E. Wilkins, K. Wickramasinghe, and M. Rayner. *Cardiovascular disease statistics 2015.* 2015.

E. Traenckner, H. Pahl, T. Henkel, K. Schmidt, S. Wilk, and P. Baeuerle. Phosphorylation of human IκB-α on serines 32 and 36 controls IκB-α proteolysis and NF-κB activation in response to diverse stimuli. *The EMBO Journal*, 14(12):2876–2883, 1995.

P. Tsao, N. Lewis, S. Alpert, and J. Cooke. Exposure to Shear Stress Alters Endothelial Adhesiveness. *Circulation*, 92(12):3513–3519, dec 1995.

C. Tung, S. Lin, H. Chou, Y. Chen, H. Lin, C. Tung, K. Huang, Y. Chen, Y. Lee, and H. Chan. Proteomics-based identification of plasma biomarkers in oral squamous cell carcinoma. *Journal of Pharmaceutical and Biomedical Analysis*, 75:7–17, 2013.

D. Tunica, X. Yin, A. Sidibe, C. Stegemann, M. Nissum, L. Zeng, M. Brunet, and M. Mayr. Proteomic analysis of the secretome of human umbilical vein endothelial cells using a combination of free-flow electrophoresis and nanoflow LC-MS/MS. *Proteomics*, 9:4991–4996, 2009.

E. Tzima, M. Irani-Tehrani, W. Kiosses, E. Dejana, D. Schultz, B. Engelhardt, G. Cao, H. DeLisser, and M. Schwartz. A mechanosensory complex that mediates the endothelial cell response to fluid shear stress. *Nature*, 437: 426–431, 2005.

M. Uhlén, L. Fagerberg, B. Hallström, C. Lindskog, P. Oksvold, A. Mardinoglu, Å. Sivertsson, C. Kampf, E. Sjöstedt, A. Asplund, I. Olsson, K. Edlund, E. Lundberg, S. Navani, C. Szigyarto, J. Odeberg, D. Djureinovic, J. Takanen, S. Hober, T. Alm, P. Edqvist, H. Berling, H. Tegel, J. Mulder, J. Rockberg, P. Nilsson, J. Schwenk, M. Hamsten, K. Feilitzen, M. Forsberg, L. Persson, F. Johansson, M. Zwahlen, G. Heijne, J. Nielsen, and F. Pontén. Tissue-based map of the human proteome. *Science*, 347(6220), 2015.

H. Urushima, M. Fujimoto, T. Mishima, T. Ohkawara, H. Honda, H. Lee, H. Kawahata, S. Serada, and T. Naka. Leucine-rich alpha 2 glycoprotein promotes Th17 differentiation and collagen-induced arthritis in mice through enhancement of TGF-β-Smad2 signaling in naïve helper T cells. *Arthritis Research & Therapy*, 19(137):1–13, 2017.

V. Velasco, M. Gruenthal, E. Zusstone, J. Thomas, R. Berson, R. Keynton, and S. Williams. An orbital shear platform for real-time, in vitro endothelium characterization. *Biotechnology and Bioengineering*, 113(6):1336–1344, 2016.

N. Venugopal Menon, H. Tay, K. Pang, R. Dalan, S. Wong, X. Wang, K. Li, and H. Hou. A tunable microfluidic 3D stenosis model to study leukocyte-endothelial interactions in atherosclerosis. *APL Bioengineering*, 2, 2018.

M. Walker, C. Zhou, A. Backen, M. Pernemalm, A. Williamson, L. Priest, P. Koh, C. Faivre-Finn, F. Blackhall, C. Dive, and A. Whetton. Discovery and Validation of Predictive Biomarkers of Survival for Non-small Cell Lung Cancer Patients Undergoing Radical Radiotherapy: Two Proteins With Predictive Value. *EBioMedicine*, 2(8):841–850, 2015.

T. Walshe, N. Dela Paz, and P. D'Amore. The role of shear-induced transforming growth factor-β signaling in the endothelium. *Arteriosclerosis, Thrombosis, and Vascular Biology*, 33(11):2608–2617, 2013.

C. Wang, B. Baker, C. Chen, and M. Schwartz. Endothelial cell sensing of flow direction. *Arteriosclerosis, Thrombosis, and Vascular Biology*, 33(9): 2130–2136, 2013a.

L. Wang, F. Du, and X. Wang. TNF-α Induces Two Distinct Caspase-8 Activation Pathways. *Cell*, 133(4):693–703, 2008.

N. Wang, H. Miao, Y. Li, P. Zhang, J. Haga, Y. Hu, A. Young, S. Yuan, P. Nguyen, C. Wu, and S. Chien. Shear stress regulation of Krüppel-like factor 2 expression is flow pattern-specific. *Biochemical and Biophysical Research Communications*, 341(4):1244–1251, 2006.

X. Wang, S. Abraham, J. McKenzie, N. Jeffs, M. Swire, V. Tripathi, U. Luhmann, C. Lange, Z. Zhai, H. Arthur, J. Bainbridge, S. Moss, and J. Greenwood. LRG1 promotes angiogenesis by modulating endothelial TGF-β signalling. *Nature*, 499(7458):306–311, 2013b.

Y. Wang, C. Chen, Q. Hua, L. Wang, F. Li, M. Li, Z. Mei, T. Zhou, B. Xiao, and Z. Tao. Downregulation of leucine-rich-α-2-glycoprotein 1 expression is associated with the tumorigenesis of head and neck squamous cell carcinoma. *Oncology Reports*, 37(3):1503–1510, 2017a.

Y. Wang, J. Xu, X. Zhang, C. Wang, Y. Huang, K. Dai, and X. Zhang. TNF-α-induced LRG1 promotes angiogenesis and mesenchymal stem cell migration in the subchondral bone during osteoarthritis. *Cell Death and Disease*, 8(3): e2715, 2017b.

C. Warboys, R. Berson, G. Mann, J. Pearson, and P. Weinberg. Acute and chronic exposure to shear stress have opposite effects on endothelial permeability to macromolecules. *American Journal of Physiology - Heart and Circulatory Physiology*, 298(6):1850–1856, 2010.

C. Warboys, A. De Luca, N. Amini, L. Luong, H. Duckles, S. Hsiao, A. White, S. Biswas, R. Khamis, C. Chong, W. Cheung, S. Sherwin, M. Bennett, J. Gil, J. Mason, D. Haskard, and P. Evans. Disturbed flow promotes endothelial senescence via a p53-dependent pathway. *Arteriosclerosis, Thrombosis, and Vascular Biology*, 34:985–995, 2014.

C. M. Warboys, M. Ghim, and P. D. Weinberg. Understanding mechanobiology in cultured endothelium: A review of the orbital shaker method. *Atherosclerosis*, 285(February):170–177, 2019.

C. Watson, M. Ledwidge, D. Phelan, P. Collier, J. Byrne, M. Dunn, K. Mcdonald, and J. Baugh. Proteomic Analysis of Coronary Sinus Serum Reveals Leucine-Rich α2-Glycoprotein as a Novel Biomarker of Ventricular Dysfunction and Heart Failure. *Circulation Heart Failure*, 4:188–197, 2011.

S. Weinbaum, J. Tarbell, and E. Damiano. The Structure and Function of the Endothelial Glycocalyx Layer. *Annual Review of Biomedical Engineering*, 9:121–167, 2007.

S. White, E. Hayes, S. Lehoux, J. Jeremy, A. Horrevoets, and A. Newby. Characterization of the Differential Response of Endothelial Cells Exposed to Normal and Elevated Laminar Shear Stress. *Journal of Cellular Physiology*, (226):2841–2848, 2011.

B. Wójciak-stothard, L. Williams, and A. Ridley. Monocyte Adhesion and Spreading on Human Endothelial Cells Is Dependent on Rho-regulated Receptor Clustering. *The Journal of Cell Biology*, 145(6):1293–1307, 1999.

C. Wong, B. Heit, and P. Kubes. Molecular regulators of leucocyte chemotaxis during inflammation. *Cardiovascular Research*, 86(2):183–191, 2010.

K. Woollard and F. Geissmann. Monocytes in atherosclerosis: subsets and functions. *Nature Reviews Cardiology*, 7:77–86, 2010.

J. Wu, X. Xie, S. Nie, R. Buckanovich, and D. Lubman. Altered expression of sialylated glycoproteins in ovarian cancer sera using lectin-based ELISA assay and quantitative glycoproteomics analysis. *Journal of Proteome Research*, 12(7):3342–3352, 2013.

J. Wu, H. Yin, J. Zhu, R. Buckanovich, J. Thorpe, J. Dai, N. Urban, and D. Lubman. Validation of LRG1 as a potential biomarker for detection of epithelial ovarian cancer by a blinded study. *PLoS ONE*, 10:1–11, 2015.

S. Xanthoulea, M. Pasparakis, S. Kousteni, C. Brakebusch, D. Wallach, J. Bauer, H. Lassmann, and G. Kollias. Tumor Necrosis Factor (TNF)

Receptor Shedding Controls Thresholds of Innate Immune Activation That Balance Opposing TNF Functions in Infectious and Inflammatory Diseases. *The Journal of Experimental Medicine*, 200(3):367–376, 2004.

X. Xie, H. Chu, Y. Xu, L. Hua, Z. Wang, P. Huang, H. Jia, and L. Zhang. Proteomics study of serum exosomes in Kawasaki disease patients with coronary artery aneurysms. *Cardiology Journal*, 2018.

Z. Xie, Y. Zhang, C. Jin, Y. Mao, and D. Fu. LRG-1 promotes pancreatic cancer growth and metastasis via modulation of the EGFR/p38 signaling. *Journal of Experimental and Clinical Cancer Research*, 38(75):1–12, 2019.

C. Xuan, H. Li, L. L. Li, Q. W. Tian, Q. Wang, B. B. Zhang, J. J. Guo, G. W. He, and L. M. Lun. Screening and Identification of Pregnancy Zone Protein and Leucine-Rich Alpha-2-Glycoprotein as Potential Serum Biomarkers for Early-Onset Myocardial Infarction using Protein Profile Analysis. *Proteomics - Clinical Applications*, 13:1–8, 2019.

W. Yang, H. Kim, J. Lee, N. Han, M. Lee, and S. Park. 1 ,25-Dihydroxyvitamin D3 Causes ADAM10-Dependent Ectodomain Shedding of Tumor Necrosis Factor Receptor 1 in Vascular Smooth Muscle Cells. *Molecular Pharmacology*, 87(3):533–542, 2015.

W. Yang, S. Moon, M. Lee, and S. Park. Epigallocatechin-3-gallate attenuates the effects of TNF-α in vascular endothelial cells by causing ectodomain shedding of TNF receptor 1. *Cellular Physiology and Biochemistry*, 38: 1963–1974, 2016.

W. Yang, S. Moon, M. Lee, E. Lee, and S. Park. Diosgenin, an Activator of 1,25D3-MARRS Receptor / ERp57 , Attenuates the Effects of TNF-α by Causing ADAM10-Dependent Ectodomain Shedding of TNF Receptor 1. *Cellular Physiology and Biochemistry*, 43:2434–2445, 2017.

T. Yap, J. Fan, Y. Chen, M. Ho, C. Choo, J. Allen, Y. Low, A. Jacobsen, and S. Nah. A novel noninvasive appendicitis score with a urine biomarker. *Journal of Pediatric Surgery*, 54:91–96, 2019.

X. Yin, S. Subramanian, S. Hwang, C. O'Donnell, C. Fox, P. Courchesne, P. Muntendam, N. Gordon, A. Adourian, P. Juhasz, M. Larson, and D. Levy. Protein Biomarkers of New-Onset Cardiovascular Disease: Prospective Study From the Systems Approach to Biomarker Research in Cardiovascular Disease Initiative. *Arteriosclerosis, Thrombosis, and Vascular Biology*, 34:939–945, 2014.

X. Yu, Y. Fu, D. Zhang, K. Yin, and C. Tang. Foam cells in atherosclerosis. *Clinica Chimica Acta*, 424:245–252, 2013.

Y. Zhan, Y. T. Yang, H. M. You, D. Cao, C. Y. Liu, C. J. Zhou, Z. Y. Wang, S. J. Bai, J. Mu, B. Wu, Q. L. Zhan, and P. Xie. Plasma-based proteomics

reveals lipid metabolic and immunoregulatory dysregulation in post-stroke depression. *European Psychiatry*, 29:307–315, 2014.

J. Zhang, Y. Zhang, N. Li, Z. Liu, C. Xiong, X. Ni, Y. Pu, R. Hui, J. He, and J. Pu. Potential diagnostic biomarkers in serum of idiopathic pulmonary arterial hypertension. *Respiratory Medicine*, 103:1801–1806, 2009.

J. Zhang, L. Zhu, J. Fang, Z. Ge, and X. Li. LRG1 modulates epithelial-mesenchymal transition and angiogenesis in colorectal cancer via HIF-1α activation. *Journal of Experimental and Clinical Cancer Research*, 35(29): 1–11, 2016a.

L. Zhang, W. Wang, J. Bai, Y. Xu, L. Li, L. Hua, L. Deng, and H. Jia. Proteomic analysis associated with coronary artery dilatation caused by Kawasaki disease using serum exosomes. *Revista Portuguesa de Cardiologia*, 35(5):265–273, 2016b.

Q. Zhang, R. Huang, Q. Tang, Y. Yu, Q. Huang, Y. Chen, G. Wang, and X. Wang. Leucine-rich alpha-2-glycoprotein-1 is up-regulated in colorectal cancer and is a tumor promoter. *OncoTargets and Therapy*, 11:2745–2752, 2018.

X. Zhang, S. Pek, S. Tavintharan, C. Sum, S. Lim, K. Ang, D. Yeo, T. Ee, C. Yip, and N. Kumari. Leucine-rich α-2-glycoprotein predicts proliferative diabetic retinopathy in type 2 diabetes. *Journal of Diabetes and its Complications*, 33(9):651–656, 2019.

Y. Zhang, X. Yang, F. Bian, P. Wu, S. Xing, G. Xu, W. Li, J. Chi, C. Ouyang, T. Zheng, D. Wu, Y. Zhang, Y. Li, and S. Jin. TNF-α promotes early atherosclerosis by increasing transcytosis of LDL across endothelial cells : Crosstalk between NF-κB and PPAR-γ. *Journal of Molecular and Cellular Cardiology*, 72:85–94, 2014.

Y. Zhang, Q. Luo, N. Wang, F. Hu, H. Jin, T. Ge, C. Wang, and W. Qin. LRG1 suppresses the migration and invasion of hepatocellular carcinoma cells. *Medical Oncology*, 32(146):1–10, 2015.

J. Zhao, Y. Fan, Y. Yang, D. Liu, K. Wu, F. Wen, C. Zhang, D. Zhu, and S. Zhao. Identification of potential plasma biomarkers for esophageal squamous cell carcinoma by a proteomic method. *International Journal of Clinical and Experimental Pathology*, 8(2):1535–1544, 2015.

D. Zhong, G. He, S. Zhao, J. Li, Y. Lang, W. Ye, Y. Li, C. Jiang, and X. Li. LRG1 modulates invasion and migration of glioma cell lines through TGF-β signaling pathway. *Acta Histochemica*, 117:551–558, 2015.

Y. Zhou, X. Zhang, J. Zhang, J. Fang, Z. Ge, and X. Li. LRG1 promotes proliferation and inhibits apoptosis in colorectal cancer cells via RUNX1 activation. *PLoS ONE*, 12(4):1–14, 2017.

A. Zink, S. Wann, R. Thompson, A. Keller, F. Maixner, A. Allam, C. Finch, B. Frohlich, H. Kaplan, G. Lombardi, M. L. Sutherland, J. Sutherland, L. Watson, S. Cox, M. Miyamoto, J. Narula, A. Stewart, G. Thomas, and J. Krause. Genomic Correlates of Atherosclerosis in Ancient Humans. *Global Heart*, 9(2):203–209, 2014.

Appendix A

IHC stain of LRG1in coronary artery sections

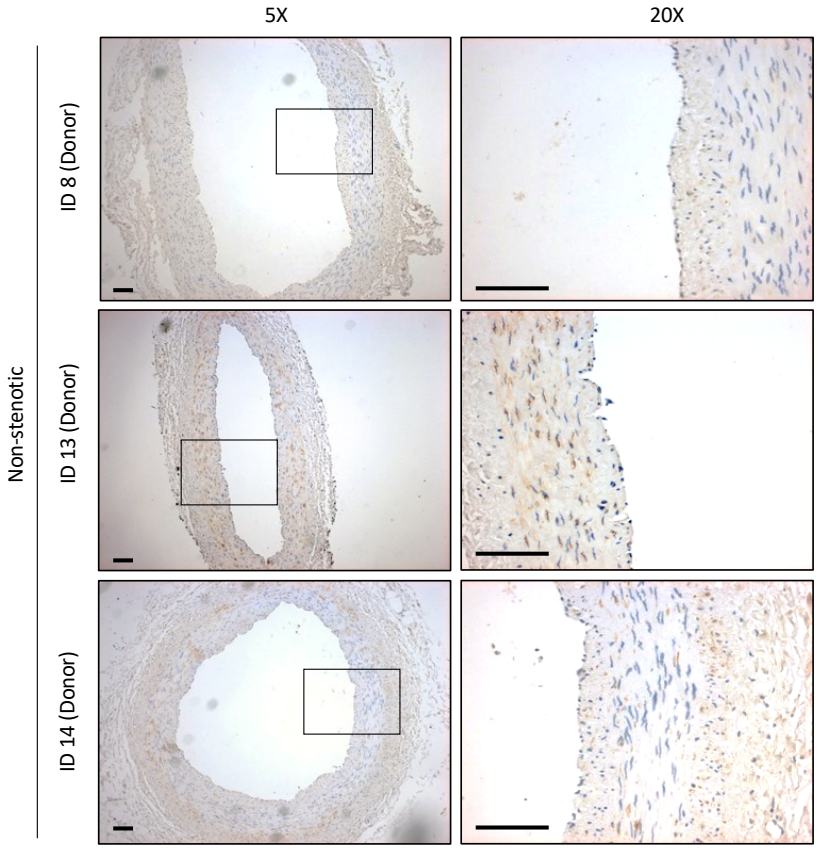

Figure A.1: IHC stain of LRG1 in non-stenotic coronary artery sections. Scale bar = 100 μm.

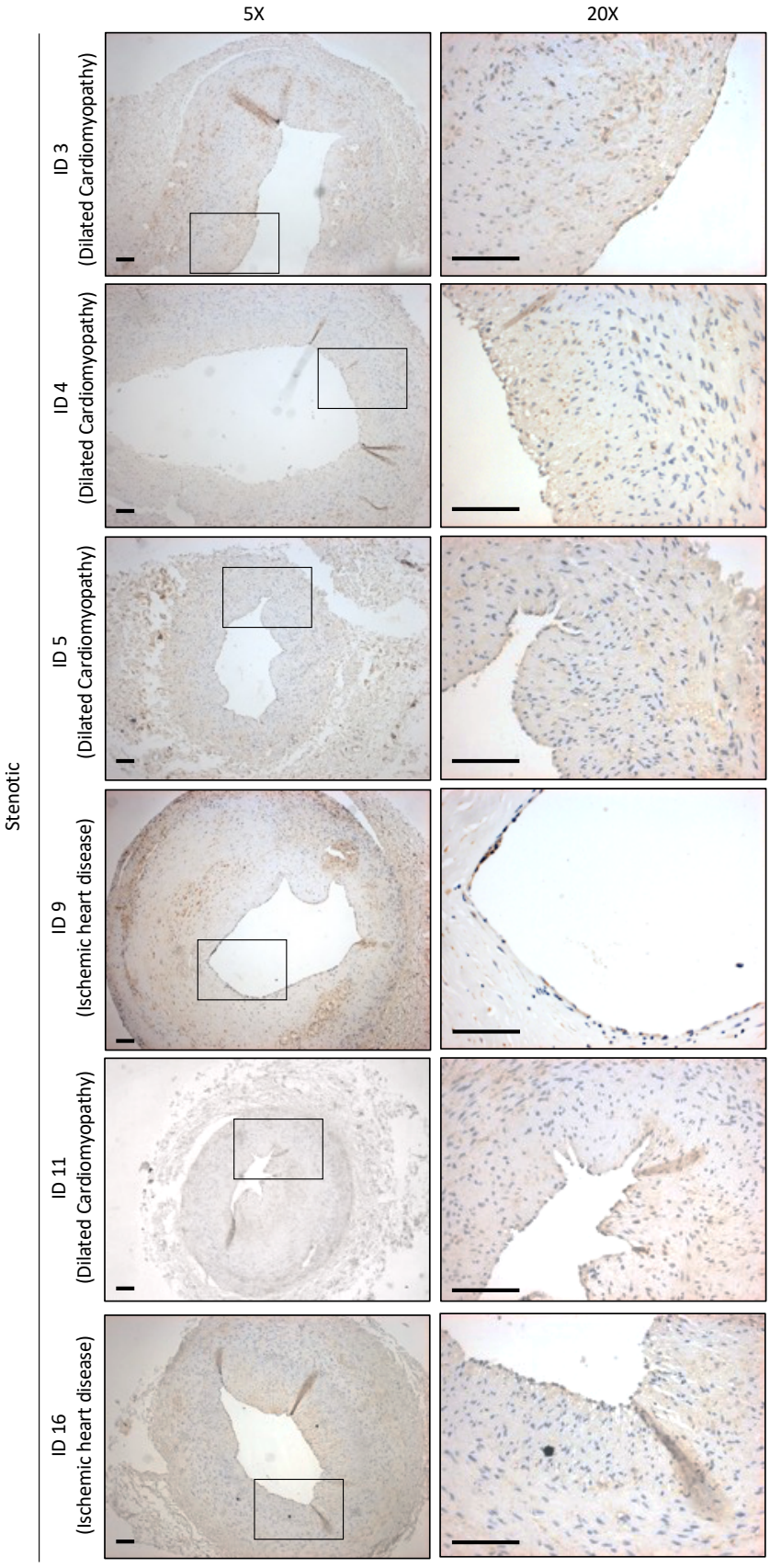

Figure A.2: IHC stain of LRG1 in stenotic coronary artery sections. Scale bar = 100 μm.

Appendix B

MATLAB code for the analysis of CFD simulation data

```
clear all;
clearvars;
close all;
clc;

%% Import data

flist=dir('WSS*.csv'); % import all csv files in current folder
nfiles = length(flist); % number of csv files imported

% read  the first file, skip headers
tmp = csvread(flist(1).name,1,0);
% initalise a big data matrix to store the results
data = zeros(size(tmp,1),size(tmp,2),nfiles);
data(:,:,1) = tmp; % paste the first table


% loop over the rest of the files, reading them in each time and stack in
% Z-direction%
for i=2:nfiles
    data(:,:,i) = csvread(flist(i).name,1,0);
end

%RawData format%
%Magnitude WSS(i) WSS(j)  WSS(k)  X  Y%

%Defining x and y values, and convert their unit to mm %
x = data(:,5,1)*1000;
y = data(:,6,1)*1000;

MeshSpacing = 0.01;
%Calculate the radius
Radius = max(x);
RadiusMax = max(x);
RadiusMin = min(x(x>=MeshSpacing));

%Customized RGB Color Vector
DarkGreen = [65 146 104] ./ 255;
DarkYellow = [240 205 19] ./ 255;
Orange = [253 168 7] ./ 255;
DarkGold = [181 142 33] ./ 255;
Brown = [141 60 14] ./ 255;
Red = [213 36 31] ./ 255;
Purple = [120 4 219] ./ 255;
Blue = [40 89 239] ./ 255;
Black = [6 21 3] ./ 255;

%% put scattered mesh values onto a regular grid that runs along a straight line

xq = (0:MeshSpacing:Radius)';
xq = round(xq,2,'decimals');
yq = zeros(length(xq),1);

%% loop through raw data and interpolate each time step onto regular grid/line
% create new big data matrix
dataNew = zeros(length(xq),size(data,2)-3,nfiles); % make new data matrix

for i=1:nfiles
    for j=1:4
        v = data(:,j,i);
        vq = griddata(x,y,v,xq,yq); % interpolate raw data at points x,y onto points↙
xq,yq
```

```
        dataNew(:,j,i) = vq; % paste into new data matrix
    end
end

%dataNew format
% X-axis > Row that represent radius
% Y-axis > WSS data (mag,i,j,k)
% Z-axis > files

% free up some memory
clear data

%% Calculate Matrices
%Calculate time averaged values
TA_data = mean(dataNew,3); % time average all columns, time is the 3rd dimension

%Calculate TAWSS
TAWSS = TA_data(:,1);

% Calculate MagMeanWSS
Averagei = TA_data(:,2);
Averagej = TA_data(:,3);
Averagek = TA_data(:,4);
MagMeanWSS = sqrt((Averagei.^2)+(Averagej.^2)+(Averagek.^2));

% Calculate OSI
OSI = 0.5*(1-(MagMeanWSS./TAWSS));

% Calculate TransWSS

%Calculate the MagMean without z-component
MagMeanWSSwoz = sqrt((Averagei.^2)+(Averagej.^2));
%Calculate the unit vector of i and j component over a cycle by dividing
%the Average i/j by the magnitude

%There are i/j because a vector is described using i/j component, hence
%this is the x/y breakdown of the mean unit vector over a cycle
XMagMeanWSS = Averagei./MagMeanWSSwoz;
YMagMeanWSS = Averagej./MagMeanWSSwoz;

%X/YMagMeanWSS multiply by every i/j component
C = bsxfun(@times,XMagMeanWSS,squeeze(dataNew(:,2,:)));
D = bsxfun(@times,YMagMeanWSS,squeeze(dataNew(:,3,:)));

Dotproduct = C+D;
E = sqrt((squeeze(dataNew(:,1,:)).^2)-(Dotproduct.^2));

TransWSS = mean(E,2);

TransWSSsmth = smooth(TransWSS,round(length(xq)/20));

clear data
%%%%%%%%%%%%
%Plot Graph%
%%%%%%%%%%%%
%_____________________________________________________%


%Plot RawMetrics Graph%
figure;hold on;
plot(xq,TAWSS,'-b','LineWidth',2.5)
plot(xq,OSI,'-r','LineWidth',2.5)
```

```
plot(xq,TransWSS,'-k','LineWidth',2.5)
axis([0 17.4 0 0.8]);
set(gca,'XTick',(0:2:17.4))
xlabel('Radial distance from centre (mm)');
ylabel('Metrics');
legend('TAWSS (Pa)','OSI','TransWSS (Pa)','CFI','TransWSSmin↙
(Pa)','location','southoutside','orientation','horizontal');

title('Unnormalized Metrics Plot');

%% Polar Plot-Compile

PolarStep = 2;
PolarRadius = [MeshSpacing:PolarStep:RadiusMax]';
PolarRadius = round(PolarRadius,2);
PolarData = zeros(size(PolarRadius,1),4,nfiles+1);

TempRow=0;
for  i=1:1:size(PolarRadius,1)
    TempRow = TempRow+1;
    Cond = xq(:,1)==PolarRadius(i);
    CondRow = find(Cond);

   for j=1:10:nfiles
       PolarData(TempRow,:,j) = dataNew(CondRow,:,j);
   end
   PolarData(TempRow,:,420) = dataNew(CondRow,:,1);
end
%Remove rows with all zero
mask = any(any(PolarData)); %// getting which layers are Non-zero Layers
PolarData = PolarData(:,:,mask);


DarkGreen = [65 146 104] ./ 255;
DarkYellow = [240 205 19] ./ 255;
Orange = [253 168 7] ./ 255;
DarkGold = [181 142 33] ./ 255;
Brown = [141 60 14] ./ 255;
Red = [213 36 31] ./ 255;
Purple = [120 4 219] ./ 255;
Blue = [40 89 239] ./ 255;
Black = [6 21 3] ./ 255;
Cyan = [0,255,255] ./ 255;
Teal = [0,128,128] ./ 255;
Olive = [128,128,0]./ 255;
DarkCyan = [0,139,139]./ 255;
CornFlowerBlue = [100,149,237]./ 255;
Magenta = [255,0,255]./ 255;
Wheat = [245,222,179]./ 255;
RosyBrown = [188,143,143]./ 255;
SlateGray = [112,128,144]./ 255;

%Create array of colors and markers
Colour={DarkGreen,DarkGold,Purple,Brown,Red,Blue,Black,Olive,CornFlowerBlue,DarkCyan,↙
Magenta,Wheat,RosyBrown,SlateGray};

%Plot Polar Plot
figure;hold on;
ax=gca;
ax.XAxisLocation = 'origin';
ax.YAxisLocation = 'origin';
```

```
%Create Legend Matrix
LegendStr = zeros(size(PolarRadius,1),1);
for i=1:1:size(PolarRadius,1)
    s1{i,1} = ' mm';
end
LegendStr = strcat(num2str(round(PolarRadius,2)),s1);

for i=[1 3 5 8 9]
    plot(squeeze(PolarData(i,2,:)),squeeze(PolarData(i,3,:)),'-*','LineWidth',↙
2.5,'MarkerSize',3.5,'color',Colour{i});
    legend(LegendStr([1 3 5 8↙
9]),'location','southoutside','orientation','horizontal');
end

x=xlabel('Radial Shear (Pa)','FontSize',10);
y=ylabel('Tangential Shear (Pa)', 'rot', 0,'FontSize',10);  % do not rotate the y↙
label
axis([-1.5 0.5 -0.6 1.5]);
set(y, 'position', get(y,'position')+[0.1,1.05,0]);  % shift the y label to the left↙
by 0.1
set(x, 'position', get(x,'position')+[-0.8,0.3,0]);

%% Polar Plot- Individual Plot

max_lim = 1.5;
x_fake=[0 max_lim 0 -max_lim];
y_fake=[max_lim 0 -max_lim 0];
h_fake=compass(x_fake,y_fake);
set(h_fake,'Visible','off');
hold on;
IndividualPolar = compass(PolarData(1,2,:),PolarData(1,3,:),'r');
set(IndividualPolar,'LineWidth',1);

% Using the code above
% Removing the label
set(findall(gcf, 'String', '30','-or','String','60','-or','String','120','-↙
or','String','150','-or','String','210','-or','String','240','-or','String','300','-↙
or','String','330') ,'String', '  ');
% Altering the angular label
set(findall(gcf, 'String', '0'),'String', '0 (Deg)');
set(findall(gcf, 'String', '  1.5'),'String', '1.5 (Pa)');


%% Plot Instanteneous WSS

TempRow=0;
IntWSS_Data = zeros(size(PolarRadius,1),nfiles,1);

for i=[1 3 5 8 9]
    TempRow = TempRow+1;
    [int_row]=find(xq==PolarRadius(i,1));

    for j=1:1:nfiles
       IntWSS_Data(TempRow,j,1) = dataNew(int_row,1,j);
    end
end
figure;hold on;

Colour2={DarkGreen,Purple,Red,Olive,CornFlowerBlue,Teal,Olive,DarkCyan,CornFlowerBlue,↙
Magenta,Wheat,RosyBrown,SlateGray};

for i=1:5
```

```
    plot(squeeze(IntWSS_Data(i,:)),'-','LineWidth',3,'color',Colour2{i});
end
set(gca,'XTick',[0 110 210 310 410]);
set(gca,'XTickLabel',{'0' '\pi/2' '\pi' '3\pi/2' '2\pi'});
xlabel('Location in orbit (radians)');
ylabel('WSS Magnitude (Pa)');
```

Appendix C

Permission to reproduce figures

Page No.	Name of work	Source of work	Copyright holder	License number
32	Figure 1.1: Atherogenesis.	P. Libby. Current Concepts of the Pathogenesis of the Acute Coronary Syndromes. Circulation, 104:365–372, 2001.	Wolters Kluwer Health, Inc.	4731361410210
35	Figure 1.2: TAWSS, OSI, and transWSS.	Y. Mohamied, E. Rowland, E. Bailey, E. Sherwin, M. Schwartz, and P. Weinberg. Change of Direction in the Biomechanics of Atherosclerosis. Annals of Biomedical Engineering, 43(1):16–25, 2014.	Authors	Creative Commons CC BY
38	Figure 1.3: Phenotype of ECs in regions of different flow profile.	C. Hahn and M. Schwartz. Mechanotransduction in vascular physiology and atherogenesis. Nature Reviews Molecular Cell Biology, 10(1):53–62, 2009.	Springer Nature	4730671119479
43	Figure 1.4: Monocyte adhesion cascade.	T. Gerhardt and K. Ley. Monocyte trafficking across the vessel wall. Cardiovascular Research, 107(3):321–330, 2015.	Oxford University Press	4730910634965
57, 122	Figure 1.5: Proposed working model of LRG1 mediated TGF-β1 endothelial cell signalling. Figure 4.1: Restriction map of pcDNA-LRG1-HIS plasmid.	X. Wang, S. Abraham, J. McKenzie, N. Jeffs, M. Swire, V. Tripathi, U. Luhmann, C. Lange, Z. Zhai, H. Arthur, J. Bainbridge, S. Moss, and J. Greenwood. LRG1 promotes angiogenesis by modulating endothelial TGF-β signalling. Nature, 499(7458):306–311, 2013b.	Springer Nature	4716011001754
68	Figure 2.2: Schematic diagram of the orbital shaker model.	P. Alpresa, S. Sherwin, P. Weinberg, and M. Reeuwijk. Orbitally shaken shallow fluid layers. I. Regime classification. Physics of Fluids, 30(032107), 2018.	AIP Publishing	4716160046265